DESIGN OF ASYMMETRIC COPLANAR STRIP FOLDED DIPOLE ANTENNAS

A THESIS SUBMITTED TO
THE GRADUATE SCHOOL OF NATURAL AND APPLIED SCIENCES
OF
MIDDLE EAST TECHNICAL UNIVERSITY

BY

KAMİL KARACİĞER

IN PARTIAL FULFILLMENT OF THE REQUIREMENTS
FOR
THE DEGREE OF MASTER OF SCIENCE
IN
ELECTRICAL AND ELECTRONICS ENGINEERING

DECEMBER 2014

Approval of the thesis:

DESIGN OF ASYMMETRIC COPLANAR STRIP FOLDED DIPOLE ANTENNAS

submitted by **KAMİL KARACİĞER** in partial fulfillment of the requirements for the degree of **Master of Science in Electrical and Electronics Engineering Department, Middle East Technical University** by,

Prof. Dr. Gülbin Dural Ünver
Dean, Graduate School of **Natural and Applied Sciences** _____

Prof. Dr. Gönül Turhan Sayan
Head of Department, **Electrical and Electronics Eng.** _____

Assoc. Prof. Dr. Lale Alatan
Supervisor, **Electrical and Electronics Eng. Dept.,METU** _____

Examining Committee Members:

Prof. Dr. Özlem Aydın Çivi
Electrical and Electronics Eng. Dept.,METU _____

Assoc. Prof. Dr. Lale Alatan
Electrical and Electronics Eng. Dept.,METU _____

Prof. Dr. Gülbin Dural Ünver
Electrical and Electronics Eng. Dept.,METU _____

Prof. Dr. Sencer Koç
Electrical and Electronics Eng. Dept.,METU _____

Kaan Temir, M.S.
ASELSAN Inc. _____

Date: **03.12.2014**

I hereby declare that all information in this document has been obtained and presented in accordance with academic rules and ethical conduct. I also declare that, as required by these rules and conduct, I have fully cited and referenced all material and results that are not original to this work.

Name, Last name: Kamil KARACİĞER

Signature:

ABSTRACT

DESIGN OF ASYMMETRIC COPLANAR STRIP FOLDED DIPOLE ANTENNAS

Karaciğer, Kamil
M. S., Department of Electrical and Electronics Engineering
Supervisor: Assoc. Prof. Dr. Lale Alatan

December 2014, 141 pages

This thesis includes the design, simulation, production and measurement of an asymmetric coplanar strip folded dipole antenna suitable to be used as an element in a linear array operating at S-band (2.7 GHz - 3.3 GHz). In this same manner, its usefulness as an array antenna is also explored in this thesis. This antenna element consists of a microstrip line feed, microstrip to coplanar stripline transition (BALUN) and asymmetric coplanar strip (ACPS) folded dipole. The planar folded dipole can be constructed using printed circuit technology, its input impedance can be adjusted over a wide range of values, and it has significantly greater bandwidth than a single half-wave dipole and conventional patch radiators. These properties make planar folded dipole antennas an appealing choice as a radiating element. A step-by-step procedure is followed during the design process of the ACPS folded dipole antenna element. The design process is based on the simple impedance matching among antenna element components, i.e. feed, transition, and antenna. First, BALUN which consists of microstrip feed line and microstrip to coplanar stripline transition is designed and simulated using Ansys HFSS®, a high frequency

electromagnetic field simulation program. Then, in order to investigate the effects of ACPS folded dipole parameters on the input impedance characteristics of the antenna, a parametric study is performed using Ansys HFSS®. By the help of the experience gained through these parametric analyses, an ACPS folded dipole is designed and simulated. Once the ACPS folded dipole is connected to the balun, the design of antenna element is completed. Before manufacturing the antenna element, the complete structure is simulated and optimized with Ansys HFSS® to achieve a good matching over the operating frequency range. Additionally, a linear array antenna comprising four asymmetric coplanar strip folded dipole antenna elements and a suitable power divider network to feed the array are designed and simulated. Finally, the antenna element and the four-element uniform linear array antenna are manufactured, measured, and their performances are compared with simulation results.

KEYWORDS: Asymmetric Coplanar Strip Folded Dipole, Balun, Microstrip to Coplanar Stripline Transition, S-Band, Linear Array

ÖZ

DÜZLEMSEL ASİMETRİK KATLANMIŞ ŞERİT DİPOL ANTENLERİN TASARIMI

Karaciğer, Kamil
Yüksek Lisans, Elektrik ve Elektronik Mühendisliği Bölümü
Tez Yöneticisi: Doç. Dr. Lale Alatan

Aralık 2014, 141 sayfa

Bu tez S-bant (2.7 GHz - 3.3 GHz) frekansında çalışacak doğrusal anten dizilerinde anten elemanı olarak kullanıma uygun düzlemsel asimetrik katlanmış şerit dipol anten tasarımını, benzeşimini, üretimini ve ölçümünü içerir. Aynı şekilde, düzlemsel asimetrik katlanmış şerit dipolün bir dizi anteni olarak kullanışlılığı da bu tezde incelenmiştir. Bu anten elemanı mikroşerit hat beslemesinden, mikroşeritten eş düzlemsel şerit hatta geçiş yapısından ve düzlemsel asimetrik katlanmış şerit dipolden oluşur. Düzlemsel katlanmış dipol baskı devre teknolojisi kullanılarak oluşturulabilir, düzlemsel katlanmış dipolün giriş empedansı geniş bir değer aralığında ayarlanabilir ve düzlemsel katlanmış dipol bir yarım dalga dipolden ve geleneksel yama antenlerinden önemli ölçüde daha yüksek bant genişliğine sahiptir. Bu özellikleri düzlemsel katlanmış dipolü bir ışıma elemanı olarak cazip bir seçim yapar. Tasarım kısmında düzlemsel katlanmış dipol anten elemanı adım adım geliştirilmiştir. Tasarım süreci, besleme, geçiş ve anten gibi anten elemanı bileşenleri arasındaki empedans uyumlamaya dayanmaktadır. İlk olarak, mikroşerit besleme hattını ve mikroşerit hattan eş düzlemsel şerit hatta geçişi içeren BALUN yapısı yüksek frekanslı elektromanyetik alan benzeşim programı Ansys HFSS® kullanılarak tasarlanmış ve benzeşimi yapılmıştır. Sonraki aşamada düzlemsel asimetrik katlanmış dipol parametrelerinin anten giriş

empedansı karakteristiği üzerindeki etkilerinin incelenmesi amacıyla Ansys HFSS® kullanılarak parametrik analizler gerçekleştirilmiştir. Parametrik analizlerden elde edinilen tecrübeyle, bir düzlemsel asimetrik katlanmış şerit dipol tasarımı yapılmıştır. Düzlemsel asimetrik katlanmış şerit dipol BALUN yapısına bağlandıktan sonra anten elemanı tasarımı tamamlanmıştır. Anten elemanı üretiminden önce, çalışma frekans aralığı boyunca iyi bir uyumlama elde etmek için anten elemanı olarak tamamlanmış yapının Ansys HFSS® ile benzeşimi yapılmış ve anten elemanı optimize edilmiştir. Ayrıca dört düzlemsel asimetrik katlanmış şerit dipol anten elemanlarından oluşan doğrusal bir anten dizisi ve bu diziyi besleyecek uygun bir güç bölücü yapısı tasarlanmış ve benzeşimi yapılmıştır. En son aşamada ise anten elemanı ve dört elemanlı düzgün doğrusal anten dizisi üretimi yapılmış, ölçümleri alınmış ve bu antenlerin performansları benzeşim programı sonuçları ile karşılaştırılmıştır.

ANAHTAR KELİMELER: Düzlemsel Asimetrik Katlanmış Şerit Dipol, Balun, Mikroşeritten Düzlemsel Şerit Hatta Geçiş, S-Bant, Doğrusal Anten Dizisi

To my wife, Gül Elmas,

ACKNOWLEDGEMENTS

I would like to express my sincere gratitude to my advisor, Assoc. Prof. Dr. Lale Alatan, for her valuable guidance, support and technical suggestions throughout the study.

I would also like to thank Prof. Dr. Özlem Aydın Çivi, Prof. Dr. Sencer Koç, Prof. Dr. Gülbin Dural and Mr. Kaan Temir being in my jury and sharing their opinions.

I would like to express my gratitude to Mr. Mehmet Erim İnal for proposing this topic to me and Mr. Can Barış Top for their invaluable help and guidance in the design and manufacturing process.

I am grateful to ASELSAN INC. for the financial and technical opportunities provided for the completion of this thesis.

I would also like to express my sincere appreciation for Mert Kalfa, Kenan Çapraz, Akın Dalkılıç and Kaan Temir for their valuable friendship, motivation and help.

Lastly, for her great support, understanding, being with me in every moment of this work and giving me the strength and courage to finish it, I am also grateful to my wife, Gül Elmas.

TABLE OF CONTENTS

LIST OF TABLES

TABLES

LIST OF FIGURES

FIGURES

CHAPTER 1

INTRODUCTION

1.1 Preface

In some applications like spacecraft, missile, aircraft and space applications, where performance, size, weight and cost are constraints, low-profile antennas with good radiation characteristics are required. In order to respond these necessities, printed antennas can be considered as an attractive alternative. In addition, low profile, low cost, and high directivity antenna arrays are required in many electronic warfare and radar systems. Due to the manufacturing on single substrates together with the feeding network, one-dimensional printed antenna arrays are commonly used solutions.

In recent years, usage areas of printed antennas are increased due to their numerous advantages. Firstly, it is pointed out that the low size, which contributes to integration antenna to systems like radar substructures, is the most important advantage of the printed antennas [1]. At the manufacturing process of printed antennas, small number of materials is used such as dielectric substrates and connectors. Thus, printed antennas are very compact and the fabrication of these antennas is cost-effective. Furthermore, dielectric substrates are thin and some of them are flexible, so printed antennas are low volume, low profile and can be conformable to curved surfaces [2]. Moreover, the printed antennas are dependable with respect to reproducibility means that the characteristics of the first produced element are exactly the same with the characteristics of new copies ones [1]. Secondly, radiation mechanisms of printed antennas are adjustable. For example,

the polarization of the printed antenna is changed easily by changing the feed configuration.

Printed antennas are produced with PCB technology, so these antennas are easily integrated into the system, which includes microwave integrated circuits. Besides, the speed of the process is the other important advantage of PCB production owing to the fact that printed antennas, matching networks and feed lines can be produced simultaneously [3].

Along with the advantages of printed antennas, they have many disadvantages. First of all, by comparison with other types of antennas, the output power level of the printed antennas is low [3] [4]. These antennas could not provide high power levels due to physical characteristics. In addition, the efficiency levels of printed antennas are also low. Narrow bandwidth is the next important disadvantage of the printed antennas [3]. In general, the frequency bandwidth of the printed antennas, especially resonant type structures like microstrip patch antennas, is at most few percents [3] [4]. Alternatively, broad bandwidth can be obtained by using the travelling wave type structures like the Vivaldi and linearly tapered slot antenna (LTSA) [5]. Nevertheless, these antennas suffer from the excitation of the substrate modes which lead to reduced efficiency, disrupted radiation pattern and strong crosstalk between antennas in an array, and they have larger electrical size than resonant type patches or slots [6]. Hence, generally pattern and/or bandwidth requirements can only be met with novel antenna configurations like Planar Inverted-F Antenna (PIFA) [7] or magneto-electric dipole antenna [8].

In parallel with the technology breakdown in the applications of RF and microwave, the low cost, low volume, lightweight and high directivity antennas are required. Since printed antennas fulfill the most of these practical needs, extensive research has been conducted to cope with the problems associated with the disadvantages of these beneficial printed antenna structures. Crucial studies have been carried on in order to especially improve the narrow bandwidth which is the major obstacle for the application in many electronic warfare and radar systems.

Since printed dipole antennas are considered within the scope of this thesis, only the studies on improving the bandwidth of these printed antenna types will be summarized.

The first studies on bandwidth enhancement of dipole antennas are initiated for wire dipole antennas. The bandwidth of the wire dipole antenna can be improved substantially by using thicker conductors [9]. Balanis quotes the narrow bandwidth of 3% for a very thin dipole, but with a thicker conductor the dipole bandwidth is approximately 30% [3]. The frequency bandwidth can be further increased by placing an additional conductor wire parallel to the dipole antenna and joining the dipole with the additional conductor at the ends to form a folded dipole antenna [10]. The radiation characteristics of a folded dipole antenna are same with those of a conventional dipole antenna [3]. Although the folded dipole antenna has enhanced frequency bandwidth over that of the conventional dipole antenna, it is main attraction at the moment lies in its ability to control the input impedance over a wide range of values. The current in the folded dipole antenna are divided asymmetrically between the two wires when the two wires do not have equal radius. This asymmetric folded dipole antenna gives an additional mean of impedance adjustment through the selection of the radius of the two wires [10].

Symmetrical and asymmetrical planar folded dipoles can also be designed and constructed using strips which can be fabricated using printed circuit board technology [11] [12]. The impedance controlling feature of wire folded dipole antenna is also valid for the antenna realized as a strip folded dipole [13]. The input impedance can be changed over a wide range of values by adjusting the widths of the parallel strips of the planar folded dipole [14]. This property of impedance control explains the increasing use of the planar folded dipoles, especially at very high frequency [15]. The planar folded dipole antenna has various additional advantages over more ordinary wire folded dipole antennas in free space. Firstly, mechanical support for the antenna is provided by the presence of the dielectric substrate and the dielectric material offers the compatibility with planar

transmission lines for planar folded dipole antennas. Wire type antennas in free space are very thin especially at high frequencies, thus they are highly fragile and difficult to feed. Secondly, using a dielectric material implies that the antenna can be miniaturized corresponding to free space wavelength. As will be shown in this study, a center to center element spacing of $\lambda_0/2$ is easily achieved with this antenna in an array environment, where λ_0 refers to a free space wavelength at the center frequency of the array. Even strict spacing may be carried out in company with the increased mutual coupling between the antenna elements in the array.

The main aim of this thesis is to design an asymmetric coplanar strip (ACPS) folded dipole antenna suitable to be used as an element in a linear array operating in S-band at frequency range of 2.7 GHz to 3.3 GHz. The designed ACPS folded dipole can be produced using printed circuit technology, its input impedance can be changed over a wide range of values, and it has significantly greater bandwidth than a single half-wave dipole and conventional patch radiators [11]. Another purpose of this study is to select the best arrangement of the physical parameters of the asymmetric coplanar strip folded dipole in order to achieve a maximum bandwidth.

1.2 Organization of the Thesis

The ACPS folded dipole antenna element is naturally fed by a coplanar strip (CPS) transmission line. However microstrip line transmission lines are generally preferred in array applications due to the ease in the design of the feed network and the convenient interface with the SMA connector. Therefore a balun also needs to be designed for the transition from the unbalanced transmission line (microstrip line) to the balanced transmission line (CPS line). In Chapter 2, the analysis methods and design formulas for ACPS folded dipole antenna are presented. The design parameters for ACPS folded dipole and CPS lines are also defined.

The design of a balun, a CPS line and an ACPS folded dipole are implemented in Chapter 3. Detailed information is offer on the design and performance of the antenna element and other components like balun. In addition, the antenna element is optimized with Ansys HFSS® [16] Chapter 3 continues with a four-element uniform linear array design. A suitable power divider network to feed the array is also designed to equally divide power to each antenna element. The simulation results obtained by Ansys HFSS® for the return loss, gain and the radiation patterns of this uniform array are given at the end of this chapter.

Following the optimization of design parameters, the asymmetric coplanar strip folded dipole antenna element and the four-element uniform linear array antenna are fabricated and measured. Chapter 4 covers the fabrication process of both the antenna element and the improved array, and provides the evaluation of the measurements results. Comparison and evaluation of the deviations from the results of simulations and measurements are also discussed in Chapter 4.

In the final chapter of the thesis, the concluding remarks about this study are given with the possible future works about asymmetric coplanar strip folded dipole antennas, which can move the knowledge and abilities a step further.

CHAPTER 2

ANALYSIS OF ASYMMETRIC COPLANAR STRIP FOLDED DIPOLES AND COPLANAR STRIPLINE STRUCTURES

2.1 Analysis of Asymmetric Coplanar Strip Folded Dipoles

Figure 2- 1 shows the structure of an ACPS folded dipole antenna in free space. In Figure 2- 1, strip S_1 is the driven strip which is centered at $x = -c$ and has width W_1, and strip S_2 is the parasitic strip which is centered at $x = +c$ and has width W_2. The spacing between the two strips is b.

A folded dipole antenna is just an extension of the conventional single wire dipole. However, since the folded dipole arms are made up of asymmetric coplanar strips, both the even and odd mode currents must be considered. A diagram representing the two modes of operation is shown in Figure 2- 2. In the odd mode, equal currents in the dipole arms travel in opposite directions, resulting in fields that are out of phase and thus cancel in the far field of the antenna [17]. This mode is named as the non-radiating (or transmission line) mode. In the even mode, currents in the dipole arms travel in the same direction. The fields generated by these currents add up in-phase, resulting in a radiating (or antenna) mode [17].

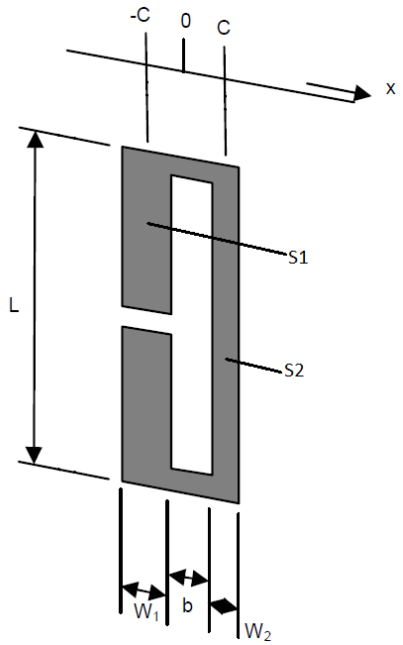

Figure 2- 1 Structure of an ACPS folded dipole in free space

The folded dipole antenna was analyzed by Thiele et al. [18]. Thiele indicates that the analysis and design of the folded dipole is extensively simplified when the spacing between the driven and parasitic conductors of the folded dipole is less than 0.01 wavelengths [18]. Provided that this constraint is met, the excitation of a folded dipole can be decomposed into two fundamental modes as discussed above [18]: the transmission line mode and the antenna mode. Figure 2- 2 shows the decomposition of the total current I into the current of the transmission line mode I_T and the antenna mode $I_A = I_1(1 + a)$, where I_1 is the current on the driven strip of the folded dipole.

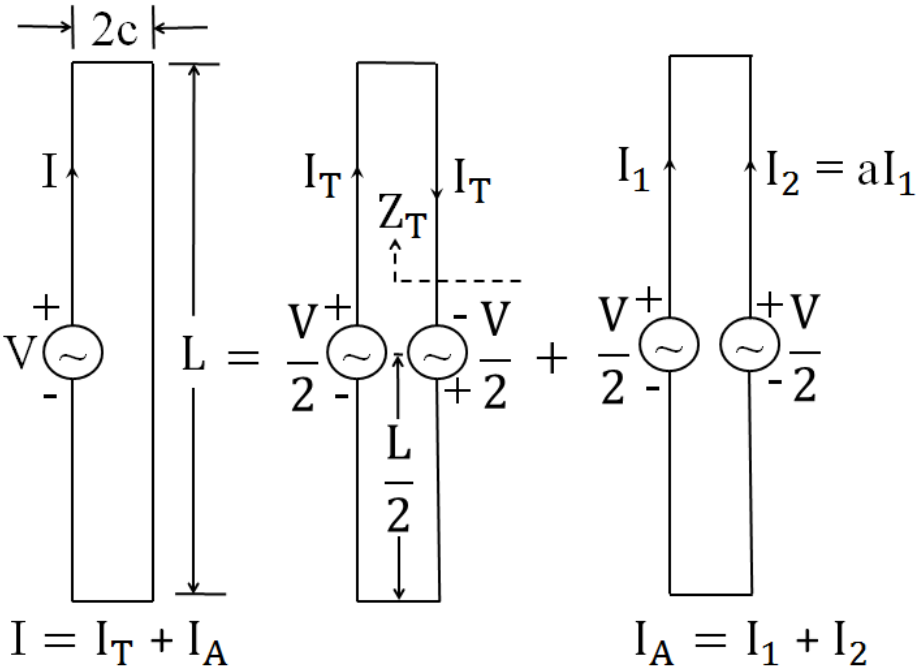

Figure 2- 2 Folded dipole and its equivalent transmission line mode and antenna mode models

Design equations for the input impedance of the ACPS folded dipole antenna (Z_{in}^{FD}) were developed by Lampe [11] [12]. There are three parameters that control the input impedance: the impedance of a cylindrical dipole having the same length with the ACPS folded dipole antenna, the step-up impedance ratio that depends on the widths of the two parallel strips and the transmission line impedance. These parameters will be studied in the following part.

The impedance Z_{in}^{FD} is given by [11] [12]:

$$Z_{in}^{FD} = \frac{2Z_T Z_A}{2Z_T + Z_A} = 2Z_T // Z_A \qquad (2.1)$$

where Z_A is the impedance of the antenna mode and Z_T is the impedance of the transmission line mode.

The antenna mode impedance is determined from [17]:

$$Z_A = (1+a)^2 Z_d \tag{2.2}$$

where Z_d is the impedance of the equivalent cylindrical dipole of having the same length with the folded dipole and the equivalent radius ρ_e, and $(1+a)^2$ is referred to as the step-up impedance ratio.

Substituting equation (2.2) to equation (2.1), the impedance Z_{in}^{FD} is found to be

$$Z_{in}^{FD} = \frac{2(1+a)^2 Z_T Z_d}{2Z_T + (1+a)^2 Z_d} \tag{2.3}$$

It is seen from equation (2.3) that the solution to the impedance Z_{in}^{FD} consists of the solution of three problems: the parameters Z_T, a and Z_d must be determined. These quantities will be presented in detail.

If we start with Z_T, for a lossless transmission line, the impedance measured at a distance (l) from the load impedance (Z_L) is given as

$$Z_{in}(l) = Z_0 \frac{(Z_L + jZ_0 \tan \beta_0 l)}{(Z_0 + jZ_L \tan \beta_0 l)} \tag{2.4}$$

where Z_0 is the characteristic impedance of the transmission line and β_0 is the propagation constant of the transmission line.

The impedance Z_T of transmission line which is the impedance of a shorted transmission line ($Z_L = 0$) of length $\frac{L}{2}$ given in Figure 2- 2 is derived by using equation (2.4) as

$$Z_T = jZ_0 \tan(\beta_0 \frac{L}{2}) \tag{2.5}$$

In particular, Z_0 is the characteristic impedance of an asymmetrical coplanar strip transmission line.

Z_0 is derived in [19] and [20] by using conformal mapping technique, and the resulting expression for Z_0 is given as [11] [12]:

$$Z_0 = \frac{120\pi}{\sqrt{\varepsilon_r}} \frac{K(k)}{K'(k)} \tag{2.6}$$

where

$$k = \begin{cases} \dfrac{\frac{b}{2}\left[1 + e\left(\frac{b}{2} + W_1\right)\right]}{\frac{b}{2} + W_1 + e\left(\frac{b}{2}\right)^2}, & W_1 \neq W_2 \text{ (asymmetric)} \\ \dfrac{b}{b + 2W}, & W_1 = W_2 = W \text{ (symmetric)} \end{cases} \tag{2.7}$$

$$e = \frac{W_1 W_2 + \frac{b}{2}(W_1 + W_2) - \sqrt{W_1 W_2 (b + W_1)(b + W_2)}}{\left(\frac{b}{2}\right)^2 (W_1 - W_2)} \tag{2.8}$$

and where the dimensions W_1, W_2 and b are given in Figure 2- 1, and ε_r is the relative dielectric constant of the medium.

In equation (2.6), $K(k)$ is the complete elliptical integral of the first kind and its complement $K'(k) = K(k')$, where $k'^2 = 1 - k^2$. The complete elliptical integral of the first kind and its complement can be evaluated using the following formulas proposed by Hilberg in [21]:

$$\frac{K(k)}{K'(k)} \cong \begin{cases} \dfrac{\ln\left[2\dfrac{\sqrt{1+k} + \sqrt[4]{4k}}{\sqrt{1+k} - \sqrt[4]{4k}}\right]}{2\pi}; & 1 \leq \dfrac{K(k)}{K'(k)} \leq \infty, \quad \dfrac{1}{\sqrt{2}} \leq k \leq 1 \\ \dfrac{2\pi}{\ln\left[2\dfrac{\sqrt{1+k'} + \sqrt[4]{4k'}}{\sqrt{1+k'} - \sqrt[4]{4k'}}\right]}; & 0 \leq \dfrac{K(k)}{K'(k)} \leq 1, \quad 0 \leq k \leq \dfrac{1}{\sqrt{2}} \end{cases} \tag{2.9}$$

For the second parameter a controls the impedance Z_{in}^{FD}, the parameter a in the step-up impedance ratio is given by Lampe in [11] [12]:

$$a = \frac{\ln\left\{4c + 2\sqrt{(2c)^2 - \left(\frac{W_1}{2}\right)^2}\right\} - \ln(W_1)}{\ln\left\{4c + 2\sqrt{(2c)^2 - \left(\frac{W_2}{2}\right)^2}\right\} - \ln(W_2)} \tag{2.10}$$

where the distances W_1, W_2 and c are indicated in Figure 2- 1.

Lastly, the impedance Z_d of the equivalent cylindrical dipole shown in Figure 2- 3 is obtained by the help of the equivalent radius ρ_e of the equivalent cylindrical dipole. Hallen determines that the theory of circular cylindrical antennas could be expanded to antennas of noncircular cross section by using the equivalent radius [22]. This parameter is given by Lampe for the asymmetric coplanar folded dipole in [11] [12]:

$$\rho_e = \left(\frac{W_1}{4}\right)^{\frac{1}{1+a}} \left(c + \sqrt{(c)^2 - \left(\frac{W_2}{4}\right)^2}\right)^{\frac{a}{1+a}} \tag{2.11}$$

where the distances W_1, W_2 and c are indicated in Figure 2- 1.

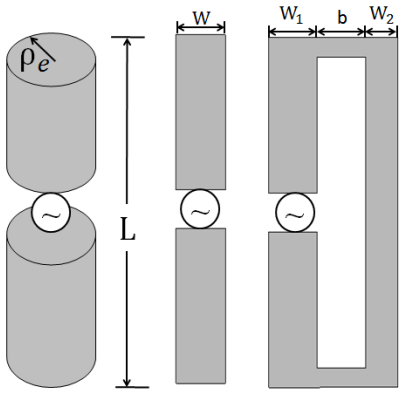

Figure 2- 3 Cylindrical dipole with the equivalent radius, strip dipole and ACPS folded dipole configurations

At the resonance frequency of the folded dipole antenna, when $L = \frac{\lambda}{2}$, transmission line impedance becomes infinite ($Z_T \rightarrow \infty$) and the expression for the Z_{in}^{FD} reduces to the following equation [11] [12]:

$$Z_{in}^{FD} = Z_A = (1 + a)^2 Z_d \tag{2.12}$$

From equation (2.12), it is seen that as the step-up impedance ratio $(1 + a)^2$ varies, the Z_{in}^{FD} changes. This flexibility in adjusting the input impedance of the antenna is one of the most attractive features of the ACPS folded dipole. In addition, the impedance tuning ability eliminates the need for a matching network, which makes the system more compact, power efficient and cheaper the produce. It can be obtained from the design equations that regardless of the spacing between the two strips, for $W_1 = W_2$, the design equations for the Z_{in}^{FD} reduce to the well-known expression for the conventional folded dipole $Z_{in}^{FD} = Z_A = 4 Z_d$.

Full wave analysis techniques such as the method of moments (MoM) and the finite integration technique (FIT) can be used in order to calculate the input impedance of the cylindrical dipole. These methods are potentially very accurate but in general these methods are considered as time consuming [23]. The cylindrical dipole impedance Z_d can be also found for equivalent radius ρ_e by using known analytical methods such as the induced EMF method [3], the Hallen's integral equation method or applying the empirical double-polyfit equations for the King-Middleton Second-Order solution [24]. While the resulting equations are easy to use, they appear to be insufficiently accurate to design antennas, especially when the radius of the cylindrical dipole increases [23].

Lampe makes some assumptions to obtain the design equations for the ACPS folded dipole. Firstly, the medium surrounding the ACPS folded dipole is supposed to be homogenous. Secondly, the effects of the presence of a dielectric material, interactions with the input transmission lines and scattering are not incorporated, and in his analysis feed region and dipole end effects are not considered [11]. Finally, it is assumed that the parallel conductor strips of the ACPS folded dipole

are very close together with regards to wavelengths, and Lampe indicates that proximity of these conductors is a necessity of the transmission line model [11].

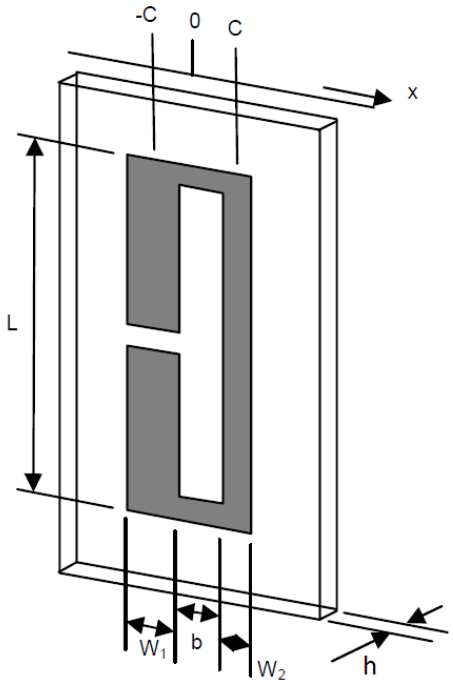

Figure 2- 4 ACPS folded dipole on a dielectric slab [23]

In practice, as seen from Figure 2- 4, the antenna will be realized on a dielectric substrate. According to Visser [10], employing the Lampe equations for this inhomogeneous case lead to relative errors in the transmission line impedance and therefore to large errors in the input impedance. Visser also shows that the impedance Z_{in}^{FD} for the antenna realized on a dielectric substrate as a function of frequency is greatly different from that of the same antenna in free space [10]. Two fundamental modes which are the transmission line mode and the antenna mode are affected by the presence of a dielectric substrate, thus Visser proposes in the following approach to the relative dielectric constant of the medium for transmission line mode [10]:

$$\varepsilon_r = \frac{\varepsilon_{rslab} + 1}{2} \tag{2.13}$$

In addition, Visser indicates that the presence of the dielectric substrate influence the transmission line mode in terms of the length L of the transmission line, thus L is increased and it is expanded to L_T where the correction for the width of the separation between parallel conductor strips is approximated by the following equation [25].

$$\tau = (0.06243 * b^{-1.038} + 3.071) * b \tag{2.14}$$

$$L_T = 2L + \tau * \lambda \tag{2.15}$$

For a large number of ACPS folded dipole antennas, having different dimensions, being positioned on dielectric substrates of different heights having different relative permittivities, the correction factors κ and χ are determined by Visser for the antenna mode of the ACPS folded dipole antenna in a uniform medium [10].

$$L_A = \kappa L \tag{2.16}$$

$$\rho_e{}' = \chi \rho_e \tag{2.17}$$

$$\kappa = \left(1 + \sqrt{h10^3}\log[\varepsilon_r]\right)^{0.45} \tag{2.18}$$

$$\chi = 1.90 \tag{2.19}$$

The accuracy offered by these correction factors for both transmission line and antenna mode is tested by comparing calculated and simulation results of the impedance $Z_{in}{}^{FD}$ for the antenna positioned on a dielectric substrate. Simulations are performed through a finite element method based commercially available EM simulator HFSS by Ansys. The center frequency of the design f_0 is chosen as 3 GHz, thus the wavelength λ_0 is 100 mm. At the frequency corresponding to resonant ($\frac{L}{\lambda} \approx 0.5$), the impedance of the transmission line mode is theoretically infinite and hence the antenna mode dominates the response. Thus, the starting values of L is set to be 50 mm. The other dimensions of the antenna are, with reference to Figure 2- 4, set to $W_1 = W_2 = b = 0.323$ mm. The asymmetric folded

dipole is positioned on a dielectric slab of thickness $h = 0.508$ mm and relative permittivity $\varepsilon_r = 2.94$. Also, the input impedance of the equivalent circularly cylindrical dipole mentioned above is obtained by applying the empirical double-polyfit equations for the King-Middleton second order solutions.

For the dimensions of the ACPS folded dipole, simulated and calculated input impedance of the ACPS folded dipole in terms of real and imaginary parts are shown in Figure 2- 5 through Figure 2- 9 as a function of frequency.

The input impedance in Figure 2- 5, Figure 2- 6 and Figure 2- 7 are calculated with the equations given above by using ε_r equal to 1, 2.94 and $\frac{2.94+1}{2}$, respectively. This means that the ACPS folded dipole is assumed to be present in a free space, a homogenous medium with relative permittivity equal to that of the dielectric substrate, and the dielectric substrate fills up a half-space.

The input impedance in Figure 2- 8 and Figure 2- 9 are calculated with the equations given above by using ε_r and the correction factors κ, χ and τ determined by Visser [10].

As seen from the figures, the impedance curves are in closer agreement with the simulation results apart from a shift in frequency. Since the gap between the parallel conductor strips of the ACPS folded dipole, b, is chosen as less then $0.01\lambda_0$, the values of the input impedance calculated as above are in accordance with the values acquired the simulations is obtained.

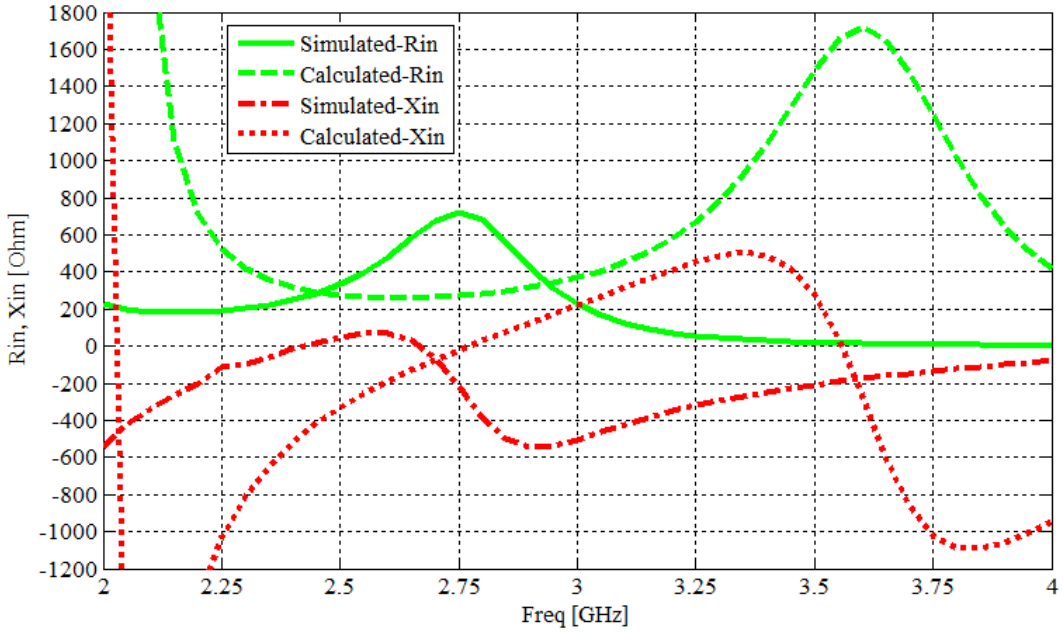

Figure 2- 5 Calculated and simulated input impedance versus frequency for initial dimensions of the ACPS folded dipole ($\varepsilon_r = 1$)

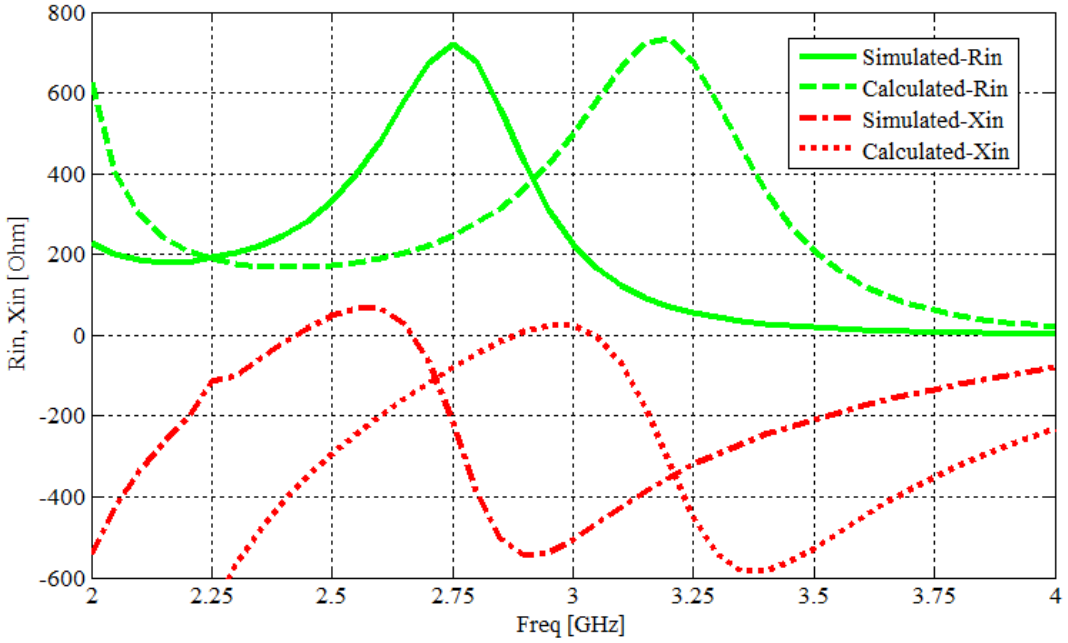

Figure 2- 6 Calculated and simulated input impedance versus frequency for initial dimensions of the ACPS folded dipole ($\varepsilon_r = 2.94$)

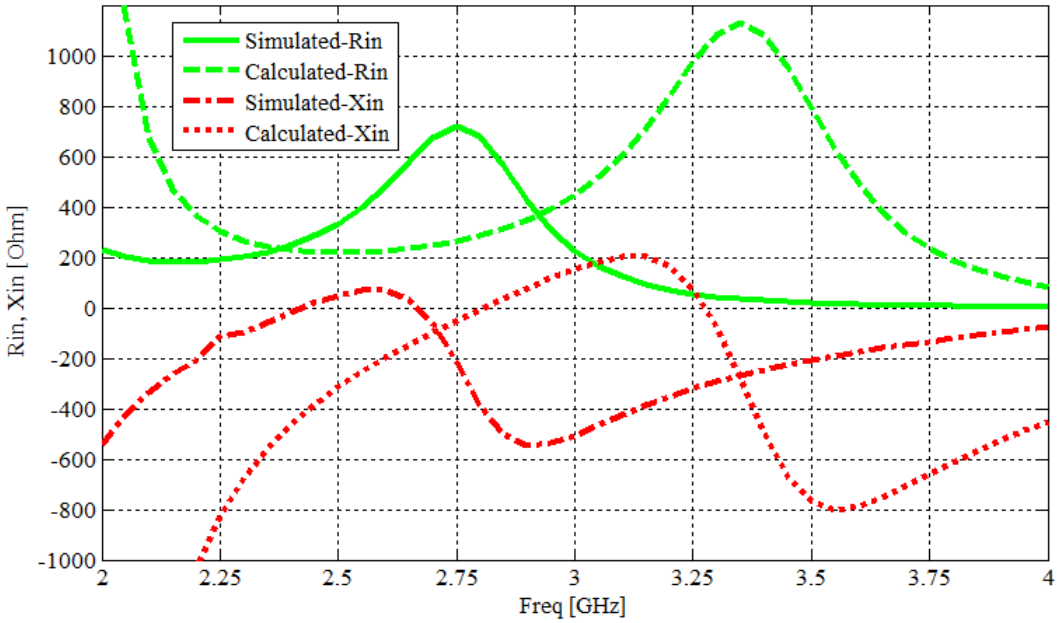

Figure 2- 7 Calculated and simulated input impedance versus frequency for initial dimensions of the ACPS folded dipole ($\varepsilon_r = (2.94 + 1)/2$)

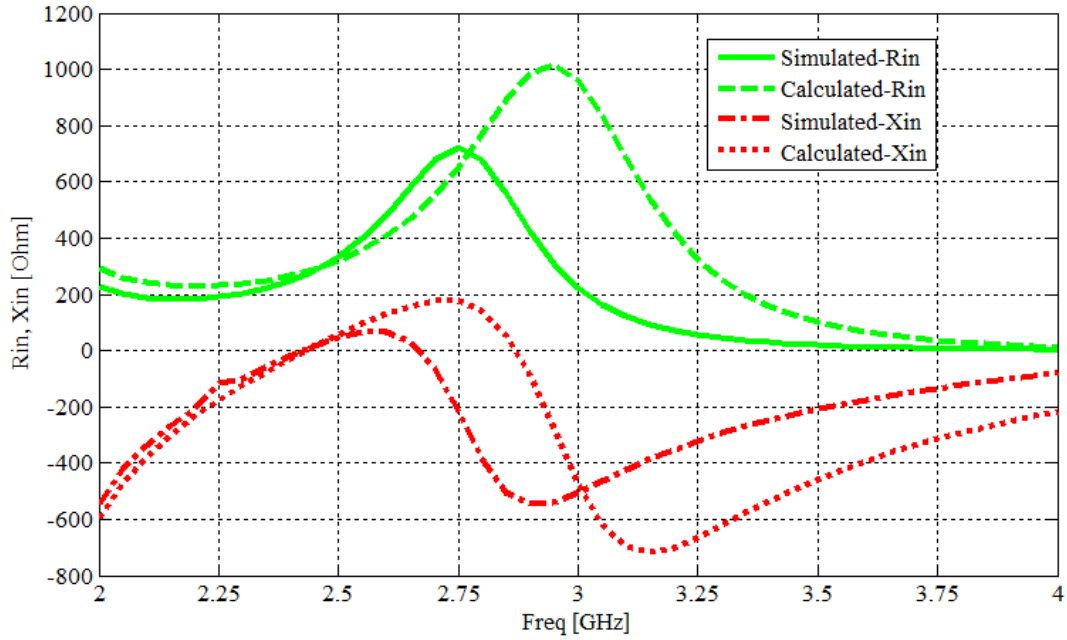

Figure 2- 8 Calculated and simulated input impedance versus frequency for initial dimensions of the ACPS folded dipole ($\varepsilon_r = 2.94$, κ and χ)

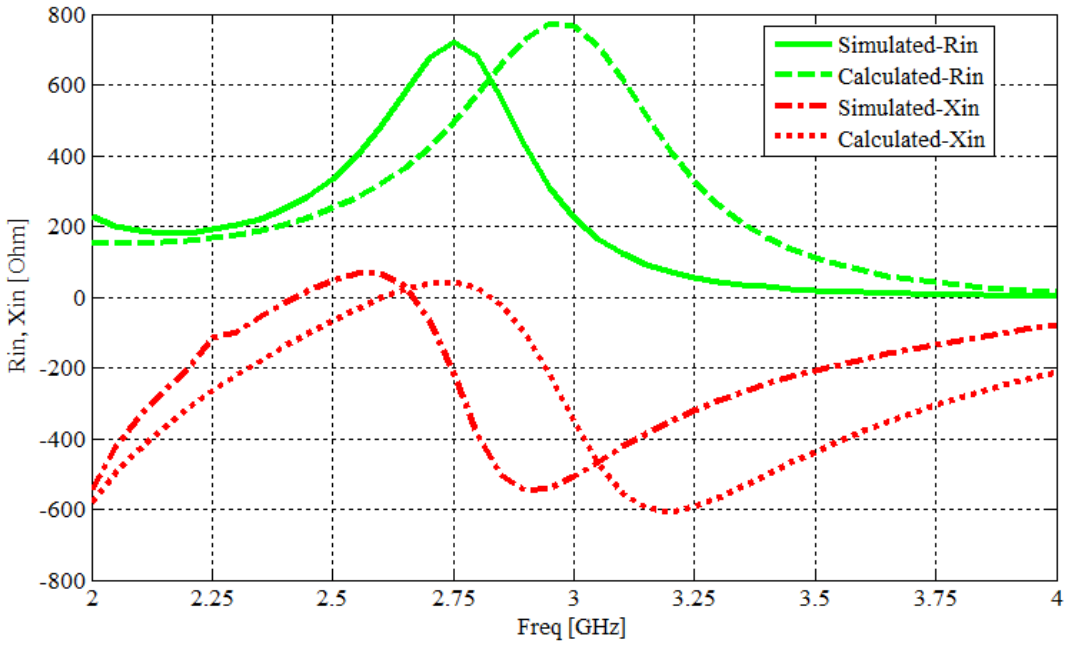

Figure 2- 9 Calculated and simulated input impedance versus frequency for initial dimensions of the ACPS folded dipole ($\varepsilon_r = (2.94 + 1)/2$, κ, χ and τ)

2.2 Analysis of Coplanar Stripline Structures

In some applications such as RF, microwave and millimeter-wave circuits, microstrip transmission line is widely used [26]. However, as a type of unbalanced transmission lines, the differential circuit cannot be directly fed by the microstrip transmission line. On the other hand coplanar stripline (CPS) which is a type of balanced transmission line can be utilized to feed the differential circuits.

The coplanar stripline (CPS) [27] was announced in the mid-1970's as a transmission line with the ability to form as an uniplanar structure [28]. The CPS is composed with two parallel conductor strips separated by a narrow gap on a dielectric substrate. Figure 2- 10 shows the basic configuration of the conventional CPS.

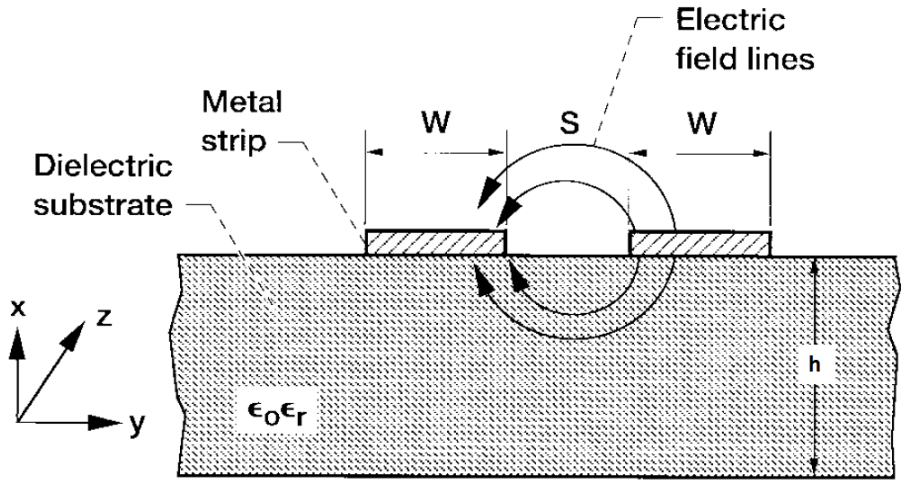

Figure 2- 10 Cross section of CPS [28]

As shown in Figure 2- 10, a thin dielectric substrate of thickness h and relative permittivity ε_r is used to support to the CPS and the electric field lines in a CPS from the strip conductors of width W reach across the slot of width S.

The advantage of CPS is that it is a type of balanced transmission line and both series as well as shunt mounting of devices is feasible [29]. Therefore the CPS transmission line is used with balanced mixers and printed dipole or folded dipole antenna for feeding network [29].

The main disadvantage of the CPS is that due to the lack of a ground plane, besides the fundamental CPS mode two other parasitic modes, namely the TE_0 and TM_0 can be generated by the CPS [29]. These undesired modes do not have a cutoff frequency and the electric fields created by these modes are mainly parallel and perpendicular to the dielectric-air interface, respectively, thus it powerfully couples to the TE_0 parasitic mode at discontinuities [29].

In determining the design equations using conformal mapping technique for the CPS transmission line, the medium supporting the CPS is supposed to be an isotropic homogenous dielectric of arbitrary thickness and relative permittivity [29].

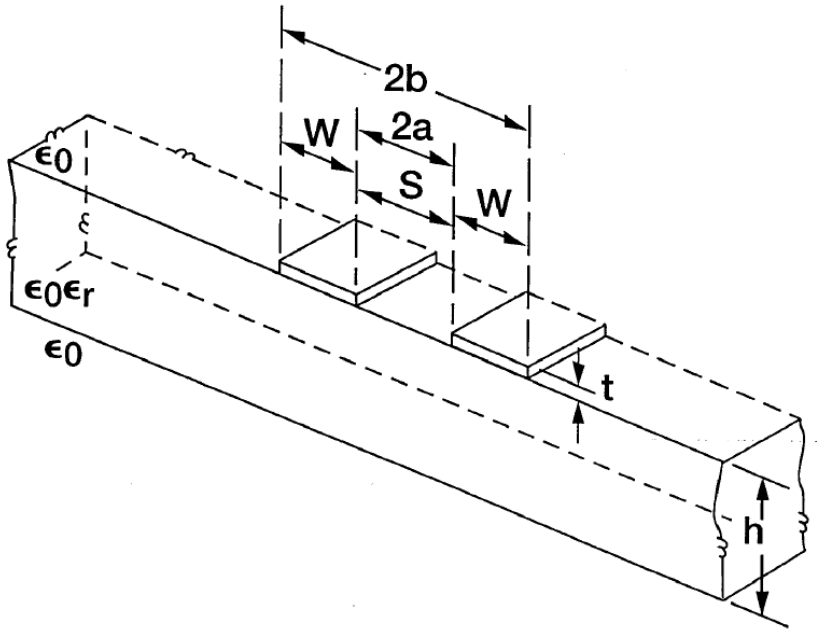

Figure 2- 11 Schematic of a CPS [29]

Figure 2- 11 shows the schematic of a CPS on a dielectric substrate with finite thickness. The effective dielectric constant $\varepsilon_{\mathrm{eff}}{}^{CPS}$ for this transmission line is as follows [29]:

$$\varepsilon_{\mathrm{eff}}{}^{CPS} = 1 + \frac{1}{2}(\varepsilon_{\mathrm{r}} - 1)\frac{K(\mathrm{k})}{K(\mathrm{k}')}\frac{K(\mathrm{k}'_{\mathrm{d}})}{K(\mathrm{k}_{\mathrm{d}})} \tag{2.20}$$

where K is the complete elliptical integral of the first kind stated before.

The arguments k and k′ are dependent on the dimensions of the CPS and are given by [29]:

$$\mathrm{k} = \sqrt{1 - \left(\frac{\mathrm{a}}{\mathrm{b}}\right)^2} \tag{2.21}$$

$$\mathrm{k}' = \sqrt{1 - \mathrm{k}^2} = \frac{\mathrm{a}}{\mathrm{b}} = \frac{\mathrm{S}}{\mathrm{S} + 2\mathrm{W}} \tag{2.22}$$

The arguments k_d and k'_d are expressed as follows [30]:

$$k_d = \sqrt{1 - \left[\frac{\sinh\left(\frac{\pi a}{2h_5}\right)}{\sinh\left(\frac{\pi b}{2h_5}\right)}\right]^2} \tag{2.23}$$

$$k'_d = \sqrt{1 - {k_d}^2} \tag{2.24}$$

where h is thickness of the dielectric substrate as indicated in Figure 2- 11.

The phase velocity and characteristic impedance are given as [29]:

$${\upsilon_{ph}}^{CPS} = \frac{c'}{\sqrt{{\varepsilon_{eff}}^{CPS}}} \tag{2.25}$$

$${Z_0}^{CPS} = \frac{120\pi}{\sqrt{{\varepsilon_{eff}}^{CPS}}} \frac{K(k')}{K(k)} \tag{2.26}$$

where c' is the velocity of light in free space.

CHAPTER 3

DESIGN OF AN ASYMMETRIC COPLANAR STRIP FOLDED DIPOLE ANTENNA

3.1 Design Requirements

In this section, the design requirements of the ACPS folded dipole antenna are explained.

The designed antenna will operate in 2.7 GHz - 3.3 GHz frequency band with return loss responses better than 10 dB. The designed antenna needs to provide a bandwidth of approximately 20% with a stable radiation pattern within this frequency range. Moreover, the designed antenna is required to be vertically polarized, and it will be the utilized in a linear array constructed in azimuth plane. Therefore, a 90^0 bend in the feed line of the ACPS folded dipole antenna (as shown in Figure 3- 1) is required to satisfy the polarization and array requirements. Moreover in order to decrease the spurious radiation that may occur due to the feed network, the feed network and antenna array are required to be on orthogonal planes as shown in Figure 3- 2. To satisfy this requirement a flexible dielectric substrate should be chosen. At the beginning of the design, dielectric substrate is chosen considering the relative permittivity, availability and flexibility of the material. As a result, Rogers Corporations material RT/Duroid 6002 substrate with copper metallization on both sides is selected [31]. Substrate thickness is 0.508 mm, copper thickness is 0.018 mm and the relative permittivity is 2.94.

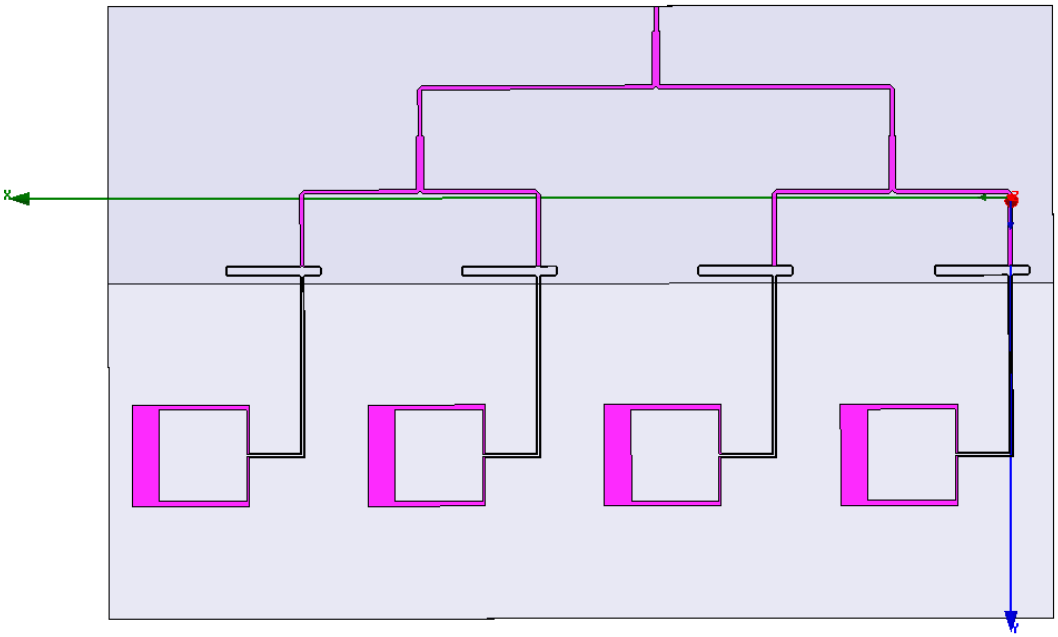

Figure 3- 1 Schematic of the ACPS folded dipole array proposed as configuration-II with feeding network

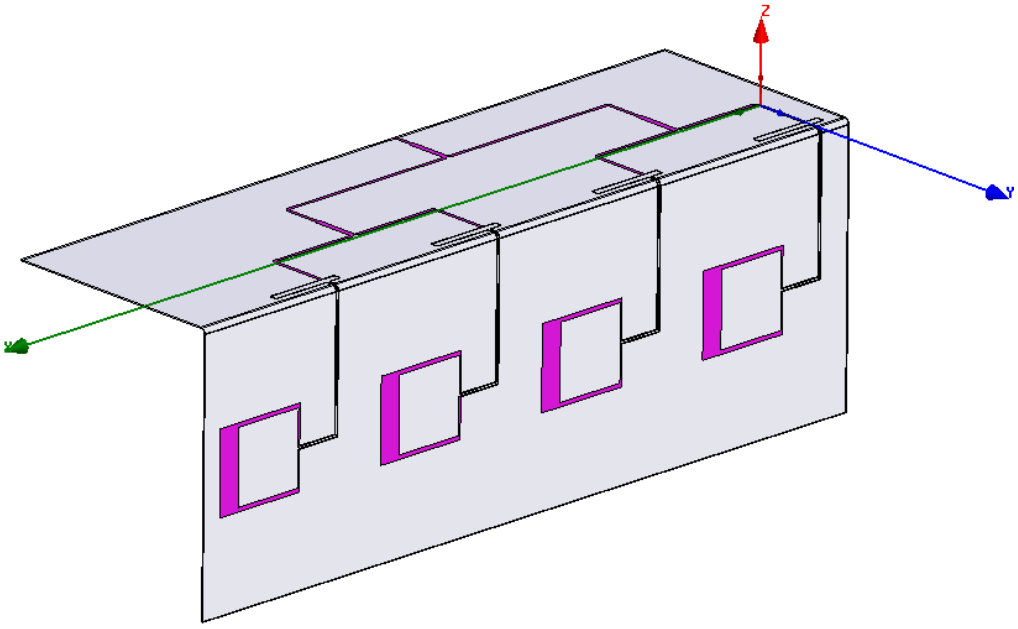

Figure 3- 2 Schematic of the ACPS folded dipole array proposed as configuration-III with feeding network

3.2 BALUN Design

The ACPS folded dipole antenna is naturally fed by a coplanar strip (CPS) which is a type of balanced transmission line. However microstrip transmission line which is a type of unbalanced transmission line is generally used for measuring and testing the performance of the antenna due to the suitable interface with the SMA connector. Thus, a balun which converts the unbalanced transmission line (microstrip line) to the balanced transmission line (CPS line) needs to be designed for connecting the antenna to the measurement systems. Coplanar stripline which is used to feed the printed dipole antennas and mounting solid state devices without via-hole is a well-recognized uniplanar transmission line [32]. Consequently, a balun consists of microstrip (MS) to coplanar strip (CPS) transition with good insertion loss and return loss is needed for feeding the ACPS folded dipole antenna. In this section of the chapter, the theoretical development and the design procedure for individual parts of the balun including MS to CPS transition are discussed.

Various methods for designing MS to CPS transitions have been improved as shown in Figure 3- 3. Via holes, radial stubs and artificial transmission lines have been utilized for MS to CPS transition in [33], [34] and [35], respectively. Due to the complicated ground alignment with the signal path or drilling via, these approaches have high fabrication cost [32]. In [36] and [37], an asymmetric T-junction which uses for signal dividing decreases the efficiency of the transition [32]. As compared with [37], another approach uses a symmetric T-junction improves the efficiency of the transition [37]. This approach employs a microstrip delay line in order to excite the odd mode of a coupled microstrip (CMS) line for transition between microstrip and CPS line [38], and the two delay line paths require to be 180 degree out of phase for excitation the odd mode of CMS line [32].

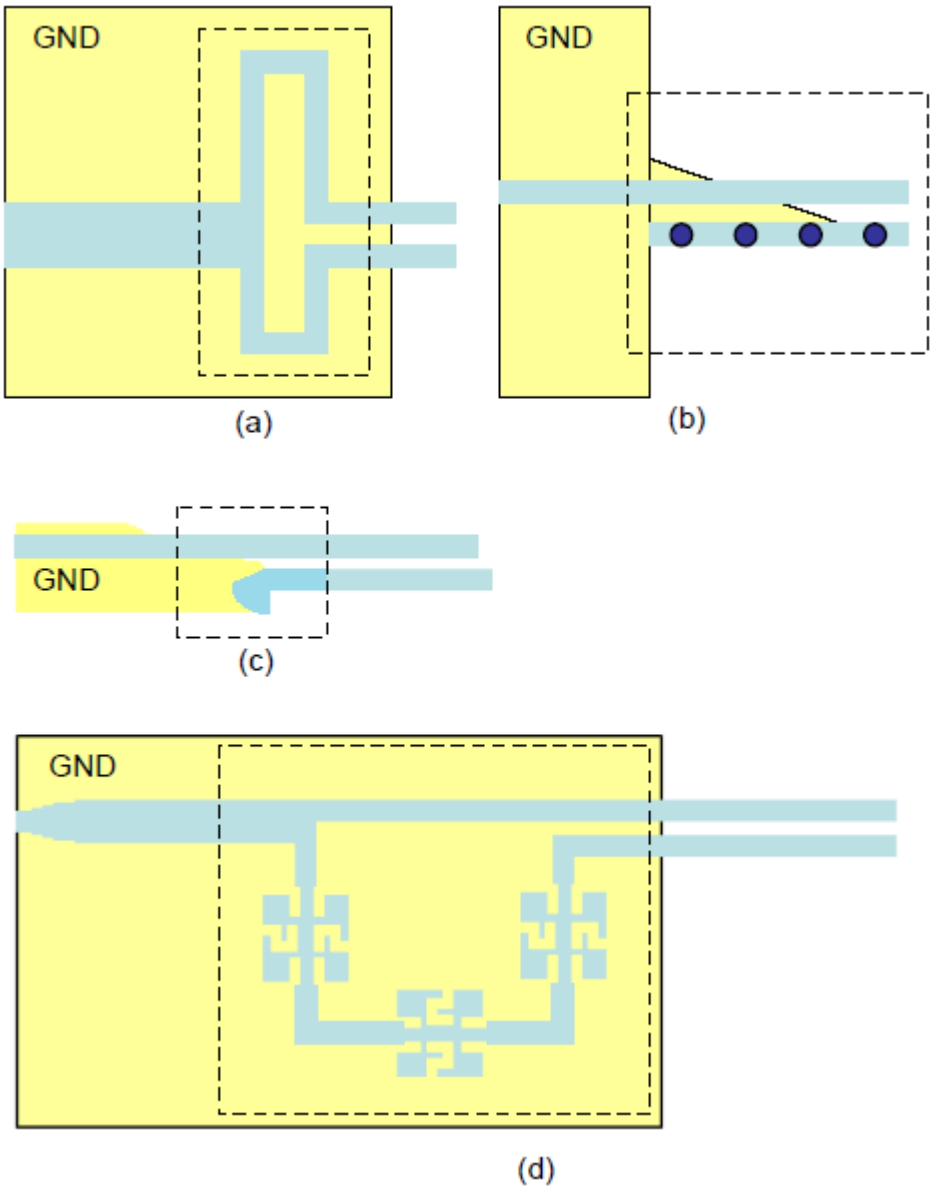

Figure 3- 3 Various methods for MS to CPS transitions: (a) square loop (b) with via holes (c) radial stubs (d) artificial transmission lines [32]

As shown in Figure 3- 4, configuration of the designed balun is inspired from the broadband uniplanar MS to CPS transition proposed by Qian and Itoh [38]. An advantage of this method is that it has a simpler design criterion due to the use of a symmetric T-junction in comparison with mentioned other transition structures.

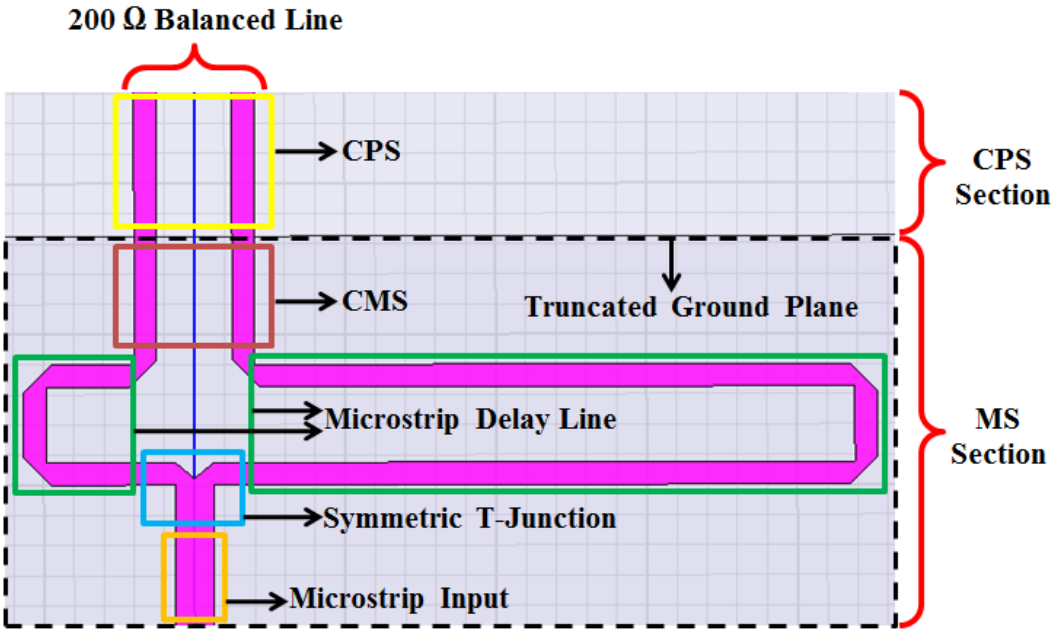

Figure 3- 4 Configuration of the designed balun

Figure 3- 5 shows the design parameters of the balun with CPS section. The input port1, where the SMA connector will be soldered, is the microstrip unbalanced transmission line which has the characteristic impedance 50 Ω.

The symmetric T-junction is a simple three port network used for power dividing/combining in any type of transmission medium. To obtain an equal power split from 50 Ω microstrip transmission line, impedance values seen from the input of each branch of the junction should be 100 Ω [39]. That leads to 200 Ω output impedance at symmetrical balanced output side [40]. This also explains why the input impedance Z_{in}^{FD} is chosen to be 200 Ω in most of the applications [40] [41]. The possibility of choosing a larger or smaller input impedance value for the ACPS folded dipole antenna is also explored. But different problems are observed for such choices. For example, when the Z_{in}^{FD} is equal to 300 Ω corresponding to a symmetric folded dipole, the width of the microstrip transmission lines consisting the coupled microstrip (CMS) for 150 Ω characteristic impedance are calculated to be too narrow resulting in manufacturing problems. On the other hand the impedance Z_{in}^{FD} can be chosen as 100 Ω which requires the characteristic

impedance of the microstrip transmission lines consist the coupled microstrip (CMS) to be 50 Ω for each. For that case an impedance transformer needs to be designed to transform the 25 Ω (50 Ω // 50 Ω) impedance to 50 Ω. Such an impedance transformer is designed and the simulation results imply that the impedance transformer leads to a narrower bandwidth for the overall structure. Hence the choice of 200 Ω for the impedance Z_{in}^{FD} is evaluated to be an optimum choice.

The balun is designed to provide 180 degrees of phase difference between the two microstrip delay line branches by setting their lengths so that $L_{dl2} - L_{dl1} \cong \frac{\lambda_g}{4}$, where L_{dl2} and L_{dl1} are half of the lengths of the two branches as seen in Figure 3-5, and λ_g is the guided wavelength in the microstrip line. At the coupled microstrip line (CMS) section, two modes are excited, the even and odd mode. The even mode is generated by the coupling between ground and a strip. The odd mode is produced by the coupling between adjacent strips. By creating 180 degree phase difference between the microstrip delay lines, the propagation mode in the coupled output will be predominantly the odd mode and can be transferred into the CPS mode easily after the ground plane is truncated [38]. Since the CPS supports the odd mode, the truncated ground plane behaves as an open end for the even mode exited in the coupled microstrip line, thus the undesired even mode exited is suppressed by the truncated ground plane.

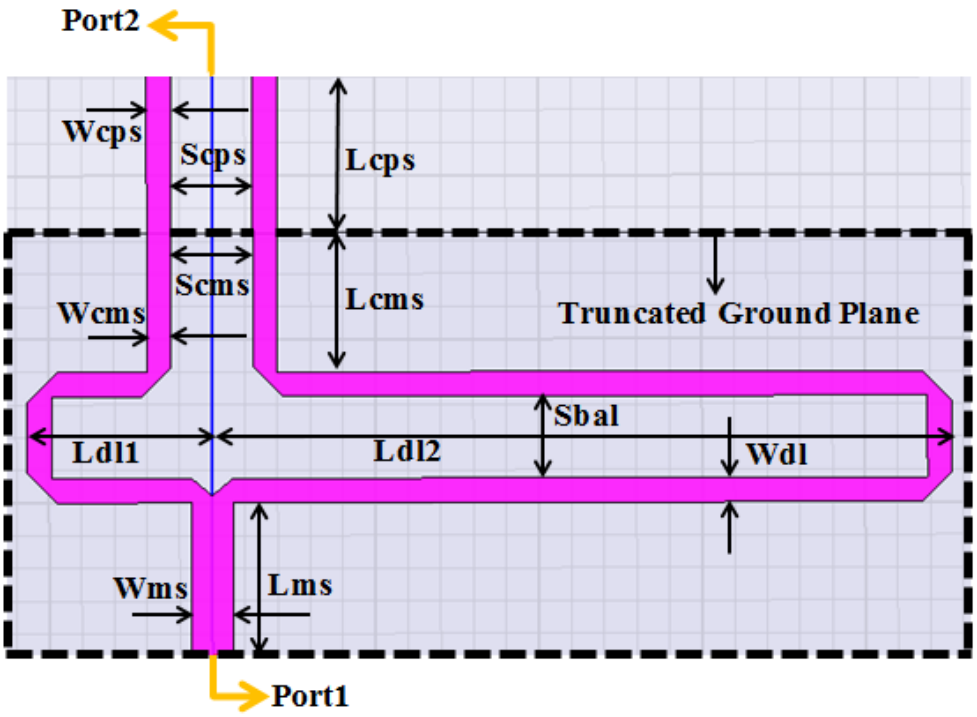

Figure 3- 5 Design parameters of the balun

Unfortunately, it is known that the phase characteristic (ψ versus frequency, f) of the microstrip line is linear. Thus, as shown in Figure 3- 6, the phase slope of microstrip A and microstrip B with respect to frequency are obviously different. Consequently, 180 degree phase difference can only be achieved at the center frequency f_0 [42]. As a result, a 180 degree phase delay is guaranteed only at the center frequency, and because of the phase shifting leg the odd mode conversion which is the fundamental characteristic of the MS to CPS transition is expected to work only for narrow frequency bandwidth [33].

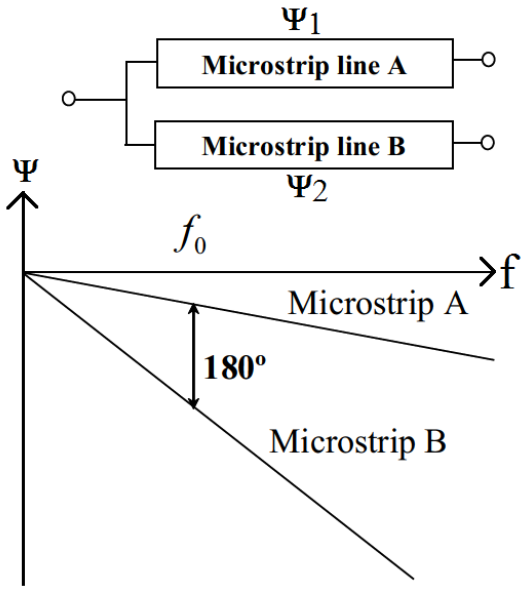

Figure 3- 6 Phase differential between two microstrip lines

Optimal miters have been used as in Figure 3- 7 in order to decrease undesired reflection and radiation losses result from the 90 degree microstrip bend and T-junction discontinuities [43] [44]. The distance between cut away point and outer corner of the un-mitered bend is $M = \frac{c}{\sqrt{2}} = 0.372\ \text{mm}$, and $L_a = W_{ms}$ and $H_a = 0.7 * W_{dl}$.

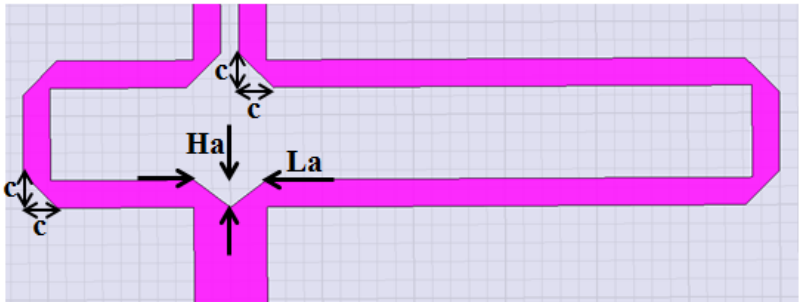

Figure 3- 7 Miter parameters of the microstrip bends and symmetric T-junction

The analytical formulation or specific software to calculate the microstrip line parameters for the chosen substrate show that the width of the 50 Ω line is 1.27 mm and 100 Ω line is 0.323 mm. Thus, W_{ms}, W_{dl} and W_{cms} are equal to 1.27 mm, 0.323 mm and 0.323 mm respectively.

In order to generate a 180 degree phase delay between the coupled lines at the center frequency, L_{dl1} and L_{dl2} are selected as $5.66\,\text{mm}$ and $22.66\,\text{mm}$ respectively. In addition, width of the coplanar stripline W_{cps} is considered to be equal to the width of coupled microstrip lines which is $0.323\,\text{mm}$. To obtain $200\,\Omega$ characteristic impedance of CPS on the chosen substrate, the gap between the coplanar striplines S_{cps} is calculated to be $0.5\,\text{mm}$. Besides, L_{cps} is initially set to $18.55\,\text{mm}$. Since the gap between the coupled microstrip lines, S_{cms}, is equal to the gap between the coplanar striplines, S_{cps}, is also set to $0.5\,\text{mm}$.

The commercial software package Ansys HFSS® is used for the analysis and design of the balun. The balun model without CPS section is shown in Figure 3- 8. Although there are many parameters that can be optimized, the most critical parameters are the gap between the meandered microstrip delay line S_{bal} and the length of the coupled microstrip lines L_{cms}. With reference to Figure 3- 5, the starting dimensions of these balun parameters are $S_{bal} = L_{cms} = 2.5\,\text{mm}$. The initial dimensions of the balun parameters are also summarized in Table 3- 1.

Table 3- 1 Initial dimensions of the balun parameters

Design Parameter	Value (mm)
L_{ms}	20,000
W_{ms}	1,270
M	0,372
L_a	1,270
H_a	0,226
W_{dl}	0,323
W_{cms}	0,323
L_{dl1}	5,660
L_{dl2}	22,660
S_{cms}	0,500
L_{cms}	2,500
S_{bal}	2,500
W_{cps}	0,323
S_{cps}	0,500
L_{cps}	18,550

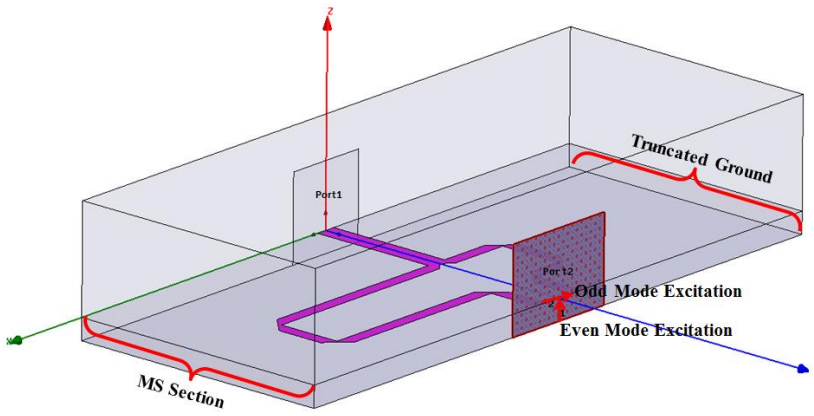

Figure 3- 8 Simulation model of the balun without CPS section in Ansys HFSS

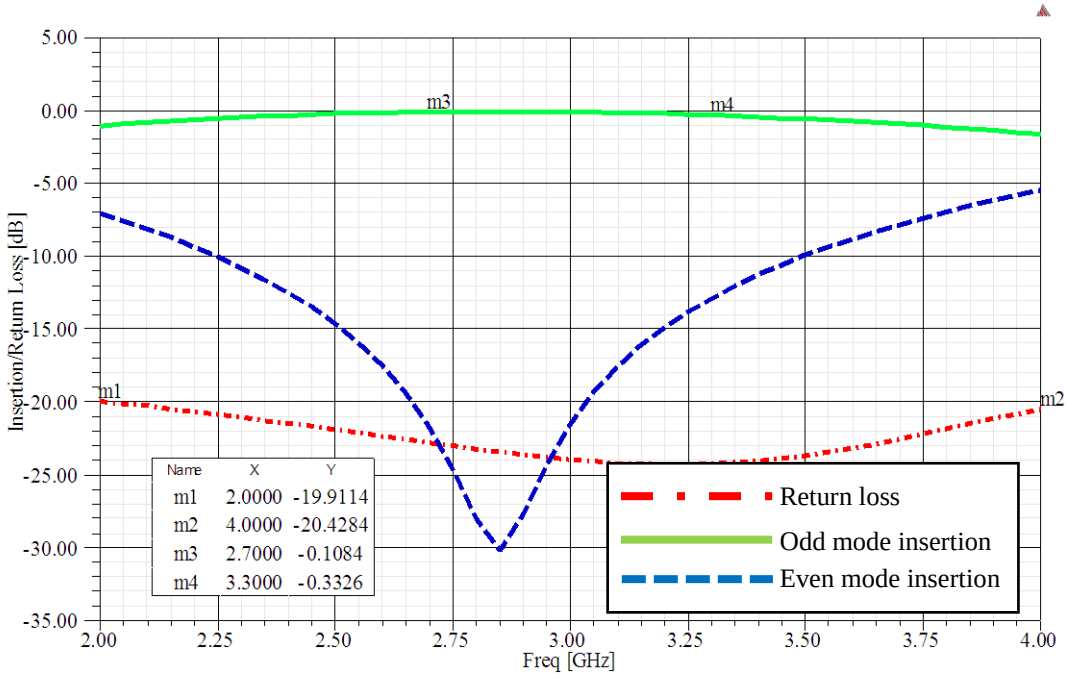

Figure 3- 9 Return and insertion loss of the balun without CPS section for initial dimensions

Figure 3- 9 gives the simulation result of S-parameters of the balun without CPS section for initial dimensions. It can be seen from the simulation result that the insertion loss of the coupled microstrip line's odd mode is fairly small (better than -1 dB) when the return loss is below -15 dB and return loss of the even mode is below -10 dB for almost entire S-band.

The balun model with CPS section is shown in Figure 3- 10.

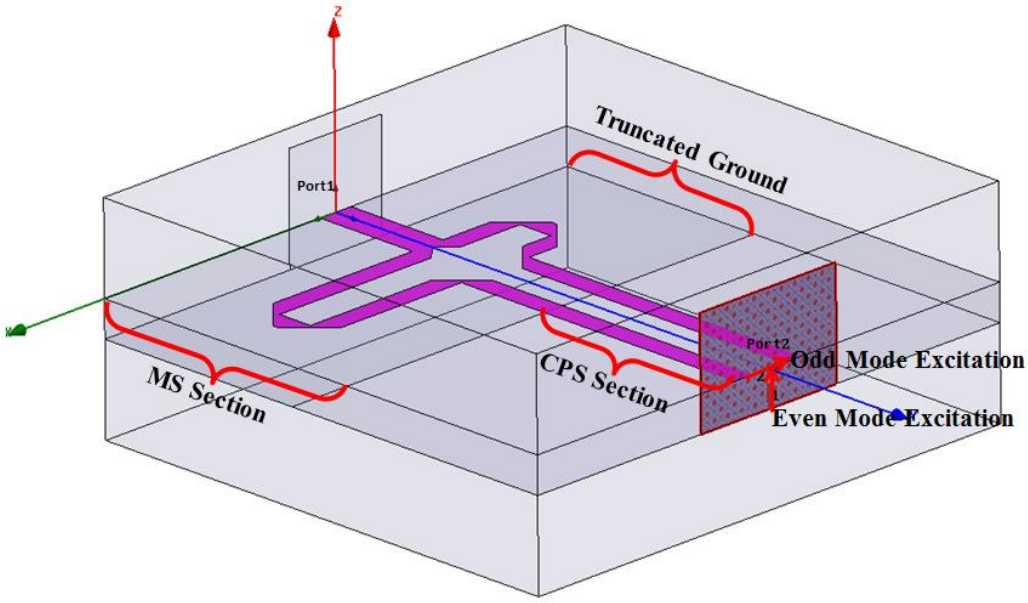

Figure 3- 10 Simulation model of the balun with CPS section in Ansys HFSS

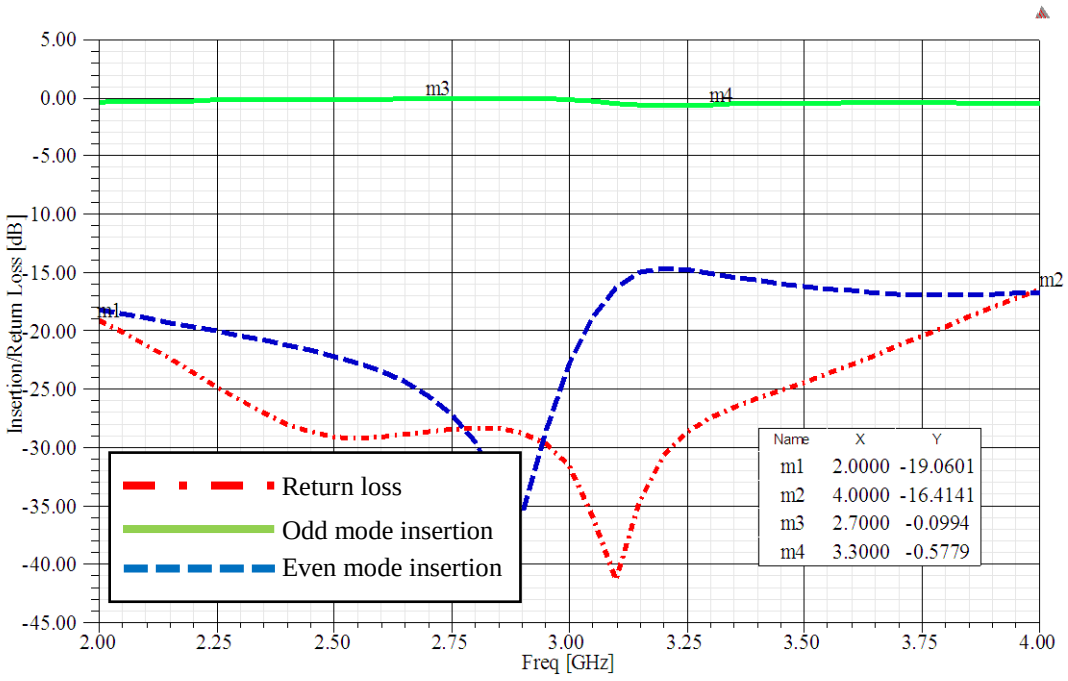

Figure 3- 11 Return and insertion loss of the balun with CPS section for initial dimensions

The simulation result of S-parameters of the balun with CPS section for initial dimensions displayed in Figure 3- 11 demonstrate a satisfactory input match to the microstrip section and maximum power transfer through the delay lines to the CPS lines.

Effects of key parameters which are the S_{bal}, L_{cms} and L_{cps} on performances of the designed balun are studied. During the parametric studies, one of the parameters is varied, and all other parameters are kept constant at their initial values.

S_{bal} affects the input impedance through mutual coupling in the balun. In addition, the input impedance is affected by L_{cms}. Fringing effects will occur if the meandered microstrip delay lines are brought too close to the truncated ground plane edge [45].

Figure 3- 12 presents the simulation results of S-parameters versus variation of S_{bal}, the gap between the meandered microstrip delay line. At the analysis, parameter value varies between 1 mm and 4 mm. From the figure it can be seen that the return loss response of the designed balun is enhanced as S_{bal} becomes larger.

Figure 3- 13 displays performance changes of the balun as the variation of L_{cms}, the length of the coupled microstrip lines. Parametrical study for this parameter is realized by changing the length value between 1 mm to 4 mm. As the figure shown, if the length is too small, the performances of the balun especially the return loss becomes worse.

Figure 3- 14 demonstrates the simulation results of S-parameters versus variation of L_{cps}, the length of the CPS. Operating frequency of the designed balun is increased when L_{cps} increases. As observed from the figures, the insertion loss of the designed balun is not significantly affected by the variations of this parameter.

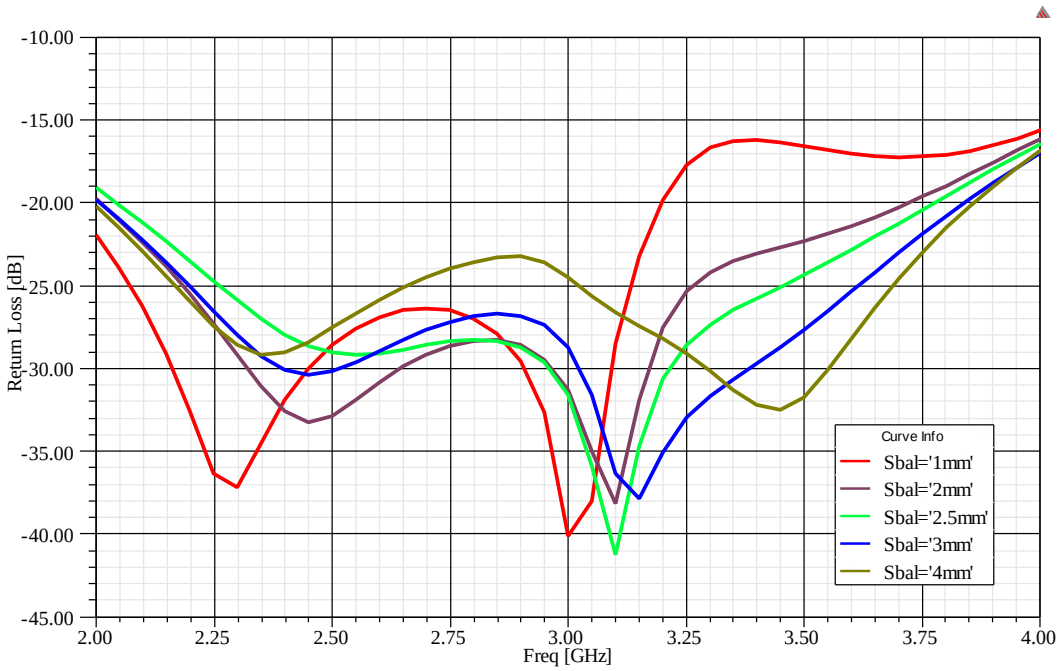

(a)

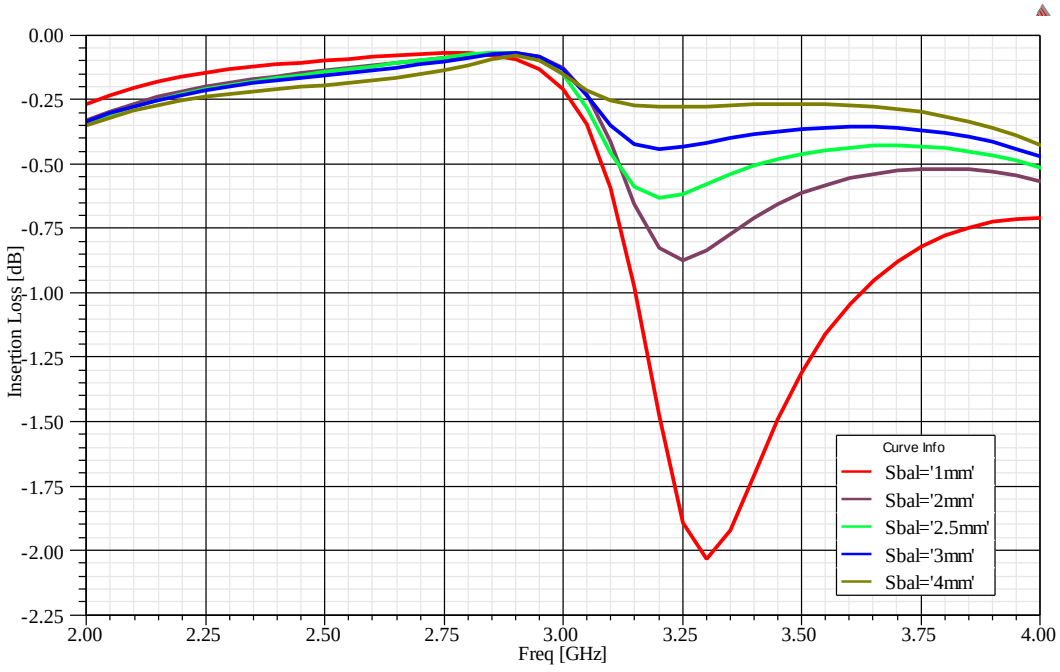

(b)

Figure 3- 12 Return and insertion loss of the designed balun versus S_{bal} : (a) S_{11} (b) S_{21}

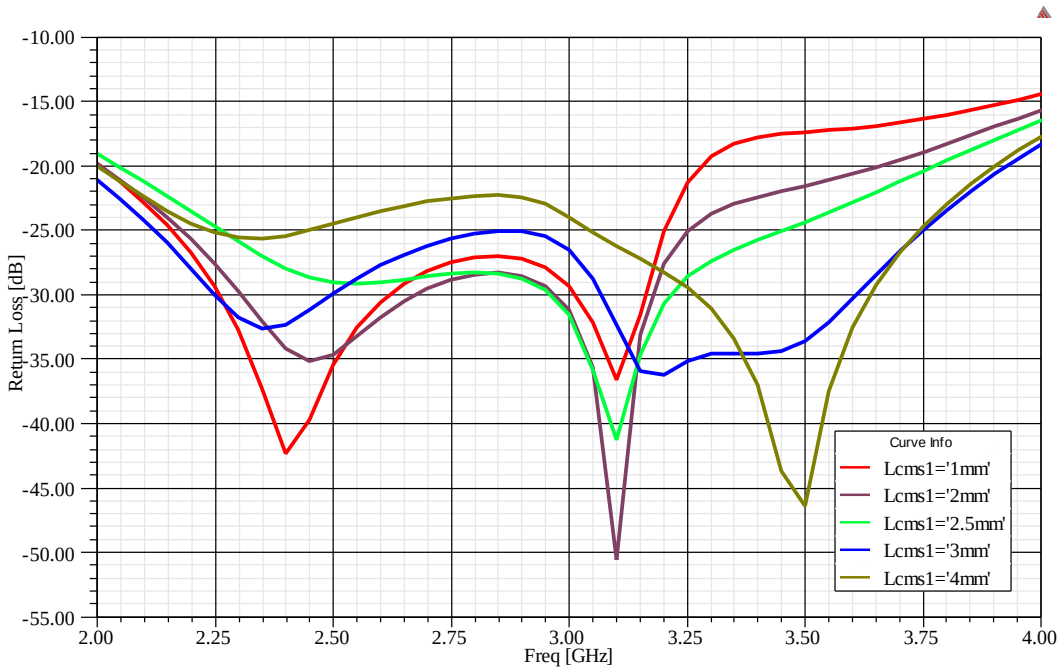

(a)

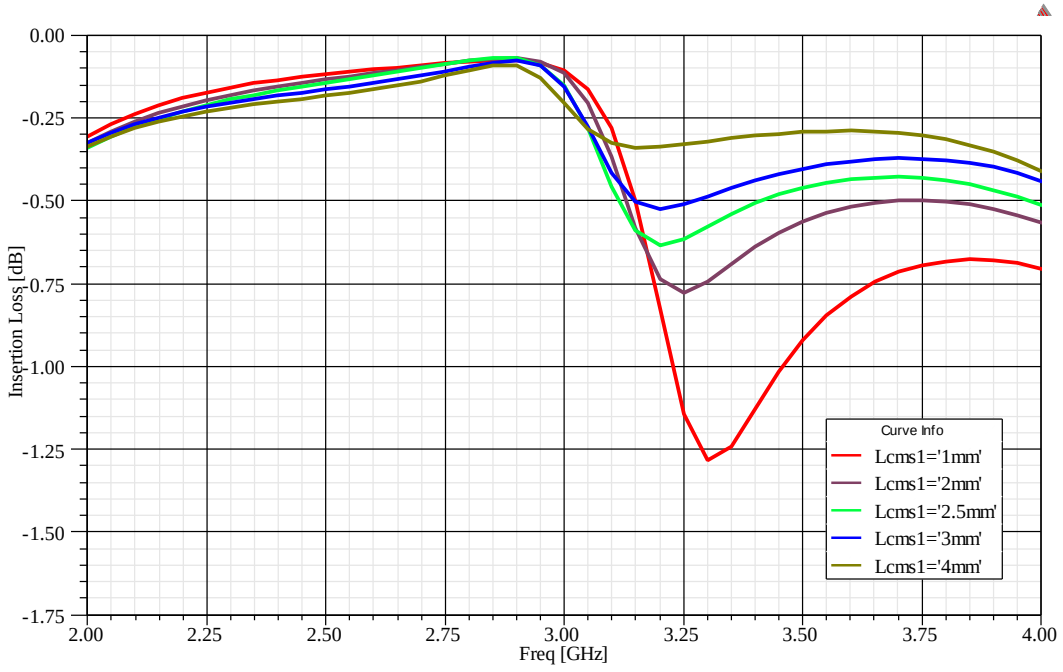

(b)

Figure 3- 13 Return and insertion loss of the designed balun versus L_{cms} : (a) S_{11} (b) S_{21}

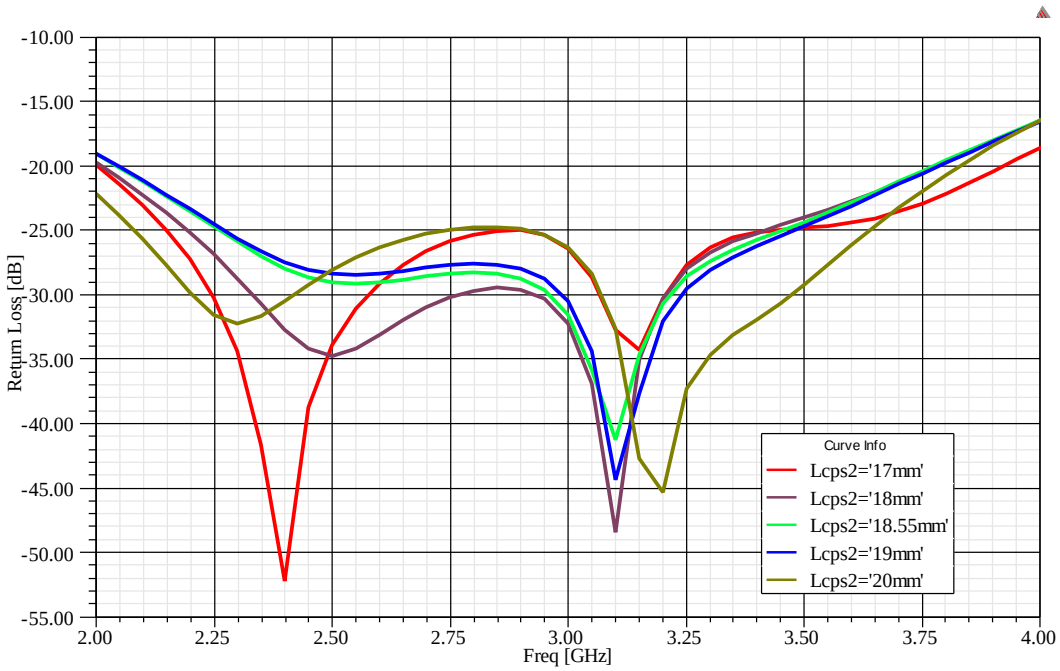

(a)

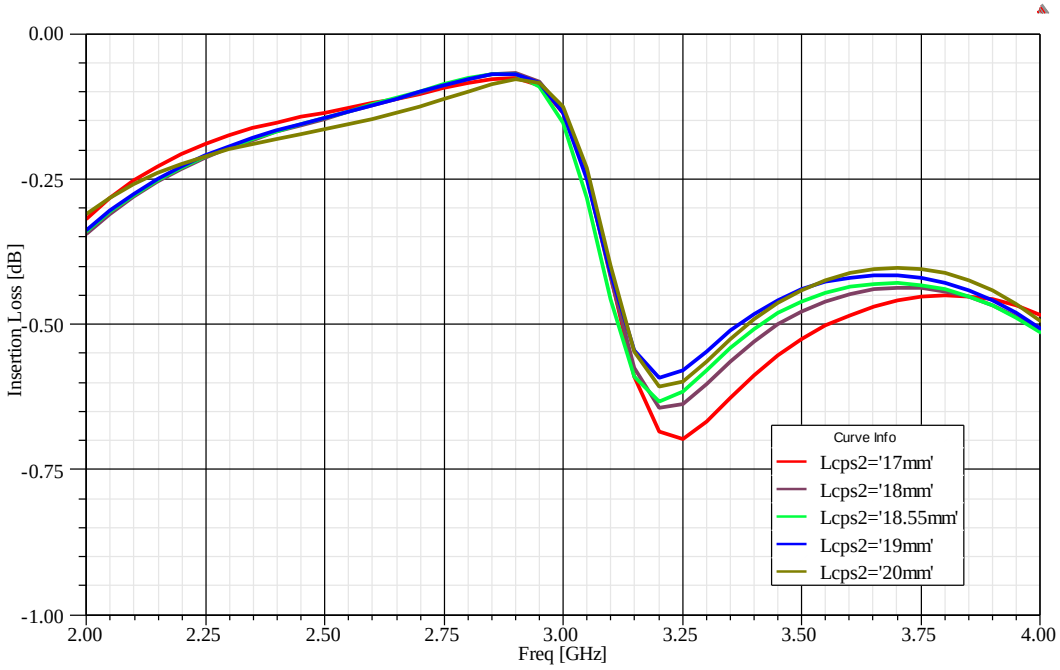

(b)

Figure 3- 14 Return and insertion loss of the designed balun versus L_{cps}: (a) S_{11} (b) S_{21}

Simulation results confirm that the designed balun has a low insertion loss less than 1 dB within the operating frequency range of 2.7 GHz - 3.3 GHz and the return loss is better than -10 dB within the entirely frequency range. The most important characteristics of baluns, which are the equal amplitudes and reversed phases between the two parallel strips of the CPS, have been accomplished. In addition, the designed balun has very compact structure and it is employed as a feeding section for the printed folded dipole antennas.

3.3 Improving the Design of Coplanar Stripline Section

The characteristic impedance of the CPS feeding line is considered to be equal to the input impedance of the antenna. This feeding system will be connected to an ACPS folded dipole antenna which has input impedance equal to 200 Ω. To obtain 200 Ω characteristic impedance of CPS on the chosen substrate, the gap between the coplanar striplines S_{cps} is calculated to be 0.5mm for the coplanar strip width equal to 0.323 mm by using the analytical formula in Section 2.2.

In order to investigate whether appropriate parameters are found for the CPS section or not, sweep analyses are performed using the lumped port excitation in Ansys HFSS®. The sweep parameters are namely, the coplanar striplines width W_{cps}, the gap between the coplanar striplines S_{cps} and lumped port impedance $\mathrm{LPort}_{\mathrm{resistance}}$.

As shown in Figure 3- 15, lumped port excitation is used for simulation of the CPS. The input and output ports are lumped port type with 50 Ω and 200 Ω impedances, respectively. Also integration line at the input port is drawn from microstrip line to truncated ground, and integration line at the output port is drawn from one stripline to the other stripline.

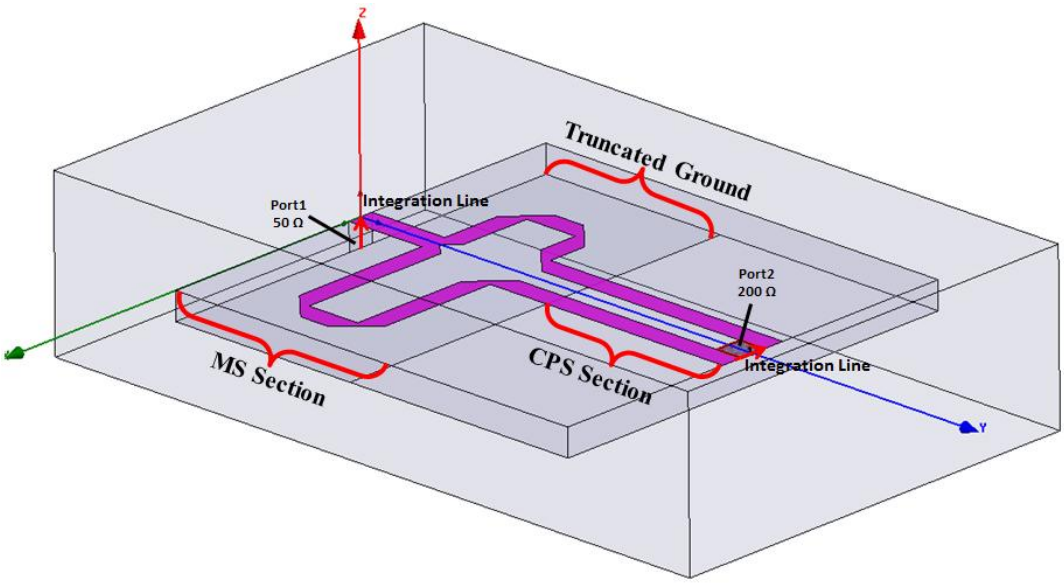

Figure 3- 15 Simulation model of the balun with lumped ports in Ansys HFSS®

Figure 3- 16 demonstrates performance changes of the balun with respect to the variation of $\mathrm{LPort_{resistance}}$. The parametrical analysis of this variable is done between 50 Ω and 250 Ω. As seen in the figure, the return loss and insertion loss of the balun are improved when $\mathrm{LPort_{resistance}}$ becomes 175 Ω. This indicates that S_{cps} and W_{cps} need to be optimized to obtain a better performance for $\mathrm{LPort_{resistance}} = 200\ \Omega$.

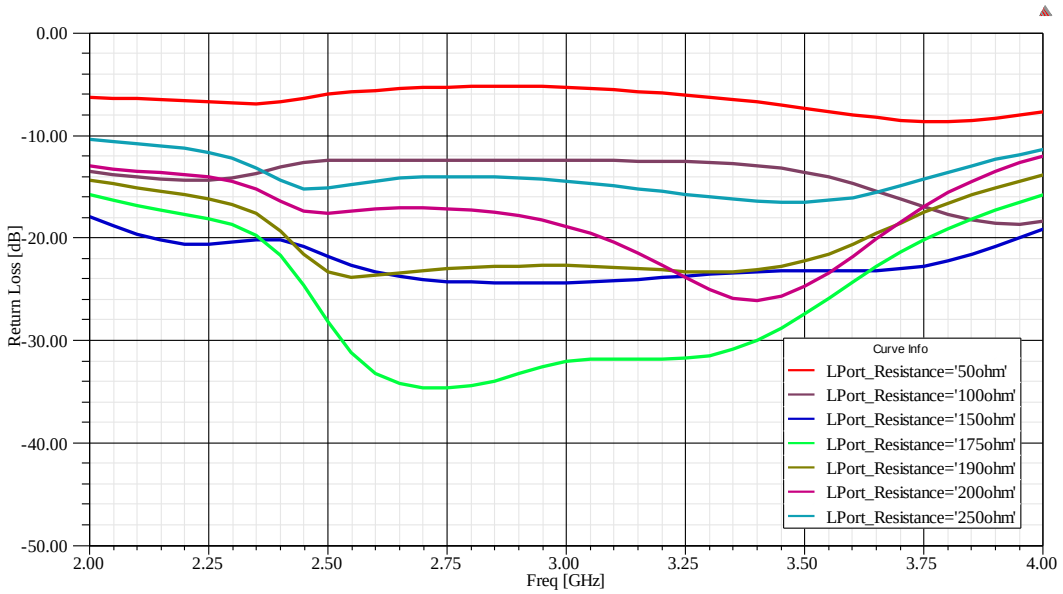

(a)

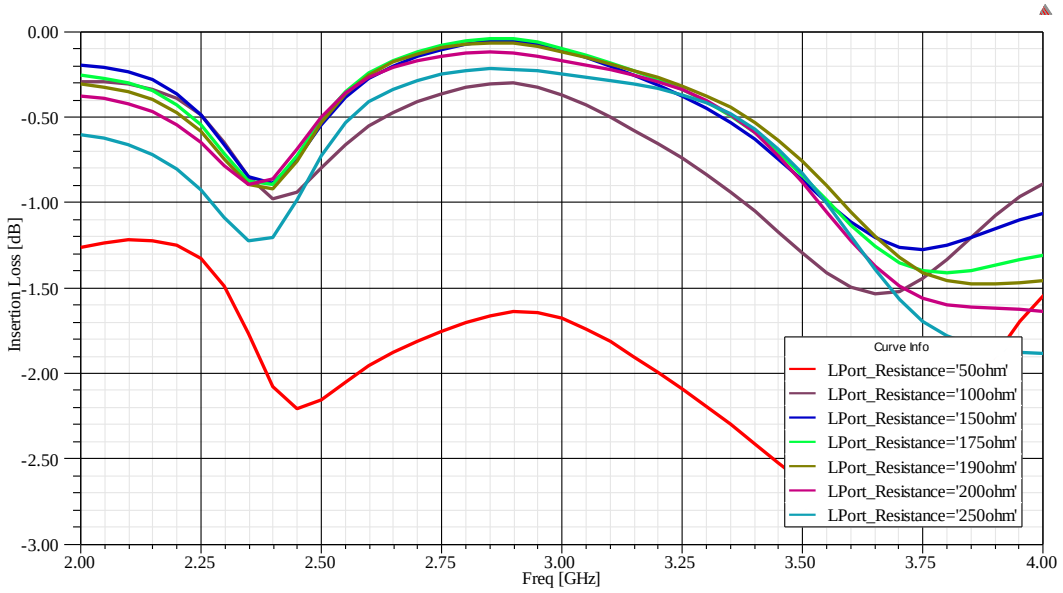

(b)

Figure 3- 16 Return and insertion loss of the designed balun versus $\mathrm{LPort_{resistance}}$ for $S_{cps} = 0.5$ mm and $W_{cps} = 0.323$ mm: (a) S_{11} (b) S_{21}

To achieve this, two parametric studies have been carried out. The parametrical analysis on the gap between the CPS is done between 0.45 mm and 0.7 mm with a step of 0.05 mm. Results of this analysis are given in Figure 3- 17. From the figure, it can be seen that the return loss of the designed balun is improved as S_{cps} becomes larger, and the best performance is achieved for S_{cps} equal 0.65 mm.

In the second analysis, the changing parameter is the CPS width W_{cps}, which is varied from 0.2 mm to 0.375 mm. As shown in Figure 3- 18, decreasing the strip width has an increasing effect on the characteristic impedance of the CPS and best performance is obtained for $W_{cps} = 0.2$ mm. Moreover, from the simulation results, it is also observed that variations of S_{cps} and W_{cps}do not affect the insertion loss of the balun significantly.

Due to the restrictions on manufacturing, instead of decreasing the strip width to 0.2 mm, increasing the gap to 0.65 mm is preferred to improve the performance.

As it may be observed from Figure 3- 19, a wider impedance match is obtained for 200 Ω load impedance, with $S_{cps} = 0.65$ mm and $W_{cps} = 0.323$ mm. The return loss is below -15 dB over 66% bandwidth and the maximum insertion loss is -1 dB from 2 GHz to 4 GHz. This broadband balun is suitable for the antennas operating within the frequency range of 2 GHz – 4 GHz.

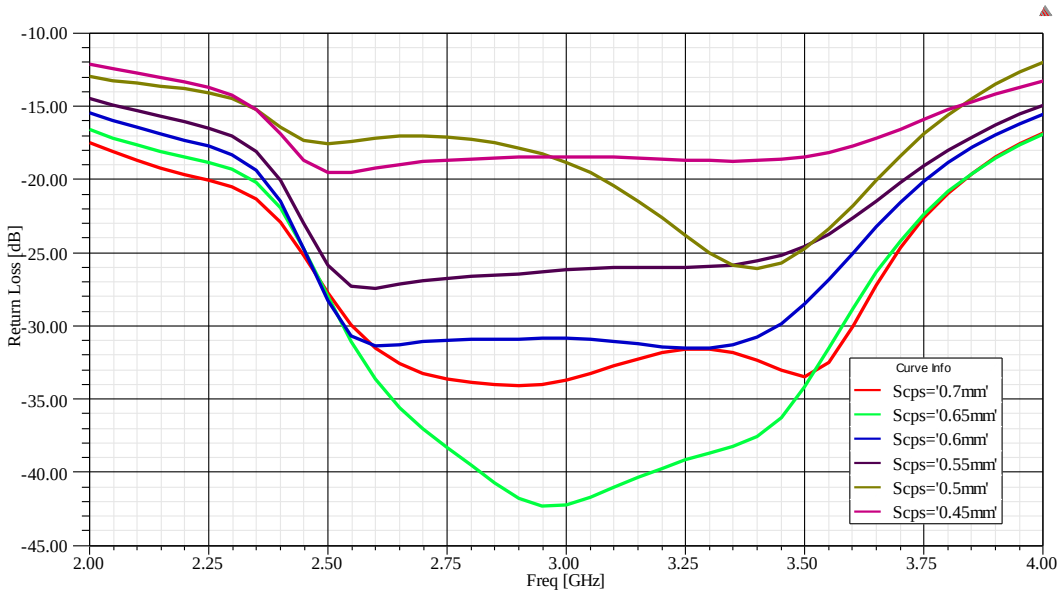

(a)

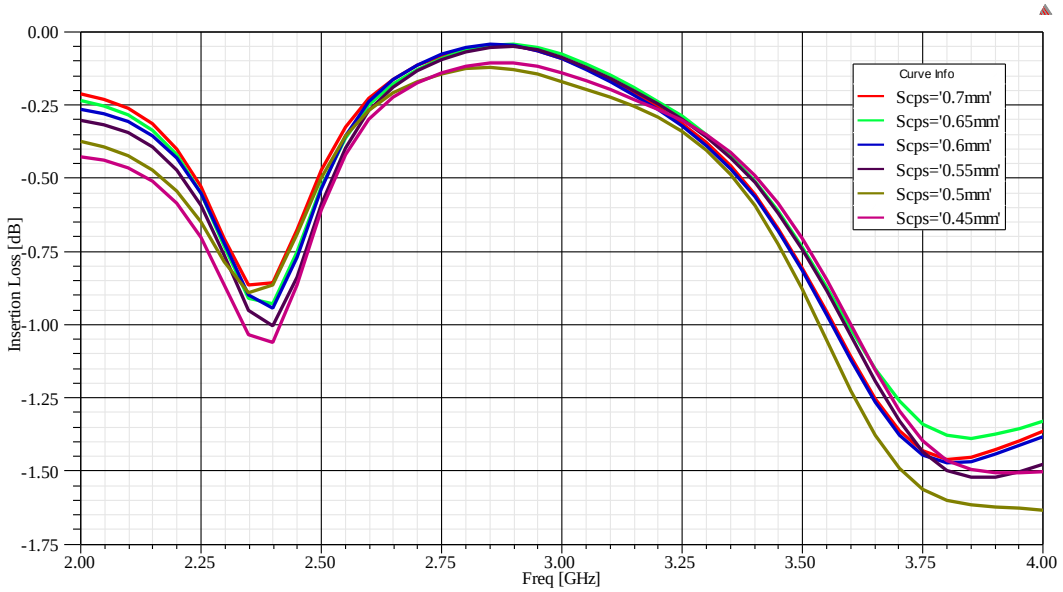

(b)

Figure 3- 17 Return and insertion loss of the designed balun versus S_{cps} : (a) S_{11} (b) S_{21}

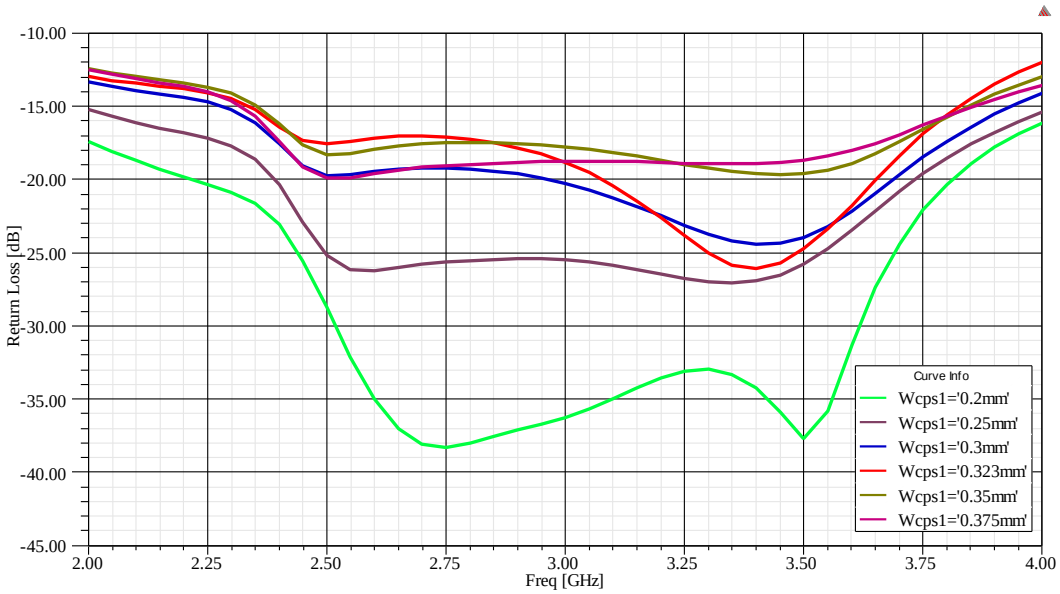

(a)

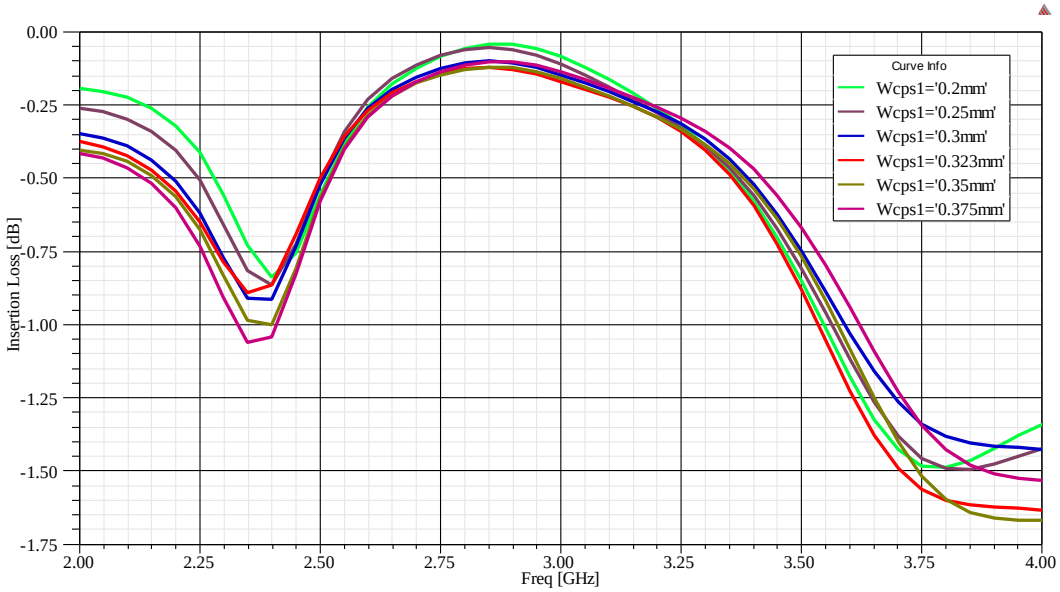

(b)

Figure 3- 18 Return and insertion loss of the designed balun versus W_{cps} : (a) S_{11} (b) S_{21}

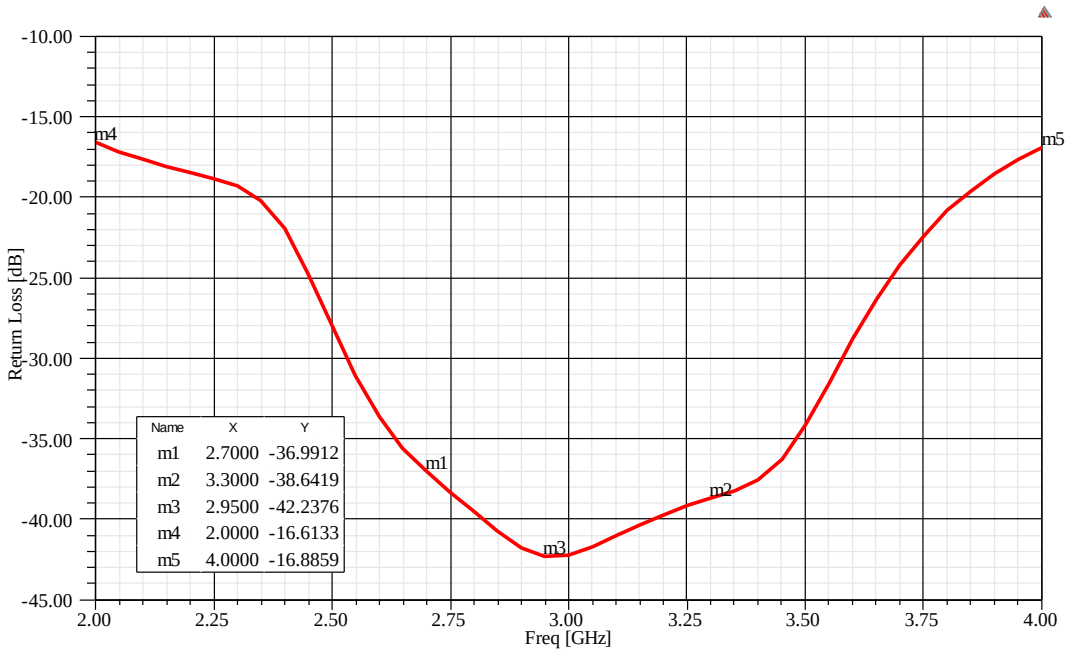

(a)

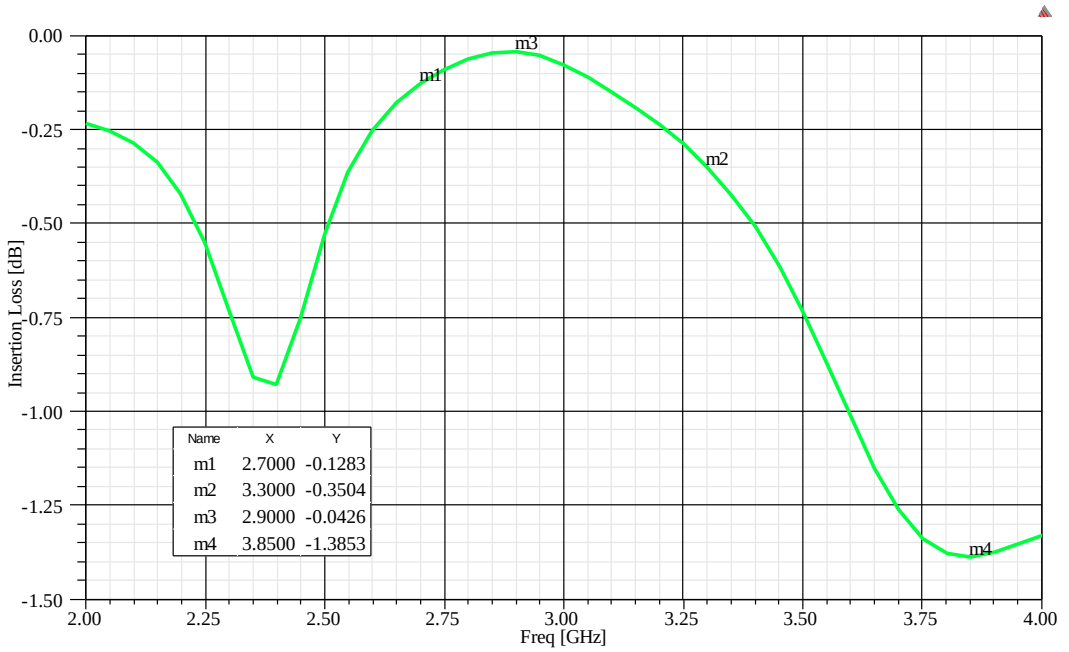

(b)

Figure 3- 19 Return and insertion loss of the designed balun for optimized dimensions: (a) S_{11} (b) S_{21}

3.4 Design of the ACPS Folded Dipole Antenna

It is the purpose of this section to find out the best choice of the physical parameters defined in Figure 3- 20, for the coplanar strip folded dipole antenna in order to achieve 20% bandwidth and an input impedance of 200 Ω.

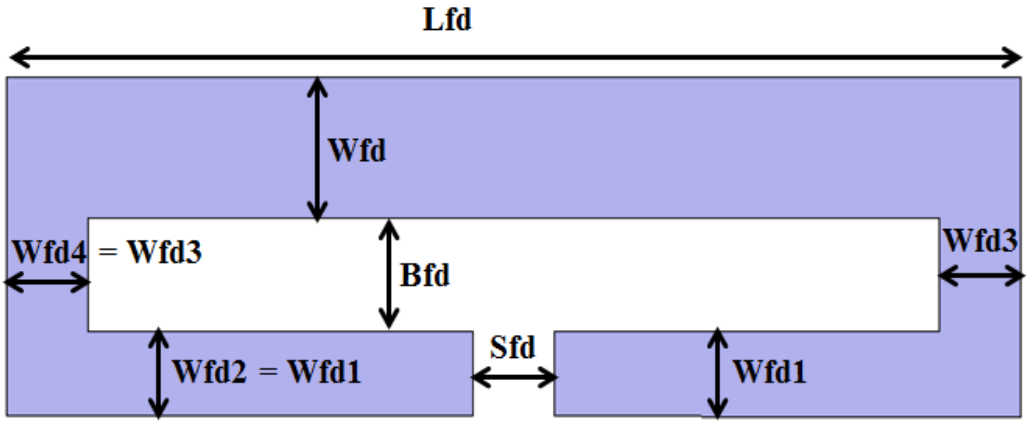

Figure 3- 20 ACPS folded dipole antenna structure

The antenna length is L_{fd}, and the widths of the upper and lower element are W_{fd} and W_{fd1}, respectively. The spacing between them is B_{fd}, and the width of the joining strips and spacing between the feed lines are W_{fd3} and S_{fd}, respectively. In the optimization, the smallest dimension of the design parameters is limited to 0.1 mm, because of the restrictions on the manufacturing process. The width W_{fd1} and the gap S_{fd} are selected to be equal to the width W_{cps} and the gap S_{cps}, respectively.

In order to investigate the effects of physical dimensions on the Z_{in}^{FD}, parametric analyses are performed using the lumped port excitation in Ansys HFSS®. The following parameters of an ACPS folded dipole antenna are crucial in the optimization of the impedance Z_{in}^{FD}: L_{fd}, W_{fd}, W_{fd1}, W_{fd3}, B_{fd} and S_{fd}. These parameters are analyzed in sequence, with the particular effect on the impedance Z_{in}^{FD}.

As shown in Figure 3- 21, input port of the ACPS folded dipole is modeled with a differential port type with 200 Ω impedance.

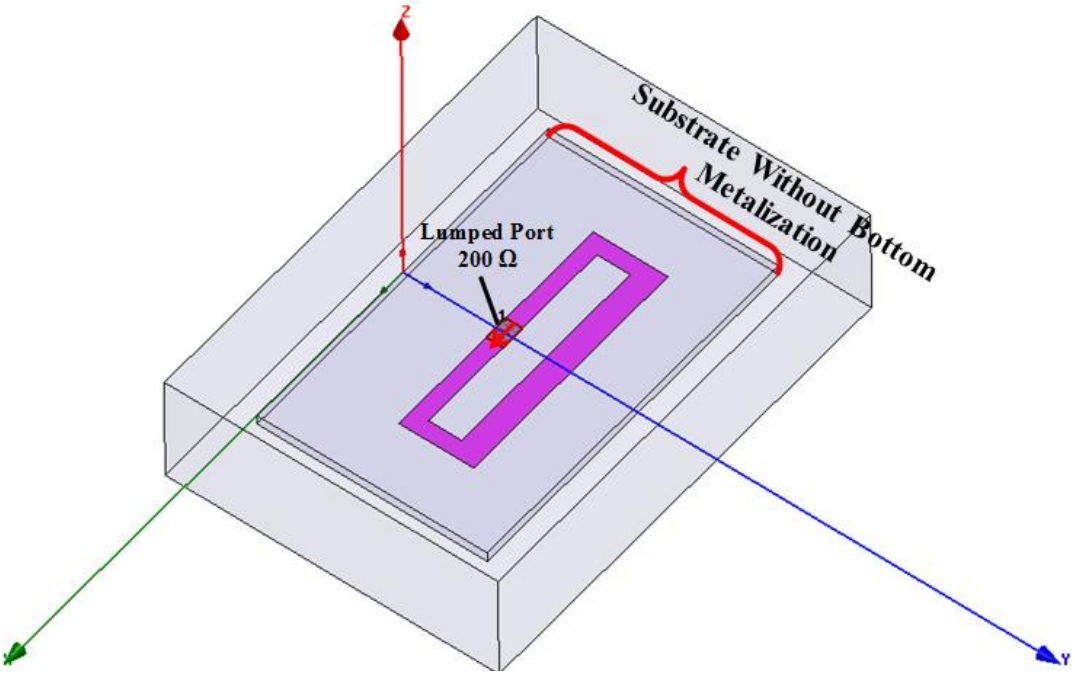

Figure 3- 21 Simulation model of the ACPS folded dipole with lumped port in Ansys HFSS®

The variation of the ACPS folded dipole input impedance with respect to the antenna length changes is investigated. Parametric analysis about the input impedance of antenna is done by varying the length of the ACPS folded dipole from 45 mm to 60 mm and the results are shown in Figure 3- 22. It is seen from the figure that the impedance Z_{in}^{FD} is close to 300 Ω around the resonant frequency and this resonant frequency of ACPS folded dipole antenna decreases when the length of the antenna increases.

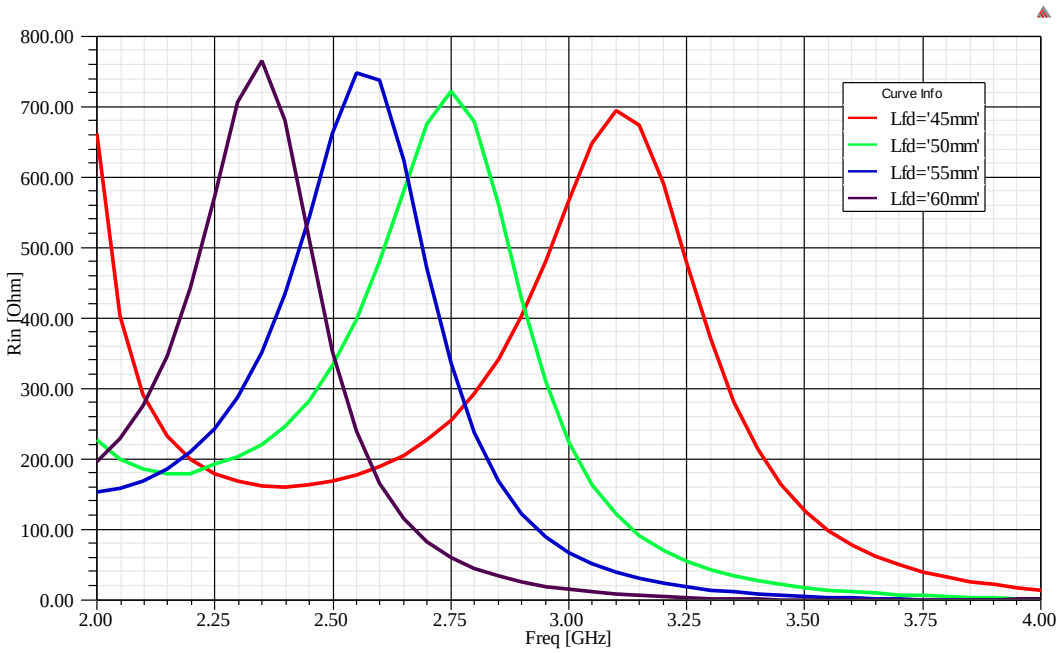

(a)

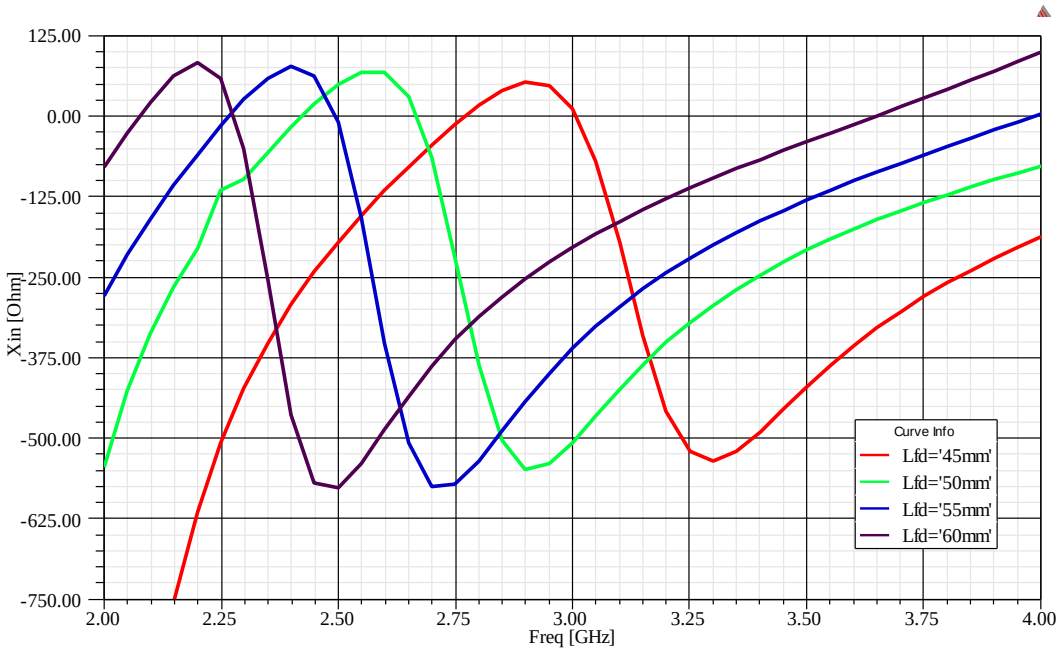

(b)

Figure 3- 22 Z_{in}^{FD} in terms of real and imaginary parts versus L_{fd} : (a) R_{in} (b) X_{in}

Effects of the spacing between the upper and lower antenna element, B_{fd}, are performed by changing this parameter between 0.1 mm and 8 mm. Figure 3- 23 shows the result of this analysis. It is concluded that B_{fd} is not an effective parameter to adjust the input impedance level of the antenna.

Effects of the width of the upper and lower conductors on input impedance of the antenna are studied. Analyses are realized by changing the W_{fd} and W_{fd1} values parametrically between 0.1 mm and 1 mm. Results of these analyses are shown in Figure 3- 24 for varying W_{fd} ($W_{fd1} = 0.323$ mm) and Figure 3- 25 for varying W_{fd1}($W_{fd} = 0.323$ mm). It is observed that both W_{fd} and W_{fd1} exhibit a negligible effect on the resonance frequency of the antenna but they significantly control the resistive part of the input impedance as expected from the theory presented in Chapter 2.

The variation of the ACPS folded dipole input impedance in terms of the joining strips width and spacing between the feed lines changes is analyzed. Analyses to explore the effects of the W_{fd3} and S_{fd} are carried out by changing the parameter values from 0.1 mm to 1 mm and 0.1 mm to 1.25 mm, respectively. From the simulation results, Figure 3- 26 and Figure 3- 27, it is observed that these parameters do not affect the input impedance significantly, but W_{fd3} and S_{fd} are used to fine tune.

Effect of the thickness of the antenna substrate on the antenna input impedance is also studied. Analysis on the input impedance is realized by changing the value parametrically between 0.254 mm and 1.016 mm. The effect of the parametric analysis on the real and imaginary parts of the input impedance is observed in Figure 3- 28. As the thickness of the substrate decreases the effective dielectric constant decreases, thus the guided wavelength and the resonance frequency increases.

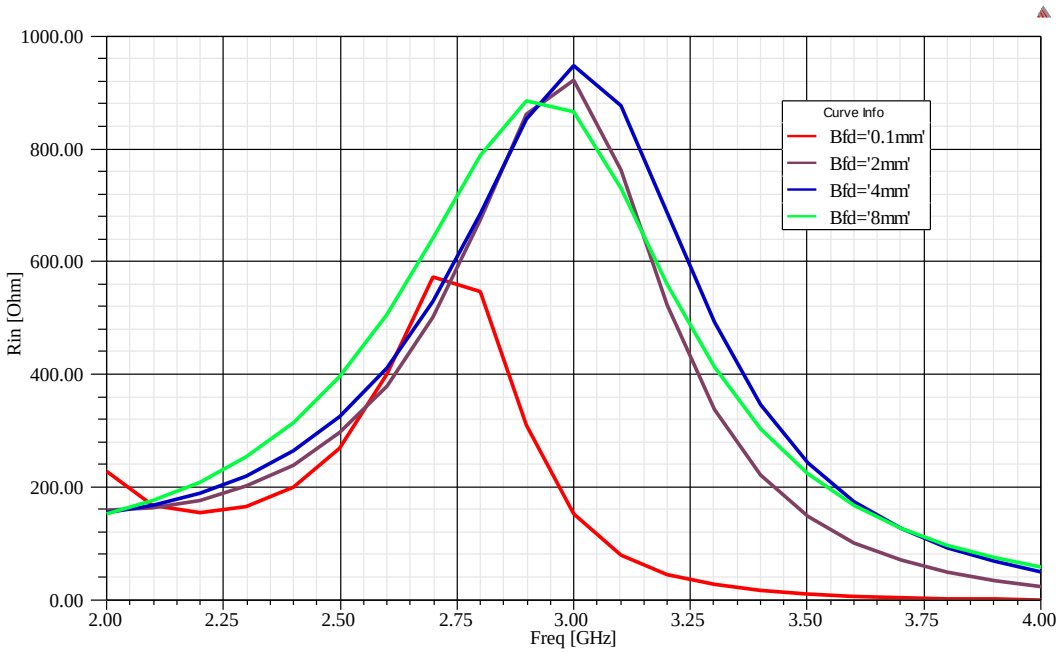

(a)

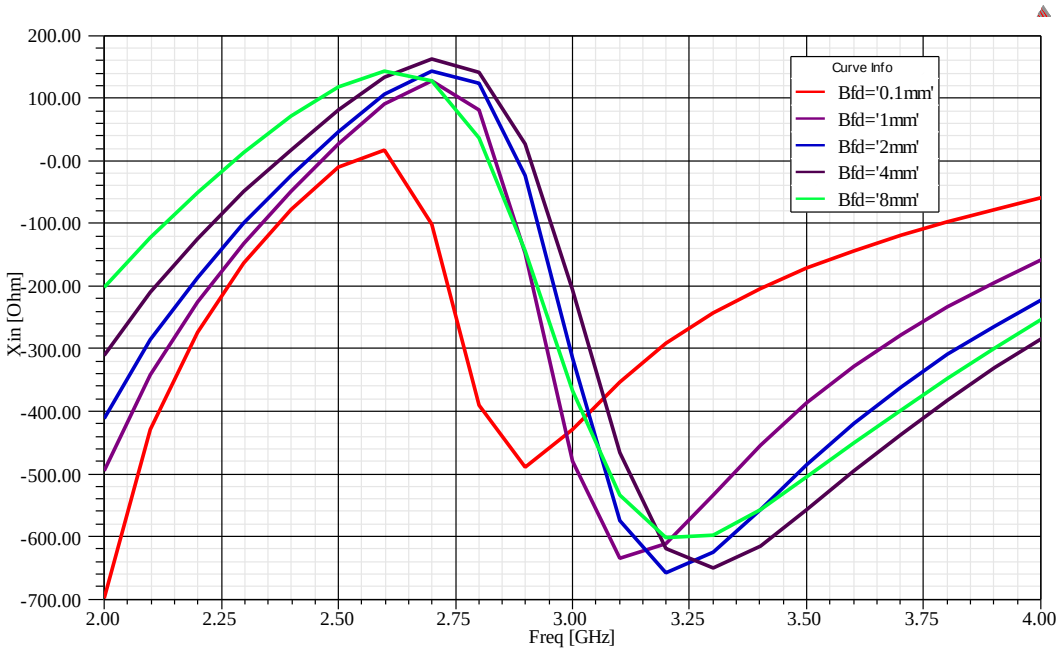

(b)

Figure 3- 23 Z_{in}^{FD} in terms of real and imaginary parts versus B_{fd} : (a) R_{in} (b) X_{in}

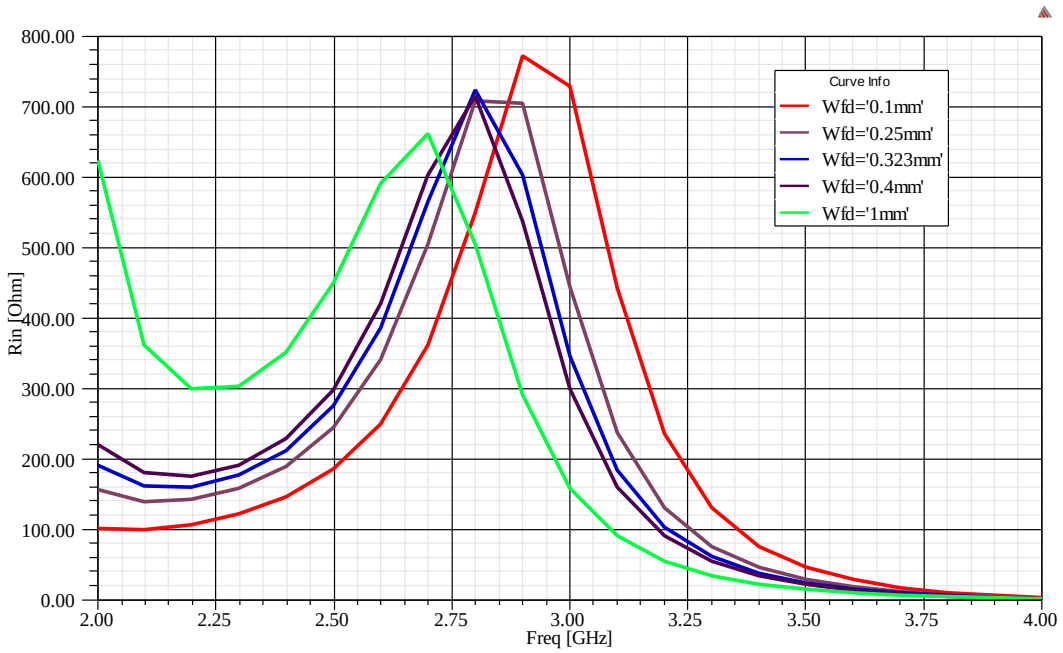

(a)

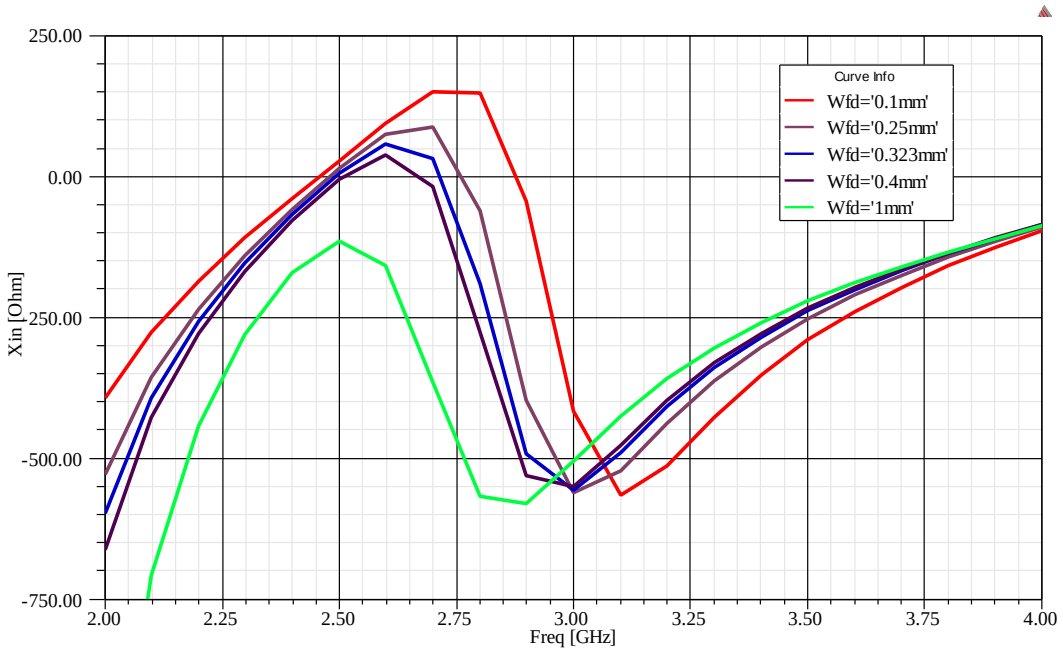

(b)

Figure 3- 24 Z_{in}^{FD} in terms of real and imaginary parts versus W_{fd} : (a) R_{in} (b) X_{in}

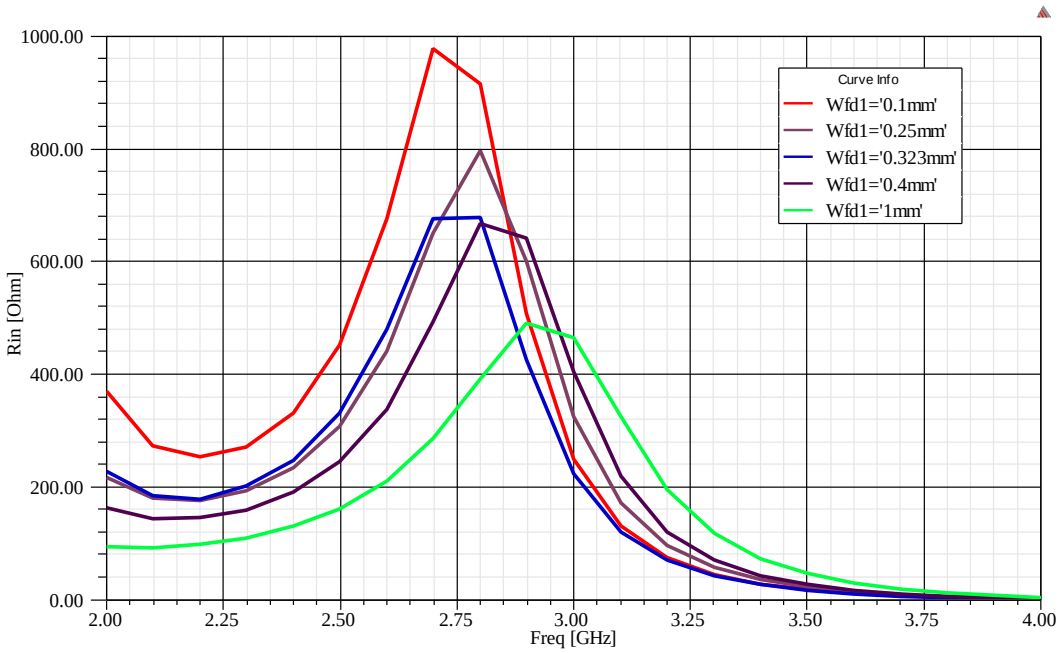

(a)

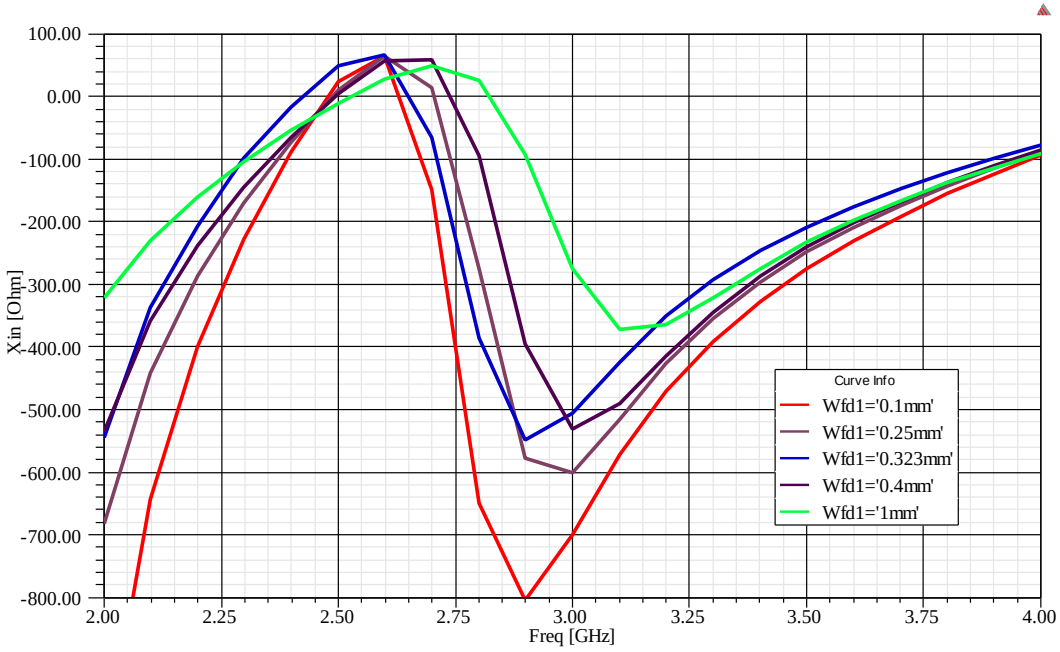

(b)

Figure 3- 25 Z_{in}^{FD} in terms of real and imaginary parts versus W_{fd1} : (a) R_{in} (b) X_{in}

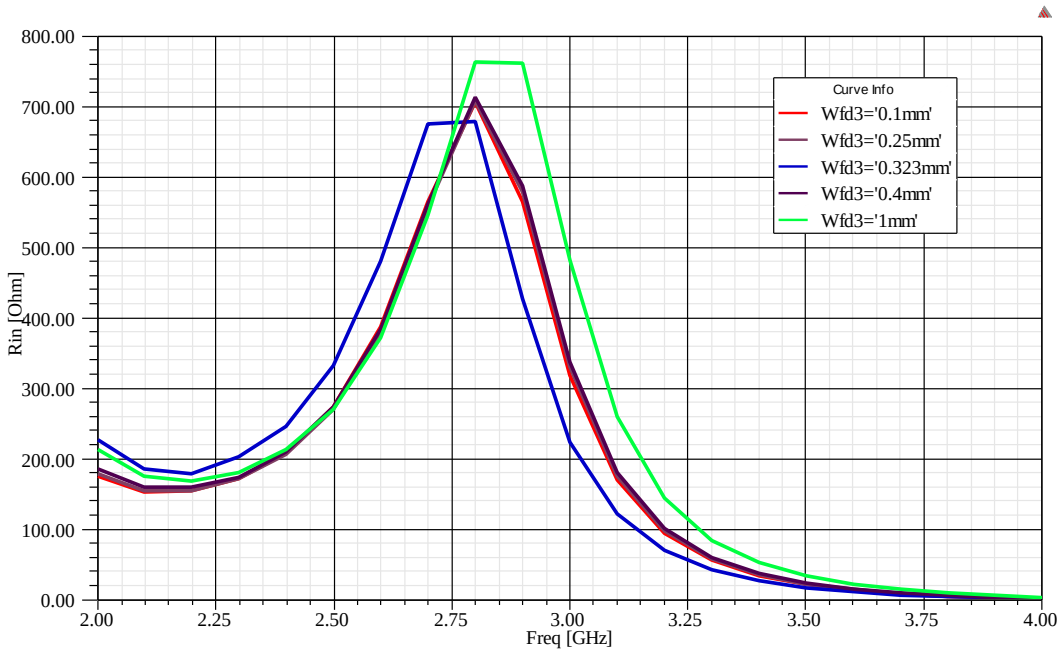

(a)

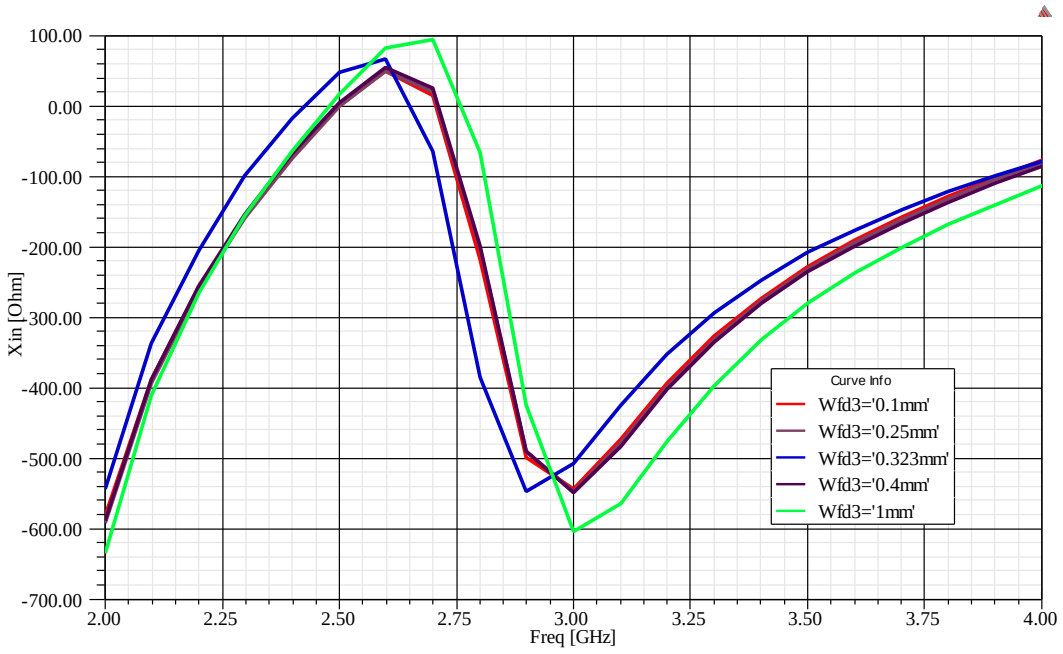

(b)

Figure 3- 26 Z_{in}^{FD} in terms of real and imaginary parts versus W_{fd3} : (a) R_{in} (b) X_{in}

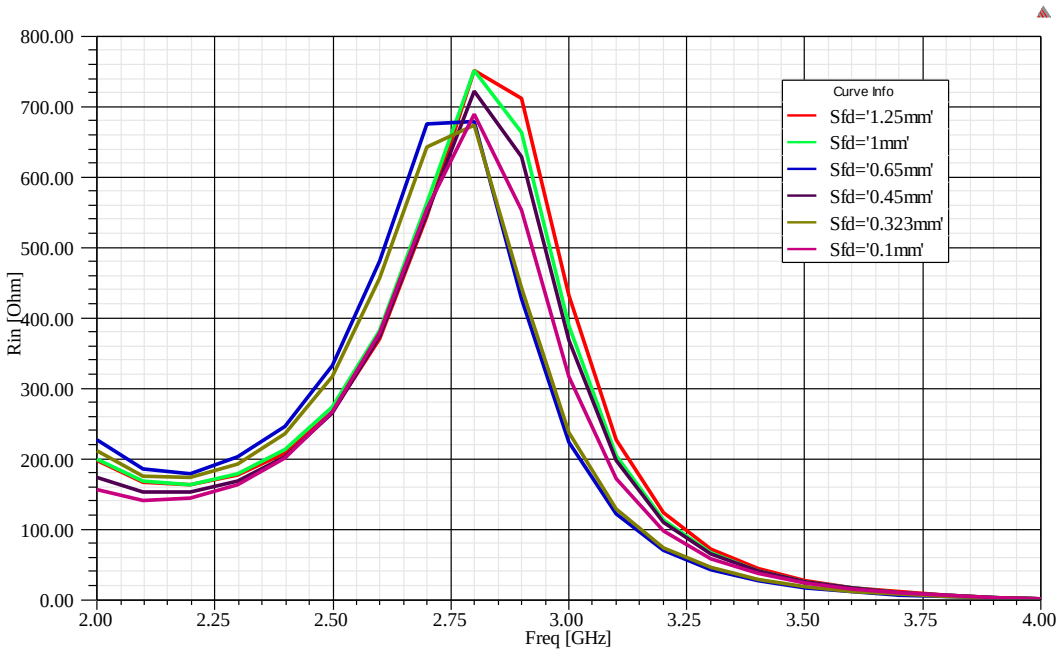

(a)

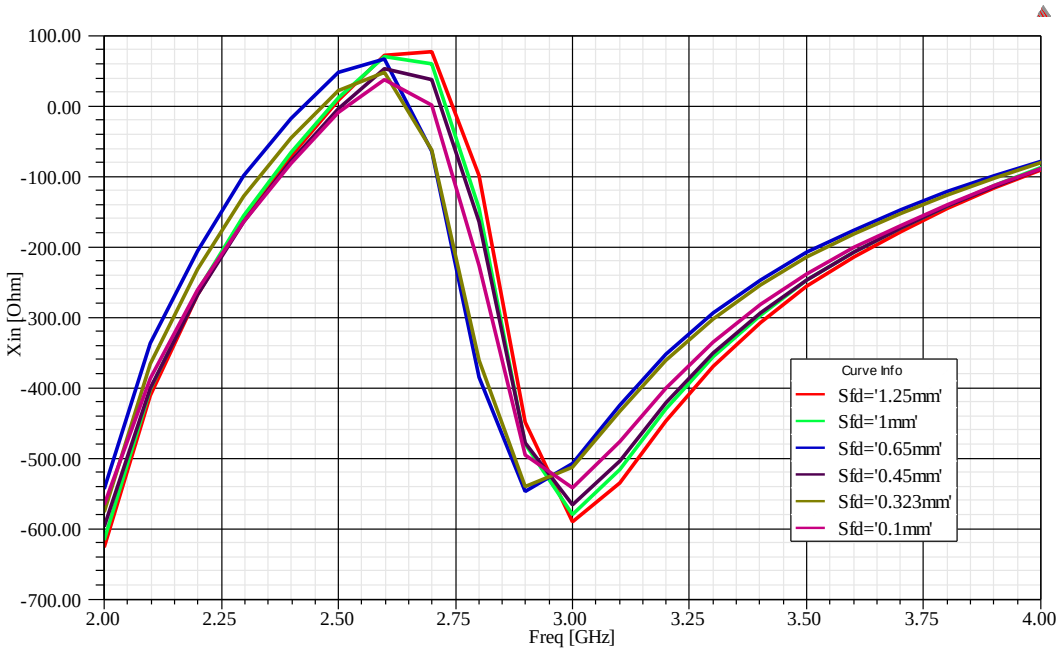

(b)

Figure 3- 27 Z_{in}^{FD} in terms of real and imaginary parts versus S_{fd} : (a) R_{in} (b) X_{in}

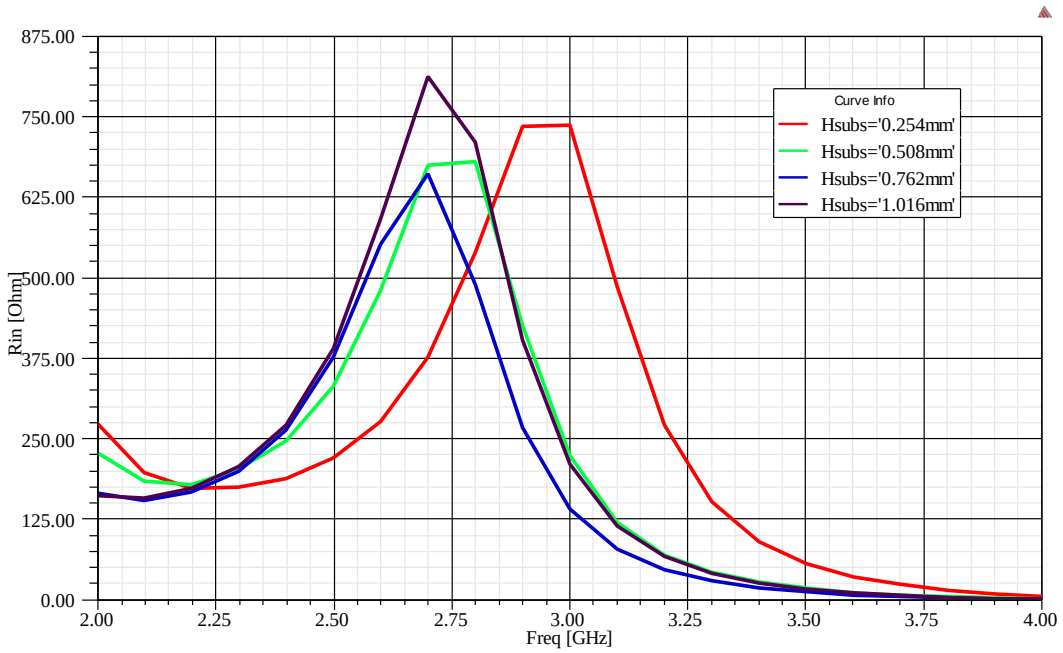

(a)

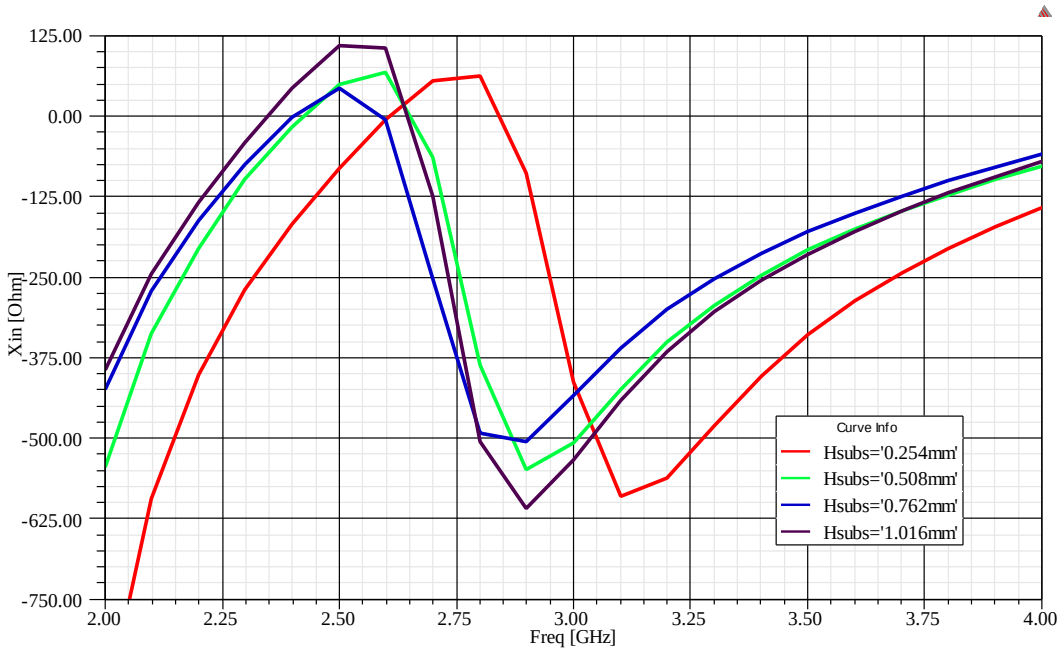

(b)

Figure 3- 28 Z_{in}^{FD} in terms of real and imaginary parts versus H_{subs} : (a) R_{in} (b) X_{in}

With the experience gained through the above summarized parametric analysis, an ACPS folded dipole antenna which has input impedance about 200 Ω and a bandwidth of 20% is designed. Values of the designed ACPS folded dipole antenna parameters are given in Table 3- 2.

Table 3- 2 Optimized dimensions of the ACPS folded dipole parameters

Design Parameter	Value (mm)
L_{fd}	30
W_{fd}	8,00
B_{fd}	26,00
W_{fd3}	1,50
W_{fd1}	0,65
S_{fd}	0,65

Note that W_{fd}/W_{fd1} ratio is large that implies a large input resistance level. However B_{fd} is also quite large that translates to a decrease in the slope of the resistance and reactance curves around the resonance. These choices were made to achieve the wide bandwidth of 20%. This result is consistent with the observations discussed in [14], which states that maximum bandwidth is achieved by using wide conducting strips with wide spacing.

Input impedance and return loss characteristics of the ACPS folded dipole for the optimized dimensions are shown in Figure 3- 29 and Figure 3- 30. 3D radiation pattern and gain of the designed ACPS folded dipole operating at 2.7 GHz - 3.3 GHz frequency band are also shown in Figure 3- 31 and Figure 3- 32, respectively. As seen from figures, 20% bandwidth requirement is provided with this design. The radiation patterns at two principle planes at 3 GHz are also presented in Figure 3- 33. It is observed that patters remain almost same throughout the bandwidth of interest. The realized total gain is 3.1 dB – 4.45 dB across the bandwidth of 2.7 GHz - 3.3 GHz.

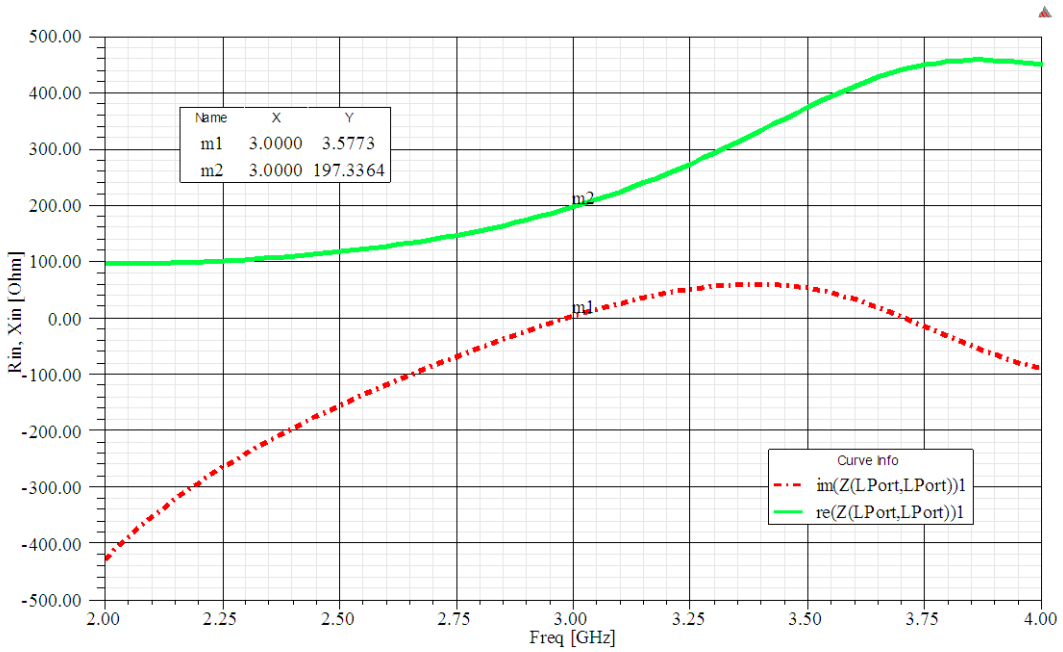

Figure 3- 29 Z_{in}^{FD} in terms of real and imaginary parts for optimized dimensions

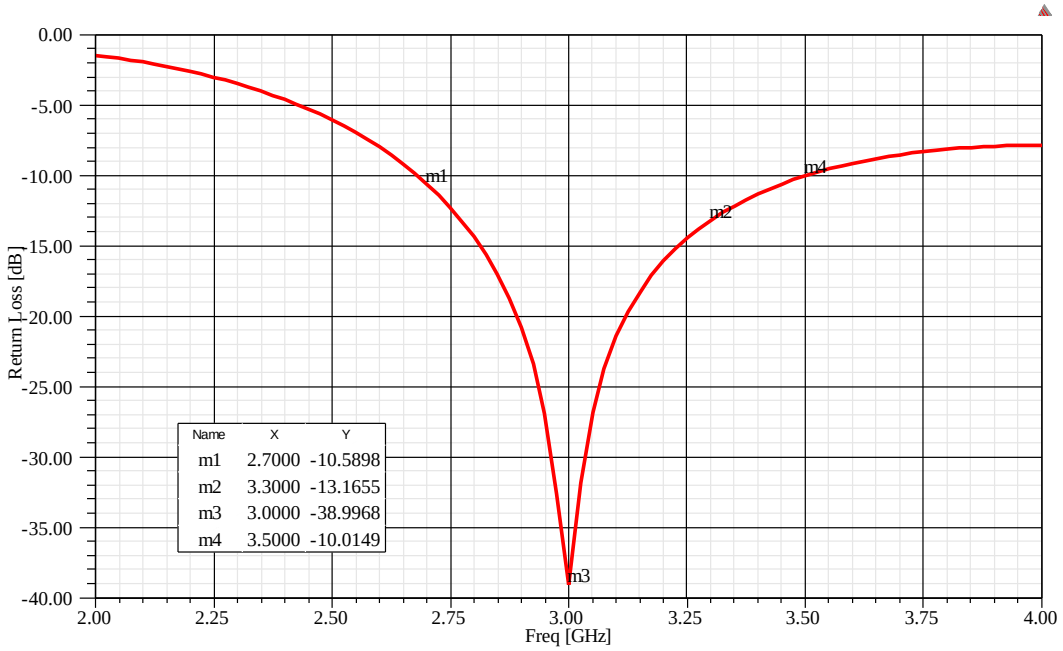

Figure 3- 30 Return loss of the ACPS folded dipole for optimized dimensions

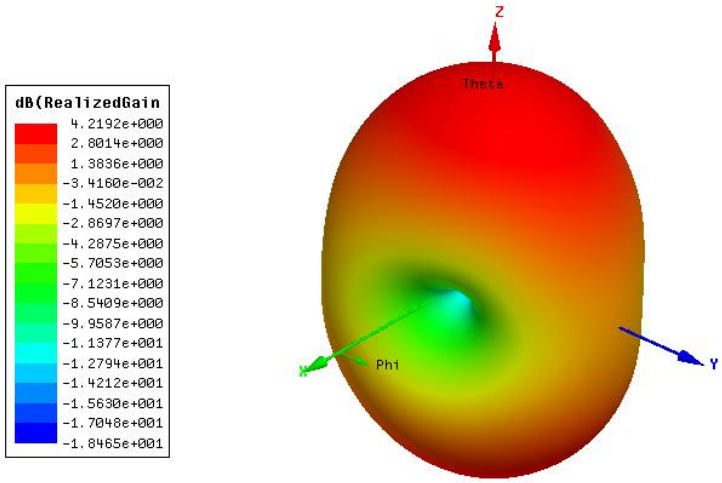

Figure 3- 31 3D radiation pattern of the ACPS folded dipole for optimized dimensions at 3 GHz

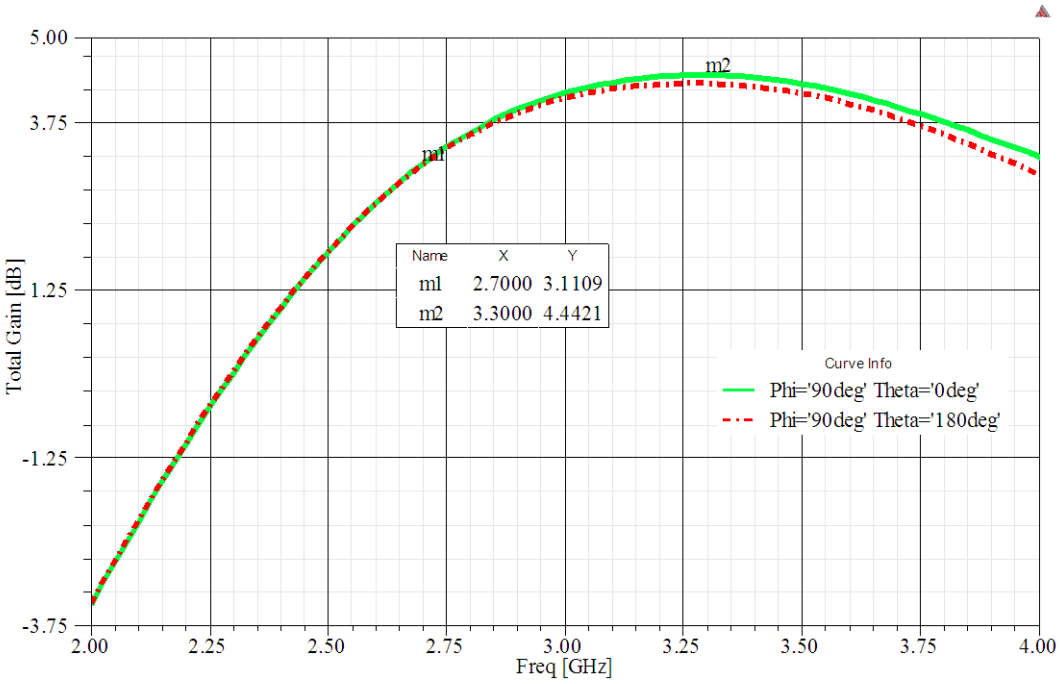

Figure 3- 32 Gains in bore-sight directions of the ACPS folded dipole for optimized dimensions versus frequency

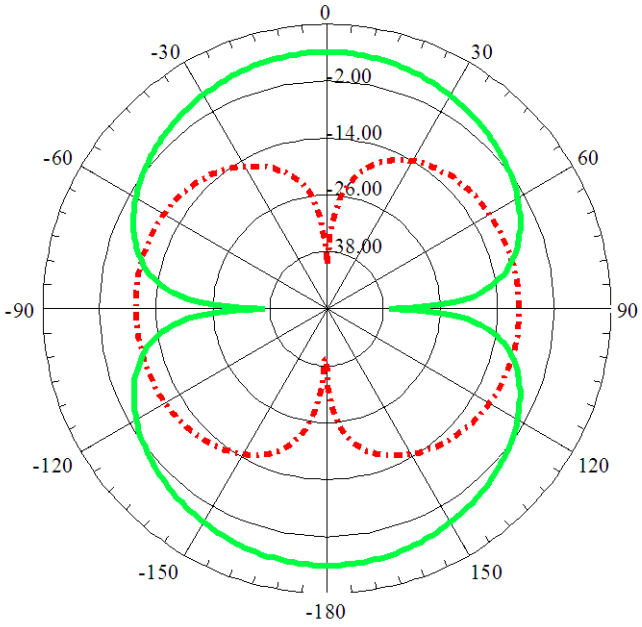

(a)

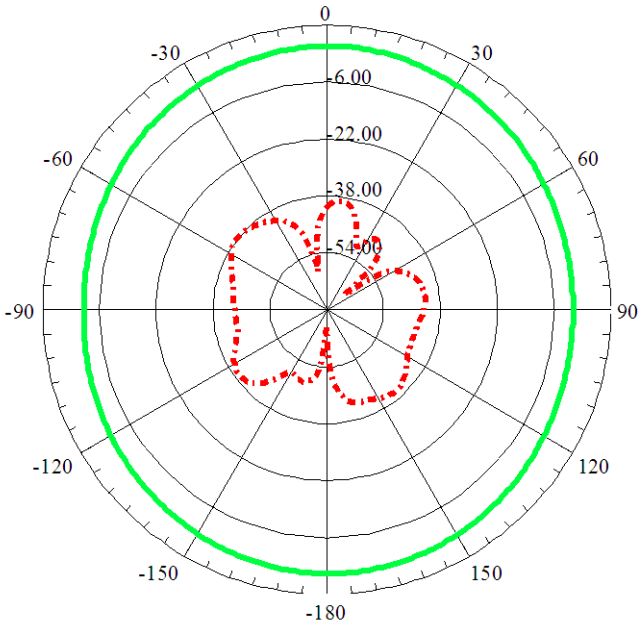

(b)

Figure 3- 33 Radiation patterns in terms of co and cross polarization of the ACPS folded dipole for optimized dimensions at 3 GHz: (a) E-plane (b) H-plane

Finally, an ACPS folded dipole antenna with a feed line is analyzed (Figure 3- 34), and the length of the feed line is optimized. The optimum length is found to be 15.5 mm and the simulation results obtained with optimized antenna parameters is given in Figure 3- 35 and Figure 3- 36.

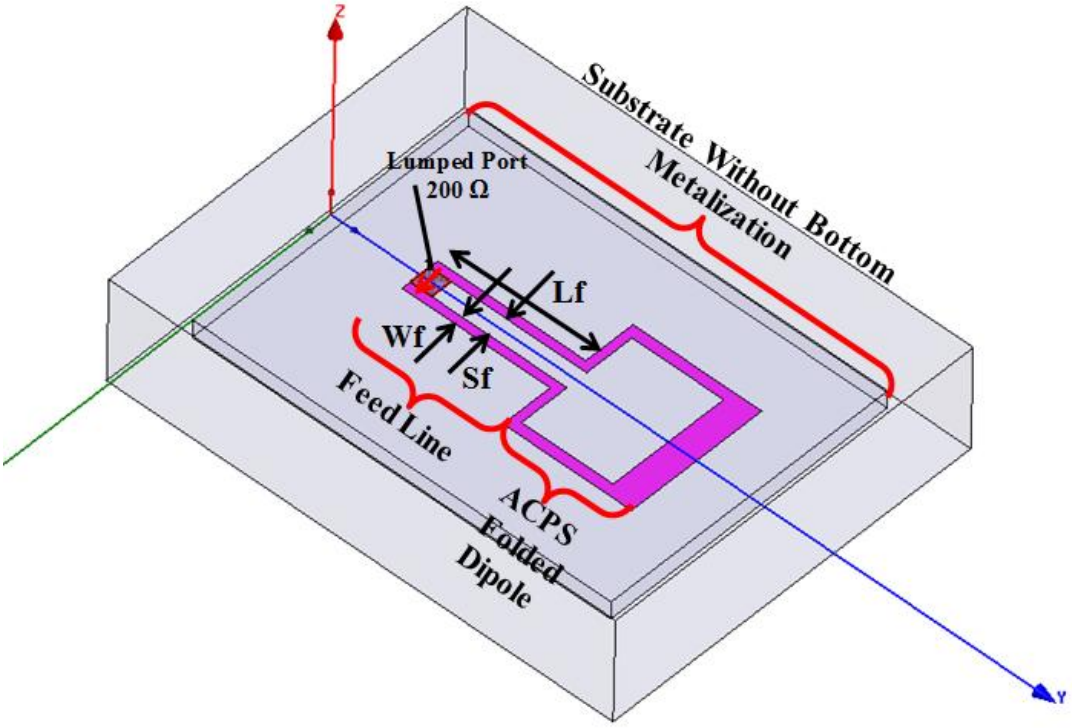

Figure 3- 34 Simulation model of the ACPS folded dipole with a feed line in Ansys HFSS®

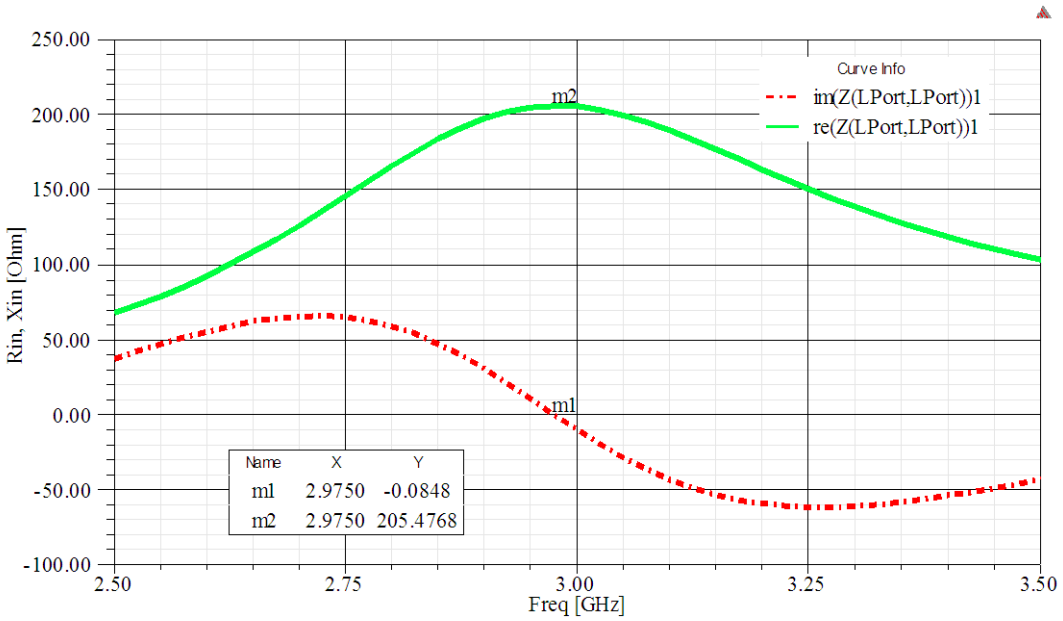

Figure 3- 35 Z_{in}^{FD} for the ACPS folded dipole with feed line in terms of real and imaginary parts for optimized dimensions

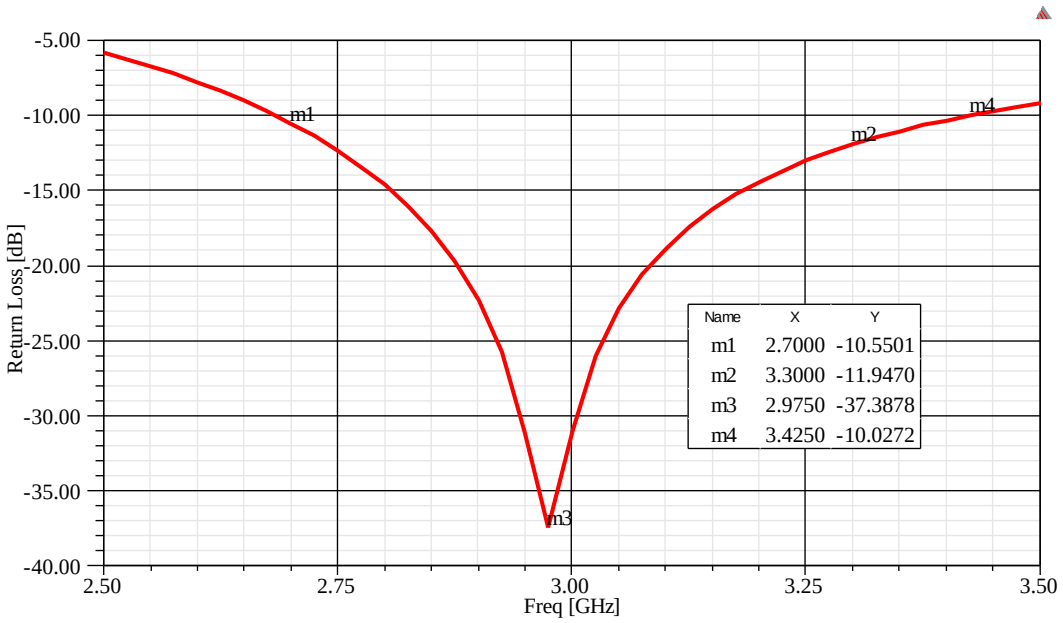

Figure 3- 36 Return loss of the ACPS folded dipole with feed line for optimized dimensions

3.5 Design of the ACPS Folded Dipole Antenna Element and Array

In this section, three different ACPS folded dipole antenna configurations are studied in order to provide polarization requirements mentioned earlier. Moreover, uniformly excited four-element linear array configurations are studied as well. The characteristics of the antennas are analyzed in terms of return loss response, gain and radiation patterns. Radiation patterns are examined at several frequencies over the operating band to determine any frequency dependence of the patterns. For the configurations that do not exhibit frequency dependence regarding the radiation patterns, only the patterns at the center frequency are presented.

Firstly, the ACPS folded dipole is directly connected with the balun as shown in Figure 3- 37 and referred as configuration-I. The simulation results of this first antenna configuration are presented in Figure 3- 38 through Figure 3- 41. It is observed from the figures that the bandwidth of the designed balun does not restrict the frequency response of the designed ACPS folded dipole antenna. While the E-plane radiation pattern remains same as the pattern for the antenna without balun, the H-plane pattern looses its omni-directional characteristic and becomes more directive due to the presence of the truncated ground plane. Consequently gain values increase slightly above 5 dB level.

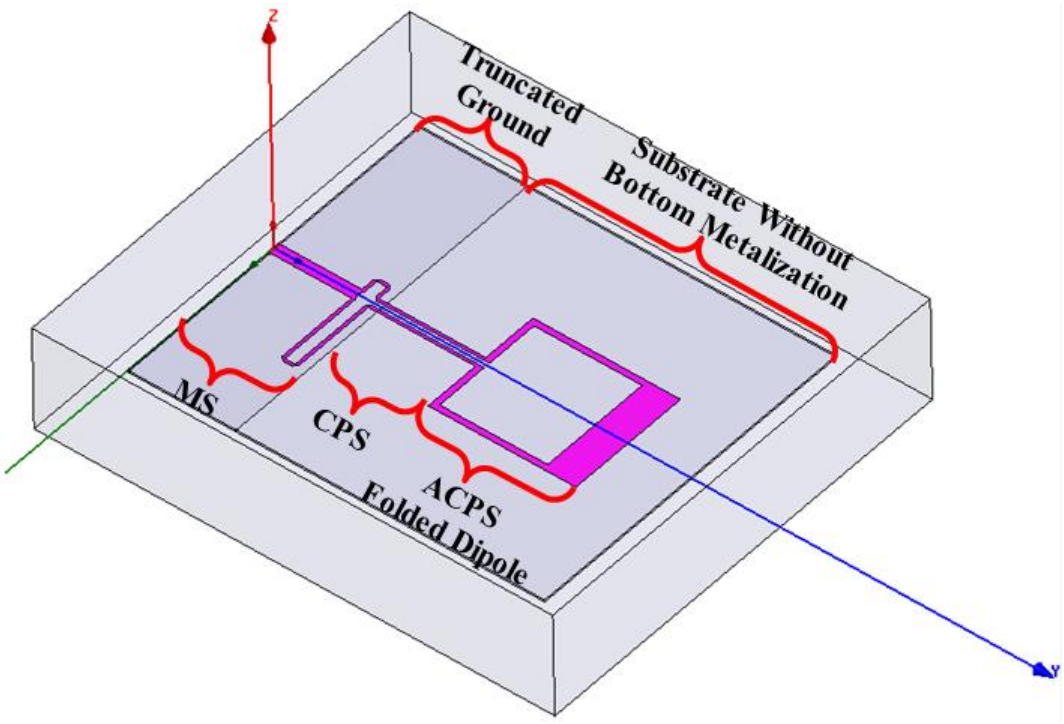

Figure 3- 37 Simulation model of the ACPS folded dipole antenna element designed as configuration-I in Ansys HFSS®

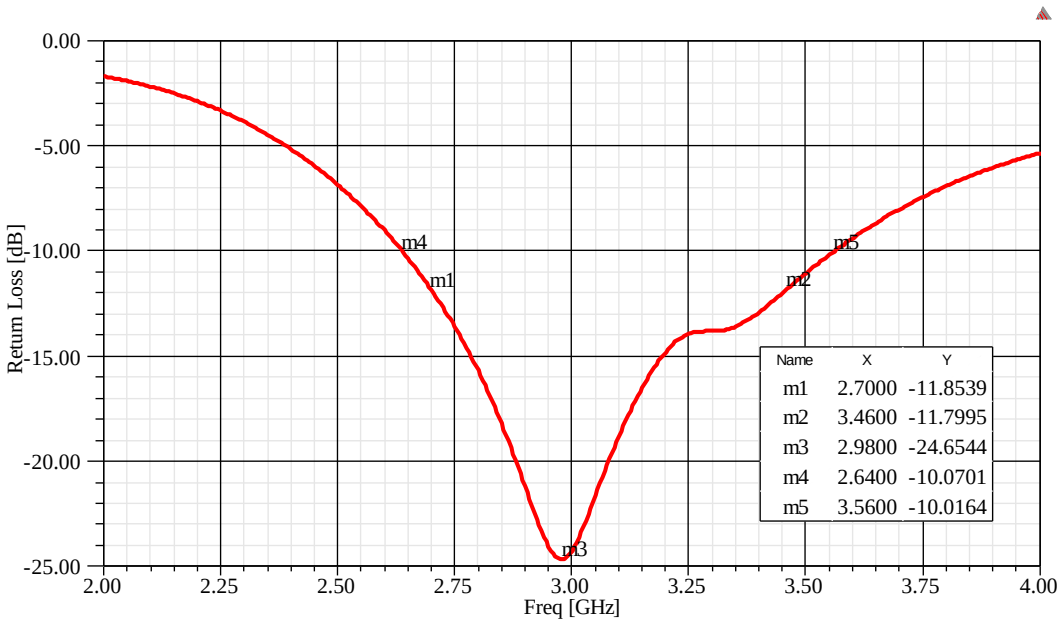

Figure 3- 38 Return loss of the ACPS folded dipole antenna element designed as configuration-I

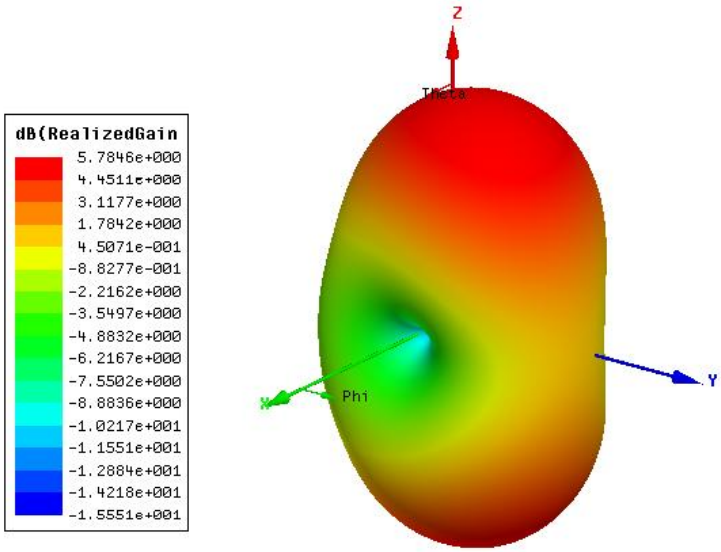

Figure 3- 39 3D radiation pattern of the ACPS folded dipole antenna element designed as configuration-I at 3GHz

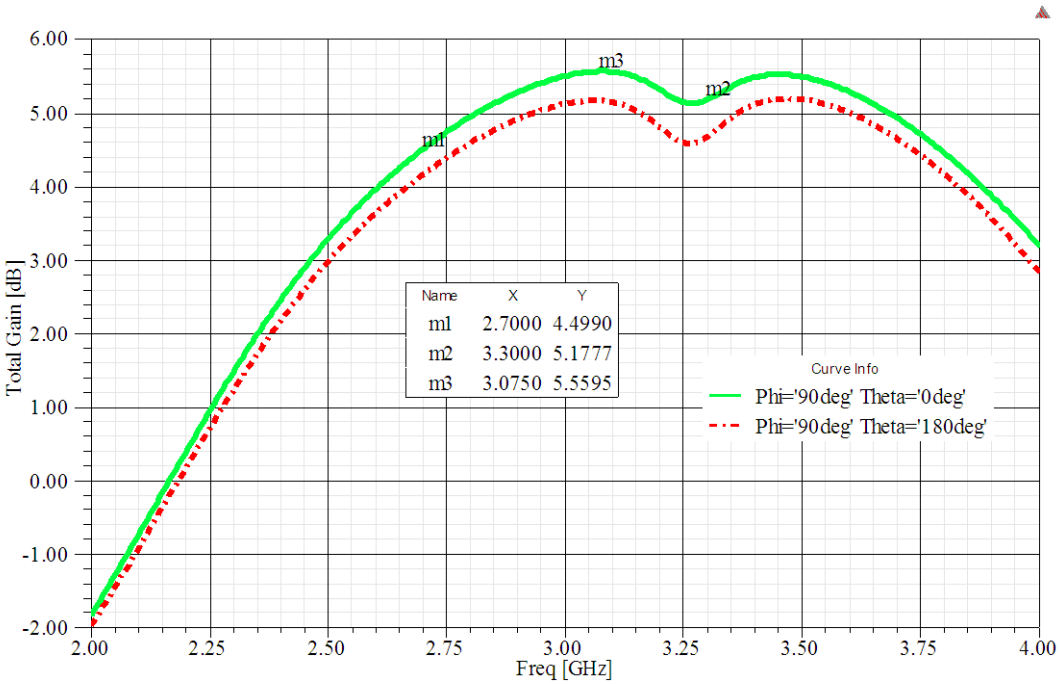

Figure 3- 40 Gains in bore-sight directions of the ACPS folded dipole antenna element designed as configuration-I versus frequency

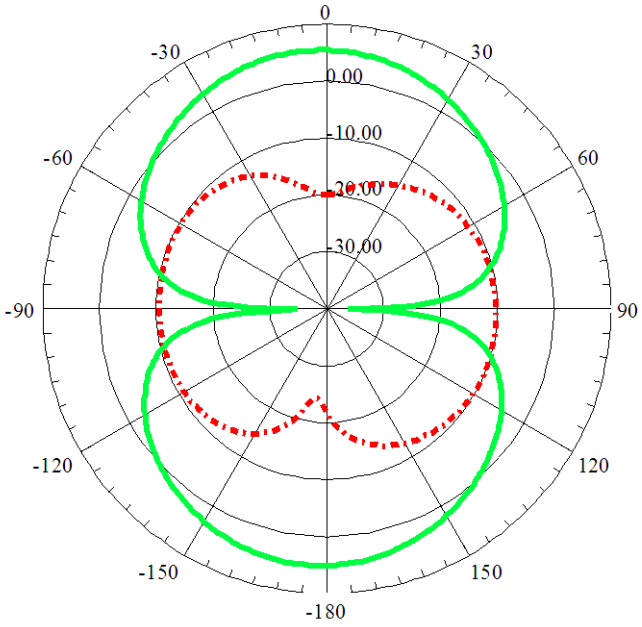

(a)

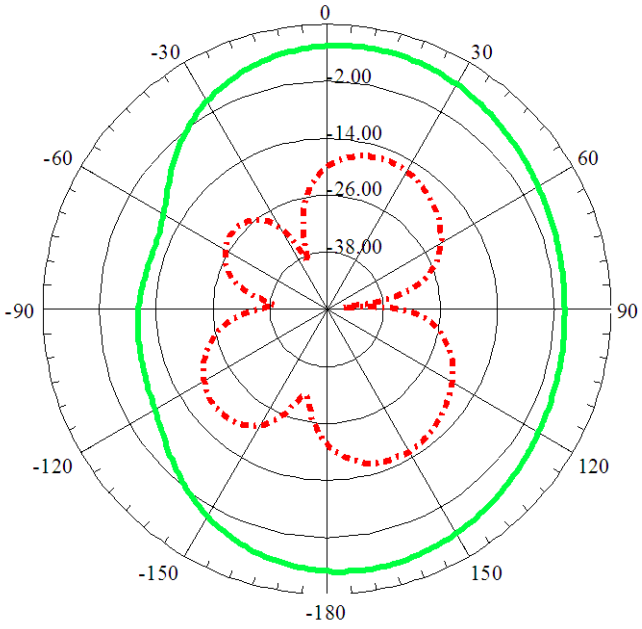

(b)

Figure 3- 41 Radiation patterns in terms of co and cross polarization of the ACPS folded dipole antenna element designed as configuration-I at 3 GHz: (a) E-plane (b) H-plane

The second configuration of the antenna element is constructed by using the CPS feed line which consists of a 90 degree right angle bend. A typical CPS 90 degree right angle bend is shown in Figure 3- 42. According to Goverdhanam et al., compensation of the CPS bend to improve VSWR is not required [28]. This fact is used in the design of the proposed antenna element which the CPS feeding line is bent without resulting in any noticeable parasitic effects due to the bend.

Simulation model of the ACPS folded dipole antenna element for configuration-II is given in Figure 3- 43. L_{cps4} is fixed at the previous length of 15.5mm and L_{cps2} is optimized. The optimum value is found to be 48 mm to minimize the effects of the ground plane. The results of this second antenna configuration are presented in Figure 3- 44 through Figure 3- 49. Note that for this configuration the ground plane is in the E-plane of the antenna. As it can be observed from the radiation pattern plots, the truncated ground plane results in increased cross-polarization levels in the E-plane. On the other hand the H-plane pattern is expected to be omni-directional as the antenna without balun. However as it seen in the radiation pattern results for 3.3 GHz, the H-plane pattern is neither omni-directional nor symmetric. This may be attributed to the CPS line which is parallel to the antenna. It can be concluded that it is more effective at higher frequencies. Therefore one expects the gain of the antenna to be similar to the antenna without balun. But the gain decreases at 2.7 GHz due to the increased cross-pol level and the gain levels at 3 GHz and 3.3 GHz increase due to the increased directivity in H-plane caused by the CPS line.

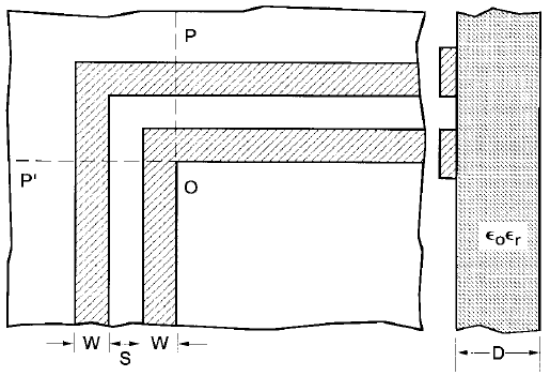

Figure 3- 42 A typical CPS 90 degree right angle bend [28]

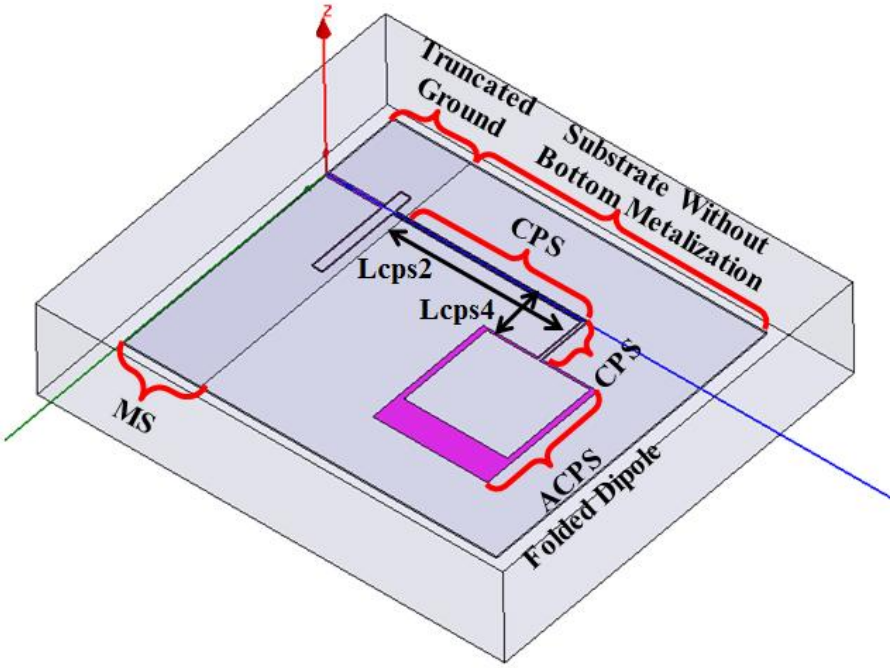

Figure 3- 43 Simulation model of the ACPS folded dipole antenna element designed as configuration-II in Ansys HFSS®

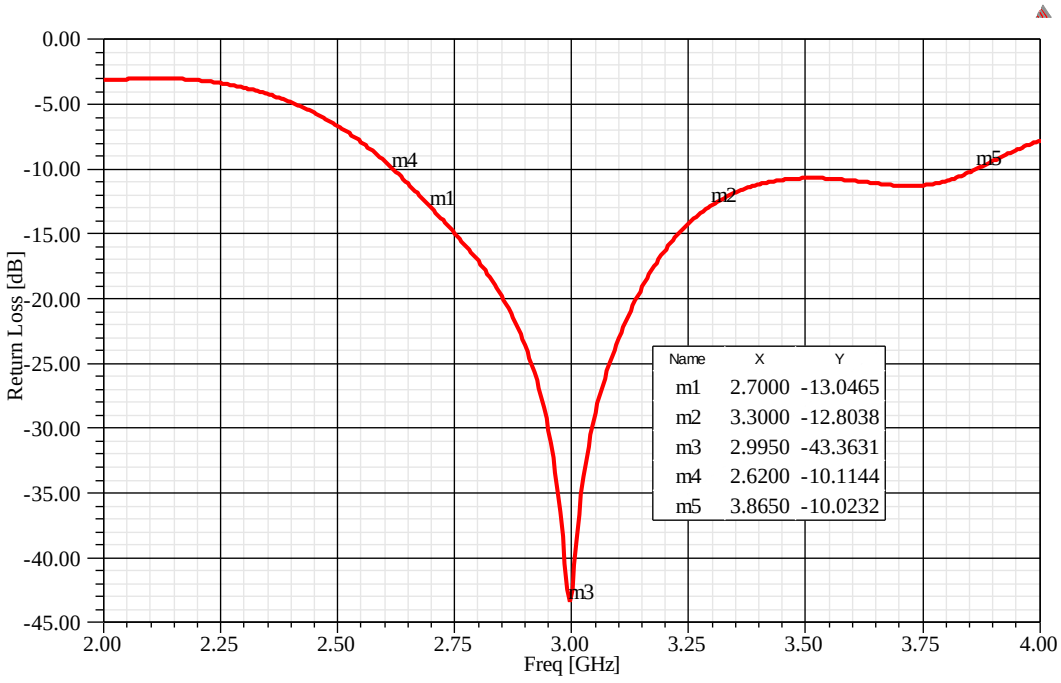

Figure 3- 44 Return loss of the ACPS folded dipole antenna element designed as configuration-II

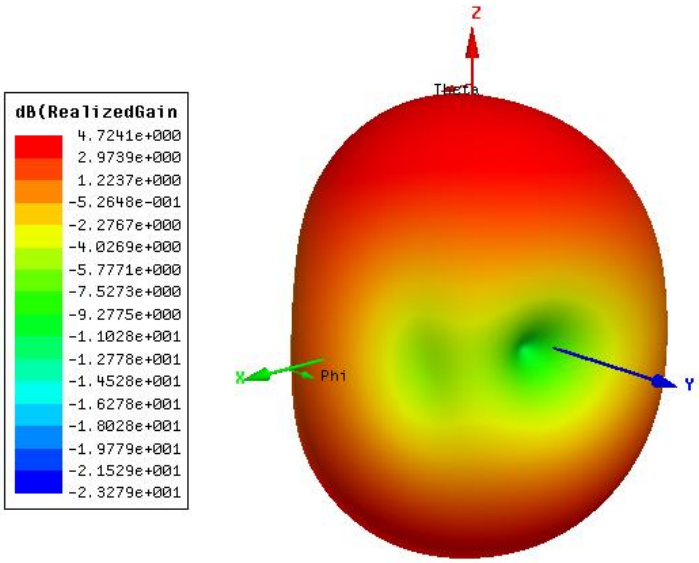

Figure 3- 45 3D radiation pattern of the ACPS folded dipole antenna element designed as configuration-II at 3 GHz

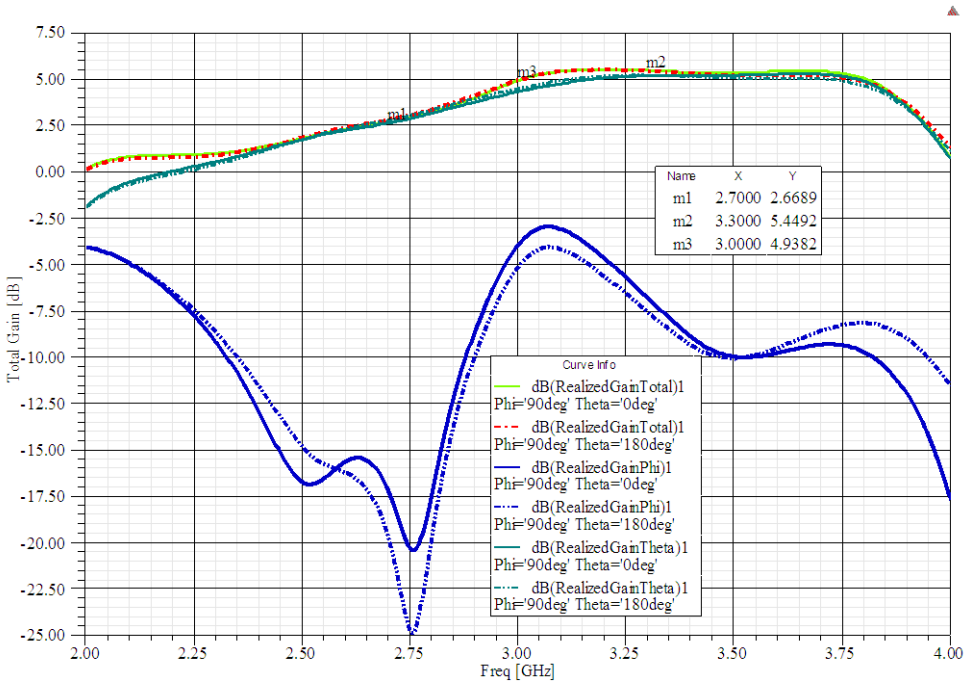

Figure 3- 46 Gains in bore-sight directions of the ACPS folded dipole antenna element designed as configuration-II versus frequency

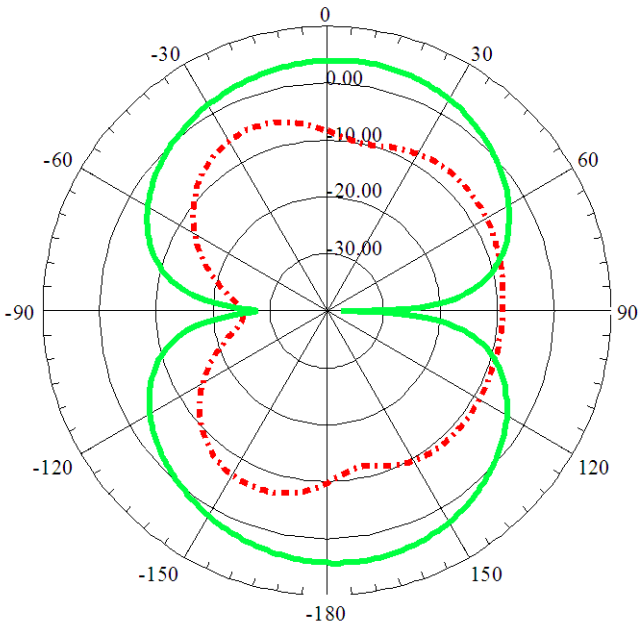

(a)

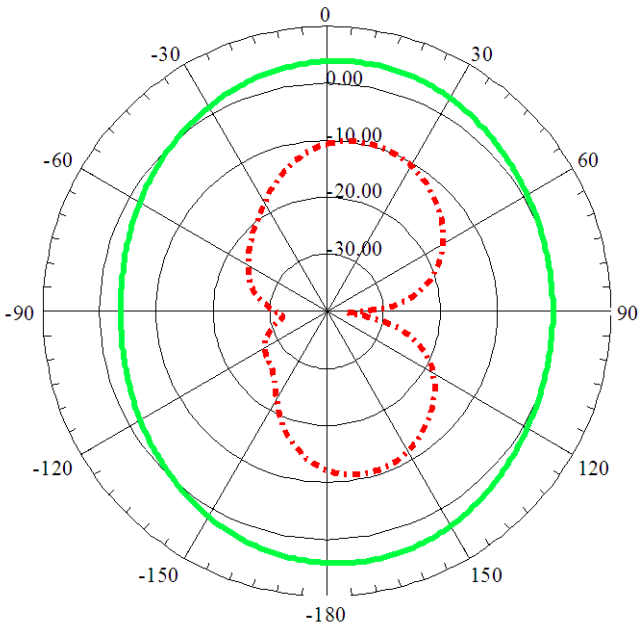

(b)

Figure 3- 47 Radiation patterns in terms of co and cross polarization of the ACPS folded dipole antenna element designed as configuration-II at 3 GHz: (a) E-plane (b) H-plane

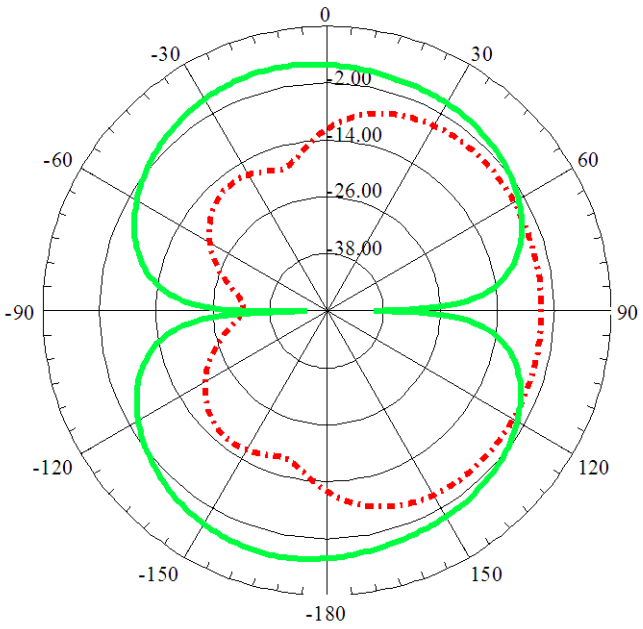

(a)

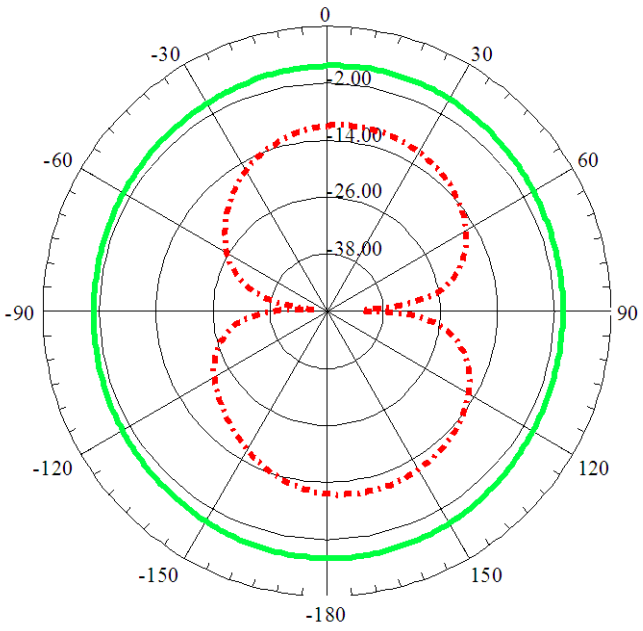

(b)

Figure 3- 48 Radiation patterns in terms of co and cross polarization of the ACPS folded dipole antenna element designed as configuration-II at 2.7 GHz: (a) E-plane (b) H-plane

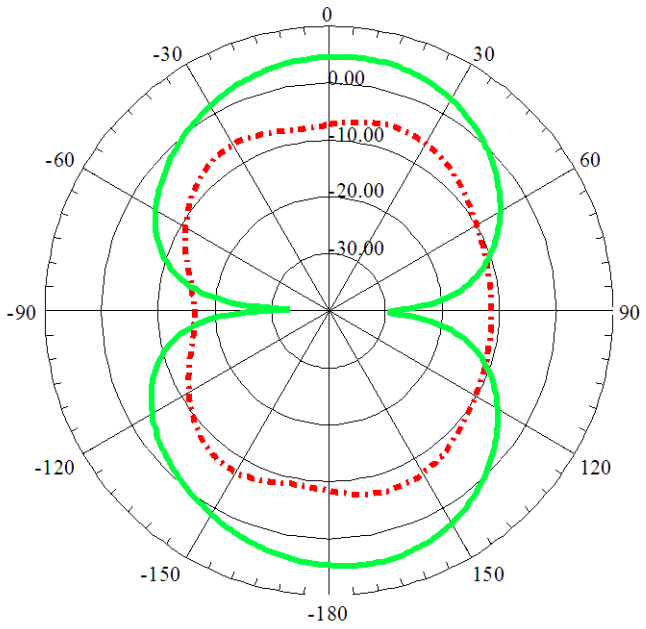

(a)

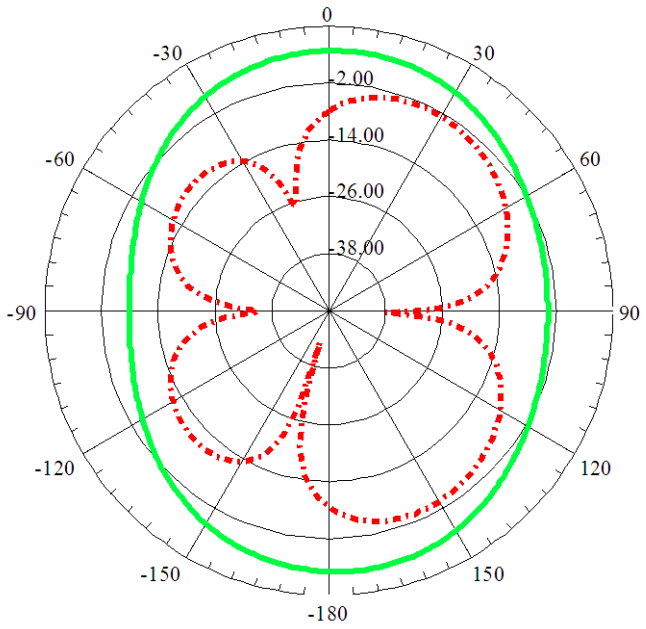

(b)

Figure 3- 49 Radiation patterns in terms of co and cross polarization of the ACPS folded dipole antenna element designed as configuration-II at 3.3 GHz: (a) E-plane (b) H-plane

Finally, as shown in Figure 3- 50 the substrate and the strips are curved to a 90 degree rotation with a specific radius after the truncated ground plane. The rotation is carried out at a specific point in order to prevent any interference in the balun performance. The position of the rotation starting point of the substrate and the radius $R_{subsbend}$ (optimum value found to be 1.524mm) of the rotation are investigated by the help of simulation and thus this discontinuity in the balun geometry does not result in impedance mismatch or any changes in balun characteristics.

Simulation model of the ACPS folded dipole antenna element for configuration-III is presented in Figure 3- 50. The simulation results of this third antenna configuration are presented in Figure 3- 51 through Figure 3- 56. A slight increase of 1 dB is observed in the gain of the antenna at 2.7 GHz, since the cross-pol levels in the E-plane are decreased due to bending. A significant change in the gain values at 3 GHz and 3.3 GHz is not observed. However, the gains at the forward and backward directions of the antenna changed due to the presence of the ground plane. Nevertheless, an additional ground plane parallel to the substrate will be used in the final design to obtain uni-directional pattern from the bi-directional antenna.

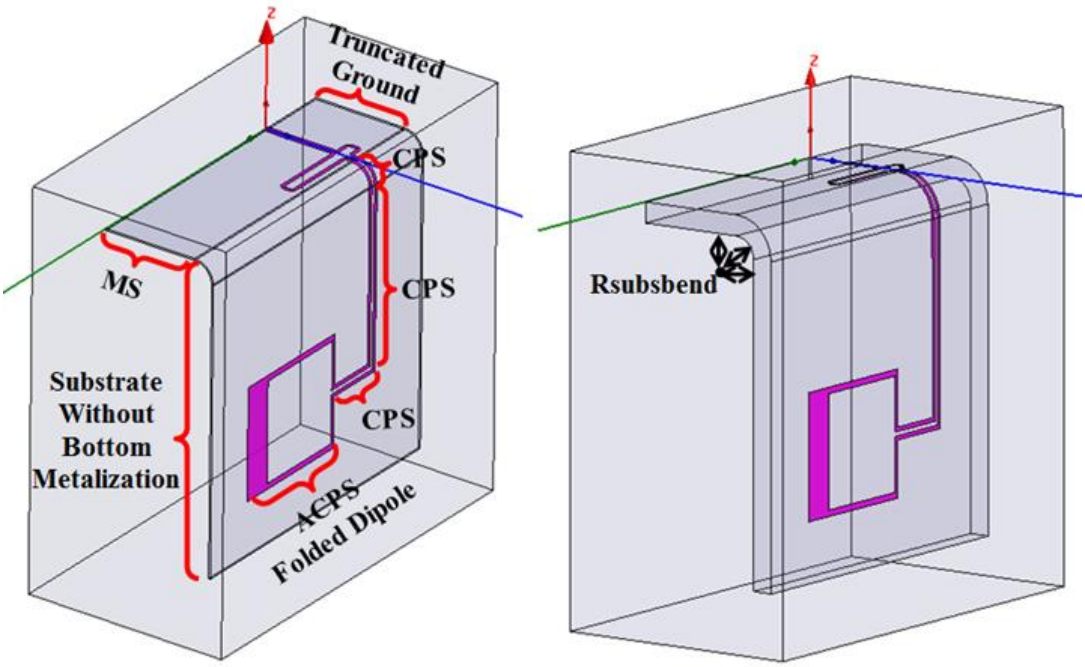

Figure 3- 50 Simulation model of the ACPS folded dipole antenna element designed as configuration-III in Ansys HFSS®

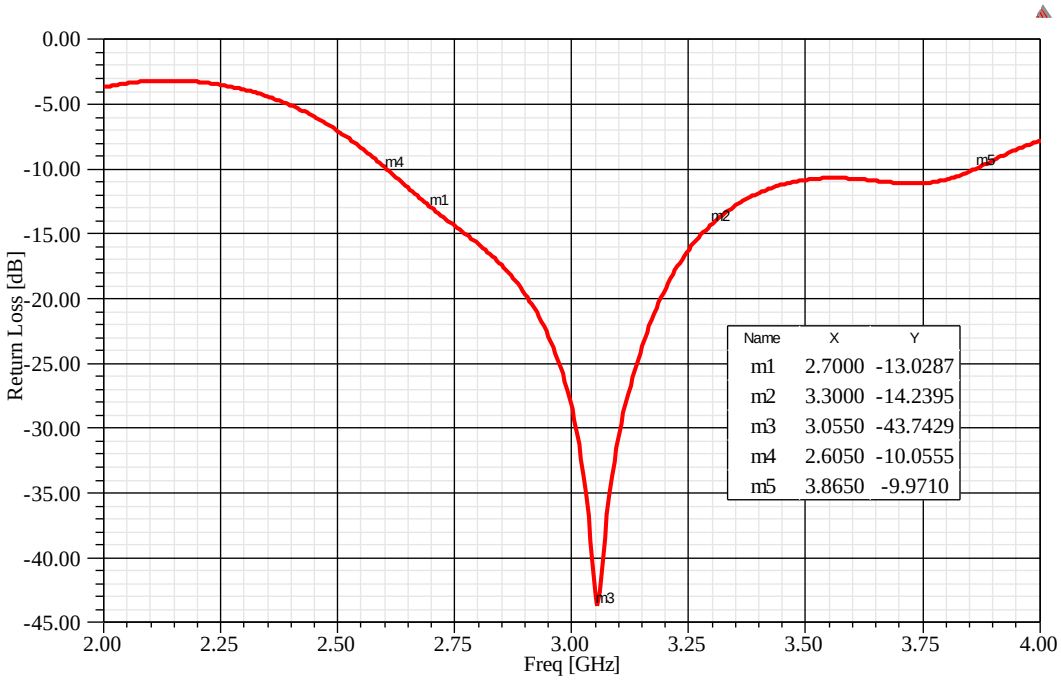

Figure 3- 51 Return loss of the ACPS folded dipole antenna element designed as configuration-III

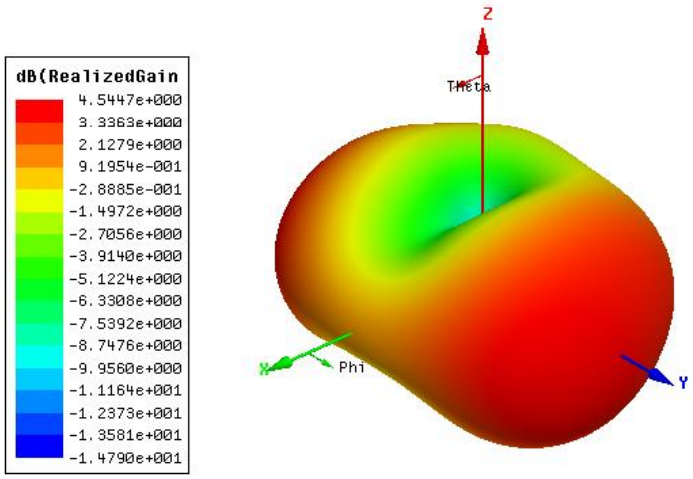

Figure 3- 52 3D radiation pattern of the ACPS folded dipole antenna element designed as configuration-III at 3 GHz

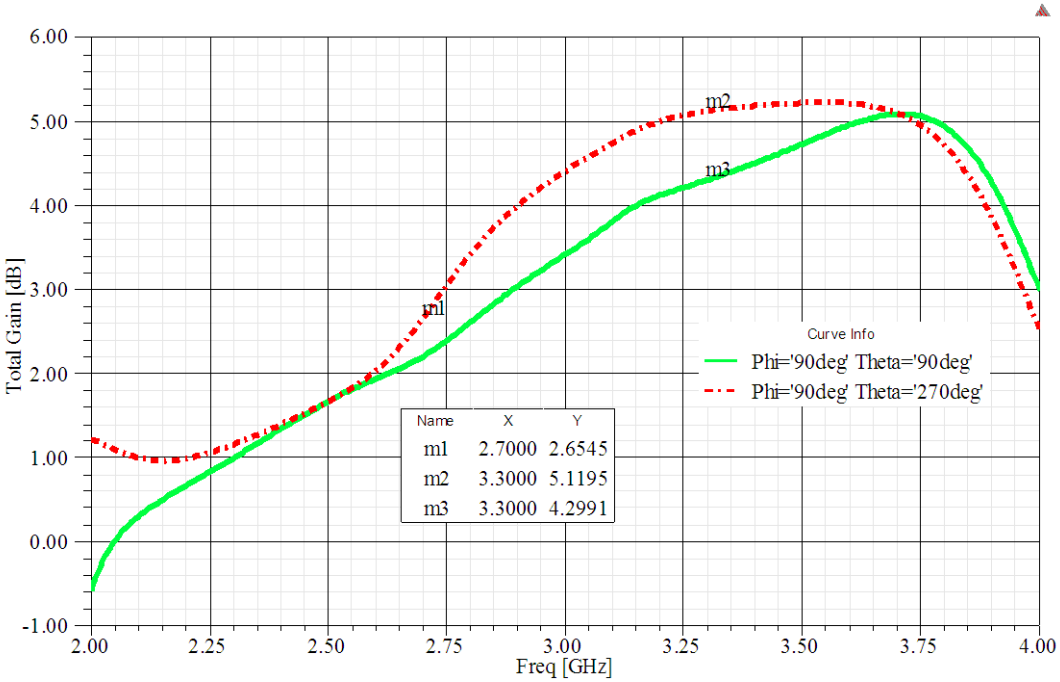

Figure 3- 53 Gains in bore-sight directions of the ACPS folded dipole antenna element designed as configuration-III versus frequency

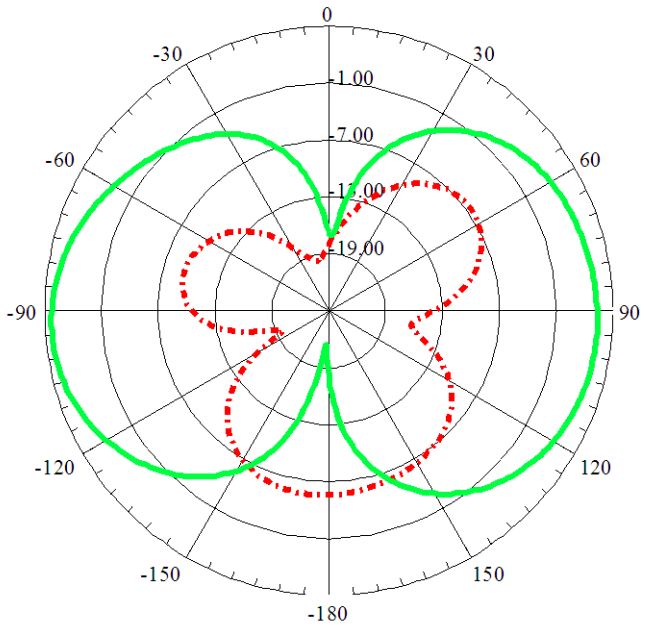

(a)

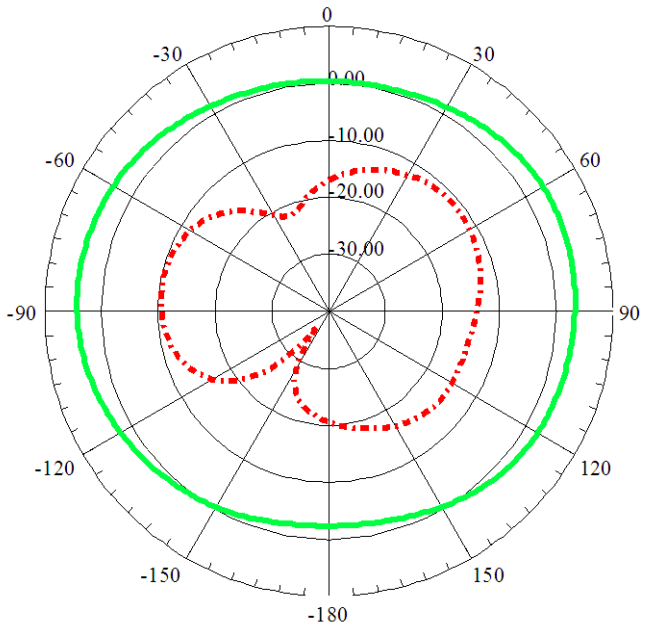

(b)

Figure 3- 54 Radiation patterns in terms of co and cross polarization of the ACPS folded dipole antenna element designed as configuration-III at 3 GHz: (a) E-plane (b) H-plane

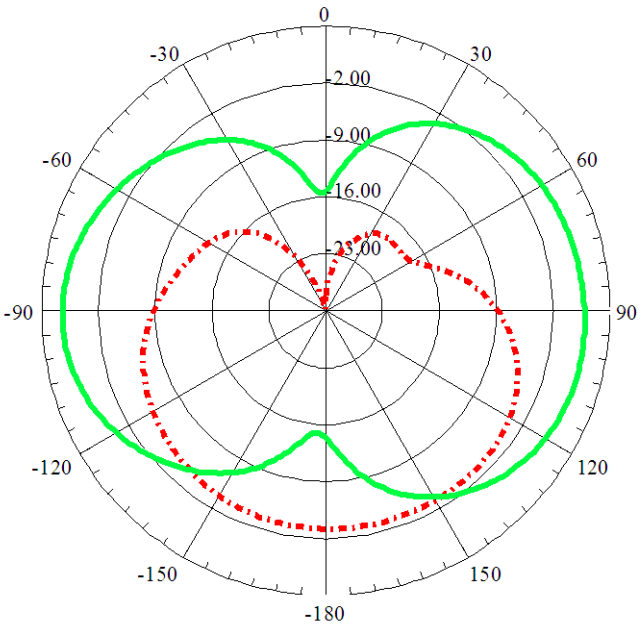

(a)

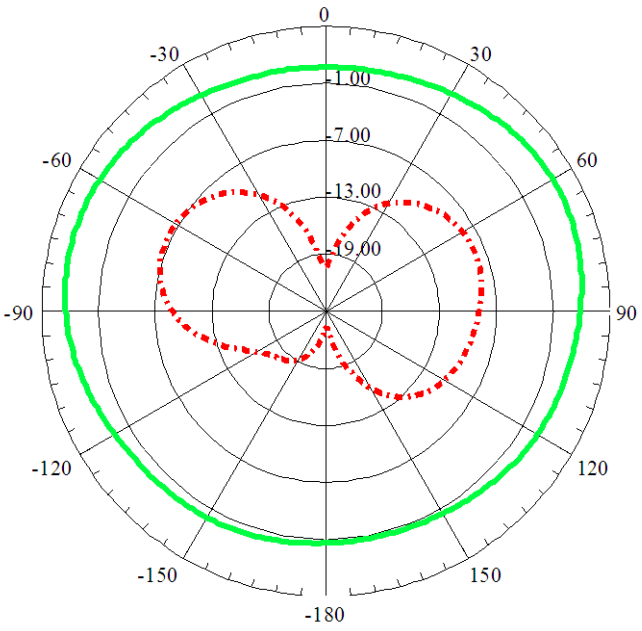

(b)

Figure 3- 55 Radiation patterns in terms of co and cross polarization of the ACPS folded dipole antenna element designed as configuration-III at 2.7 GHz: (a) E-plane (b) H-plane

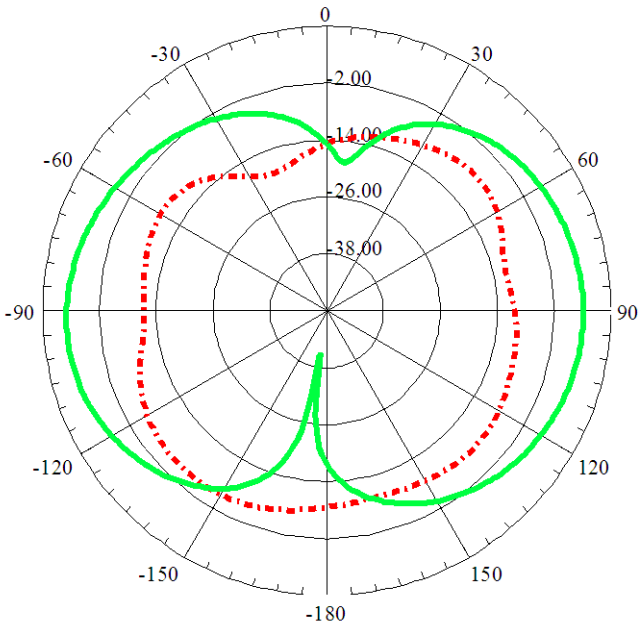

(a)

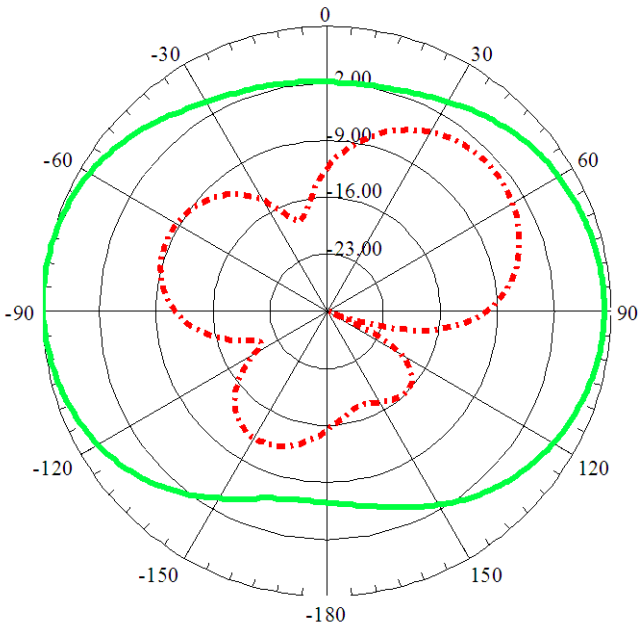

(b)

Figure 3- 56 Radiation patterns in terms of co and cross polarization of the ACPS folded dipole antenna element designed as configuration-III at 3.3 GHz: (a) E-plane (b) H-plane

Finally for better comparison of these three configurations, the simulated gain results and radiation patterns are represented altogether in Figure 3- 57 through Figure 3- 63.

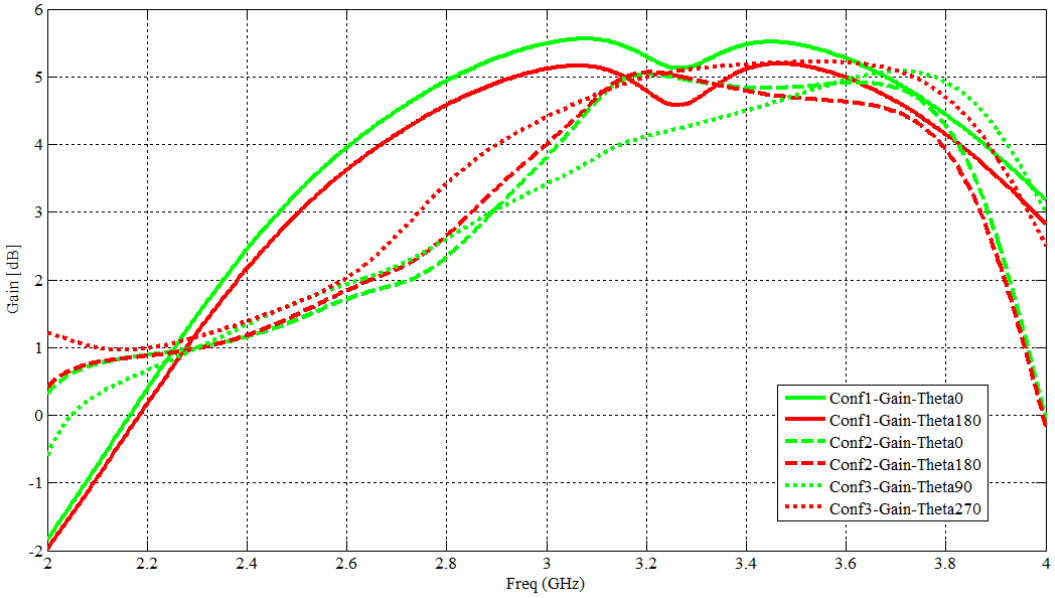

Figure 3- 57 Gains in bore-sight directions for the three ACPS folded dipole antenna elements versus frequency

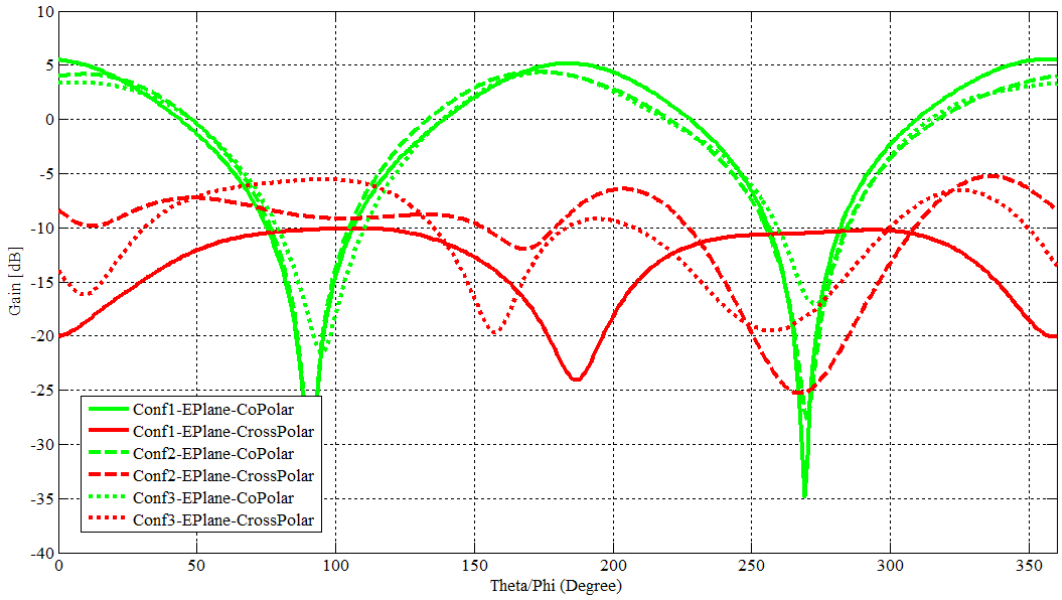

Figure 3- 58 E-plane radiation patterns for the three ACPS folded dipole antenna elements at 3 GHz

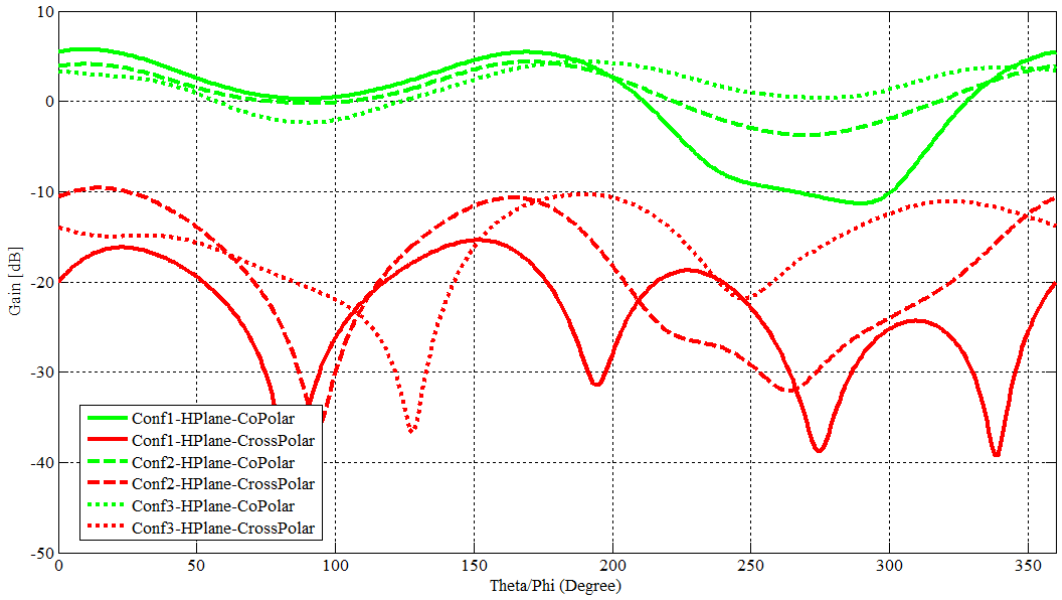

Figure 3- 59 H-plane radiation patterns for the three ACPS folded dipole antenna elements at 3 GHz

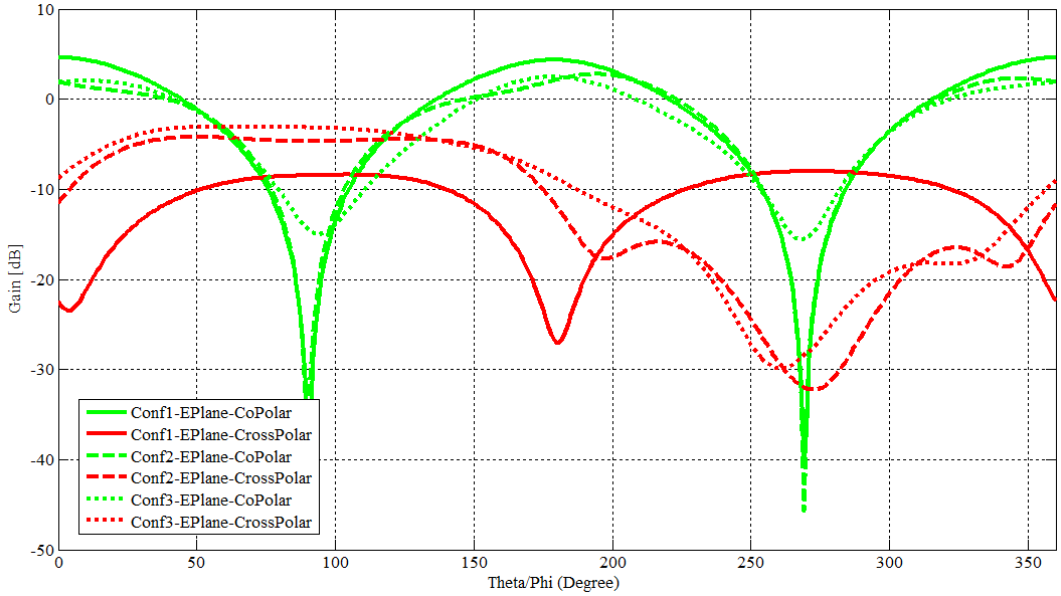

Figure 3- 60 E-plane radiation patterns for the three ACPS folded dipole antenna elements at 2.7 GHz

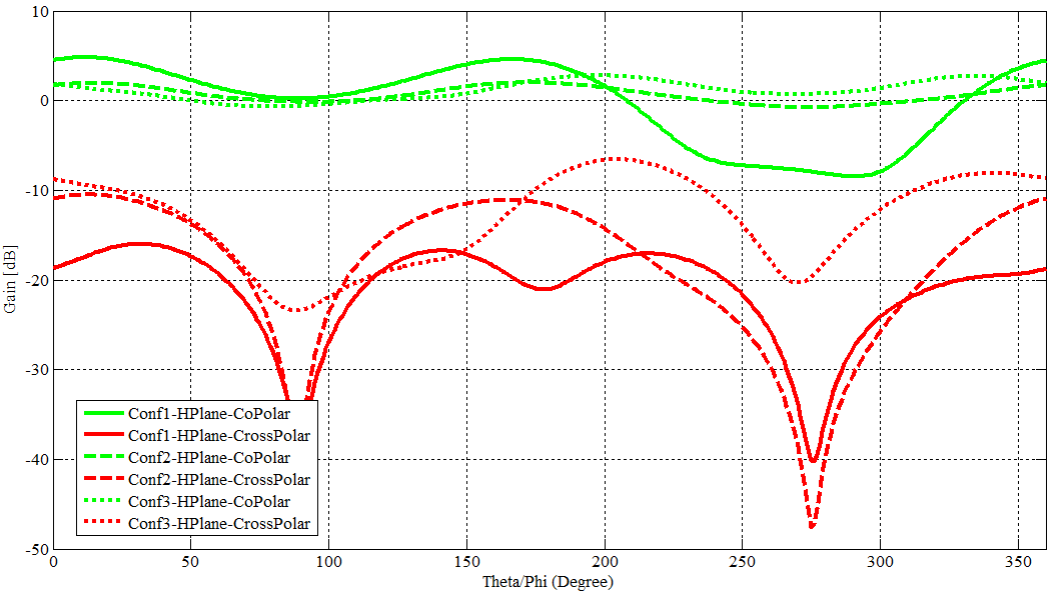

Figure 3- 61 H-plane radiation patterns for the three ACPS folded dipole antenna elements at 2.7 GHz

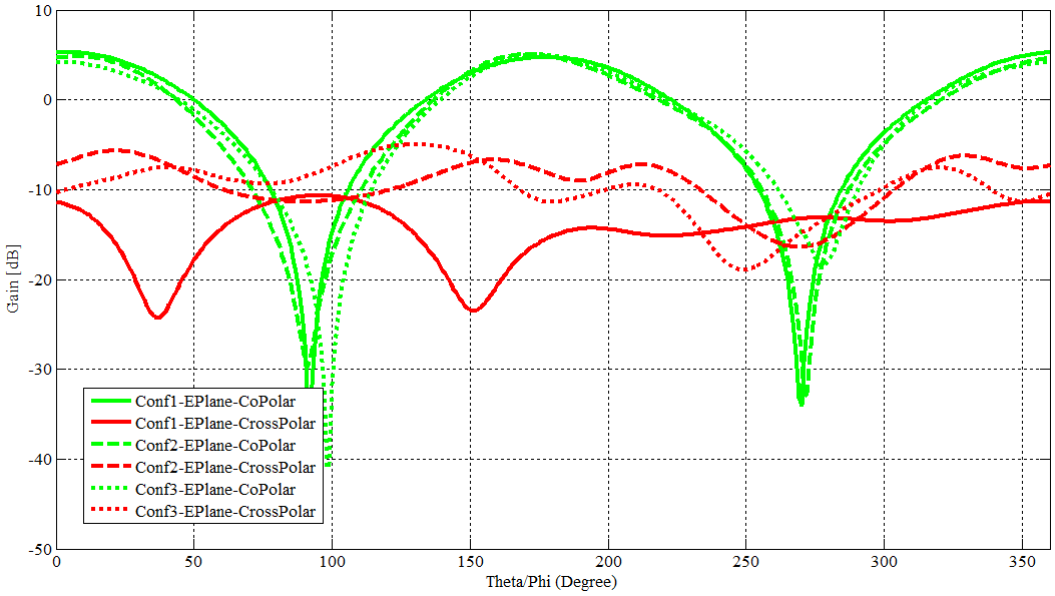

Figure 3- 62 E-plane radiation patterns for the three ACPS folded dipole antenna elements at 3.3 GHz

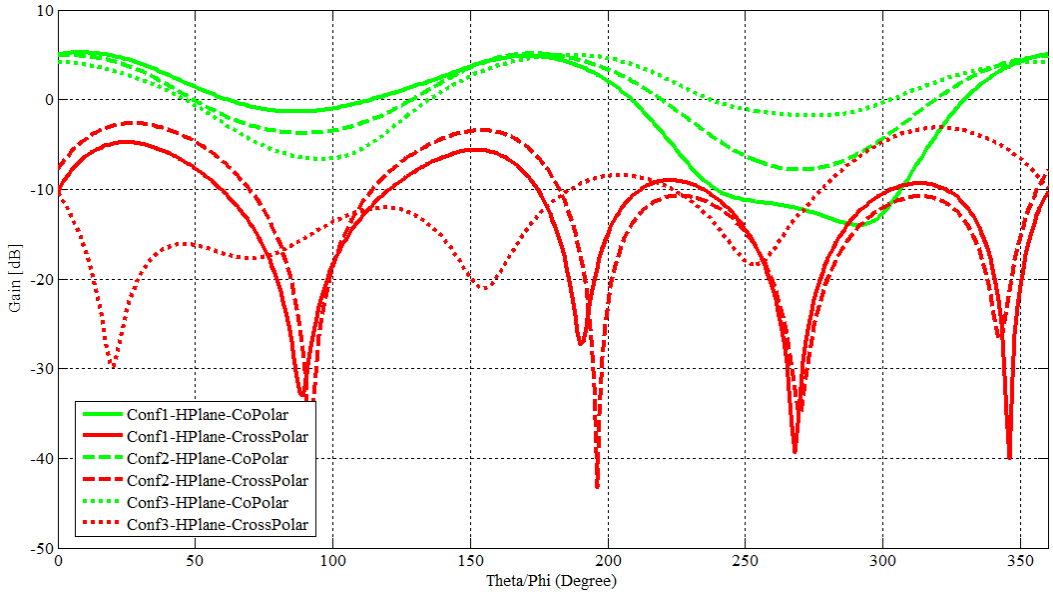

Figure 3- 63 H-plane radiation patterns for the three ACPS folded dipole antenna elements at 3.3 GHz

A simple equal-amplitude and equal-phase four-element linear array is used to find out the viability of the ACPS folded dipole as an array element. Four identical single element ACPS folded dipole antennas designed above are arranged along a straight line in x-axis as a linear array configuration. Simulation models of the ACPS folded dipole antenna element for configuration-II and configuration-III are given in Figure 3- 64 and Figure 3- 71, respectively. A simple corporate feed topology with binary dividers consists of quarter-wave transformers and symmetric T-junctions is used for each array.

A four-way power divider is designed in order to obtain equally distribute power to each single element antenna. Symmetric T-junctions are employed to divide power from a one-way to a two-way path. The symmetric T-junction lines are all designed to be 50 Ω so that the feeding network size is kept small. Also, three 35.4 Ω quarter-wavelength transformers are sufficient for the feeding network. As the 90 degree microstrip bend and T-junction discontinuities result in undesired reflection and radiation losses, the microstrip lines are mitered at each bent corner.

A center to center spacing L_{es} is defined between two adjacent single element antennas. Choosing the array structure and designing the feeding network, the element spacing L_{es} shall be determined next. Besides the mutual coupling effect between the individual antennas, grating lobes should be considered in this step. In order to avoid grating lobes completely, array spacing should be smaller than one-half wavelength of the maximum operating frequency. However, smaller spacing will increase mutual coupling. Effects of the element spacing on grating lobes are investigated. Analyses are carried out parametrically so that the effect on the characteristics in terms of return loss, radiation patterns and gain is investigated. At the end of these analyses the final value $L_{es} = 0.7\lambda_0 = 70\,\text{mm}$ is chosen to minimize the grating lobes level.

The dimensions defined for the feed network are summarized in Table 3- 3. The simulated return loss response, gain and radiation patterns of both configuration-II and configuration-III, respectively, are given in Figure 3- 65 through Figure 3- 70 and Figure 3- 72 through Figure 3- 77 below. Radiation patterns for two four-element uniform linear arrays are presented at three different frequencies which are 2.7 GHz, 3 GHz and 3.3 GHz, with respect to the lowest, middle and highest frequencies of the operating band of the antennas.

Table 3- 3 The dimensions defined for the feed network

Design Parameter	Value (mm)
W_{msx_fnx}	1,270
L_{msx_fnx}	7,500
W_{qwx_fnx}	2,118
L_{qwx_fnx}	15,890
L_{ax_fnx}	2,118
H_{ax_fnx}	0,889
M_{msx_fnx}	0,985
$L_{ms\_output\_fn}$	2,500
$W_{ms\_output\_fn}$	1,270
L_{es}	70

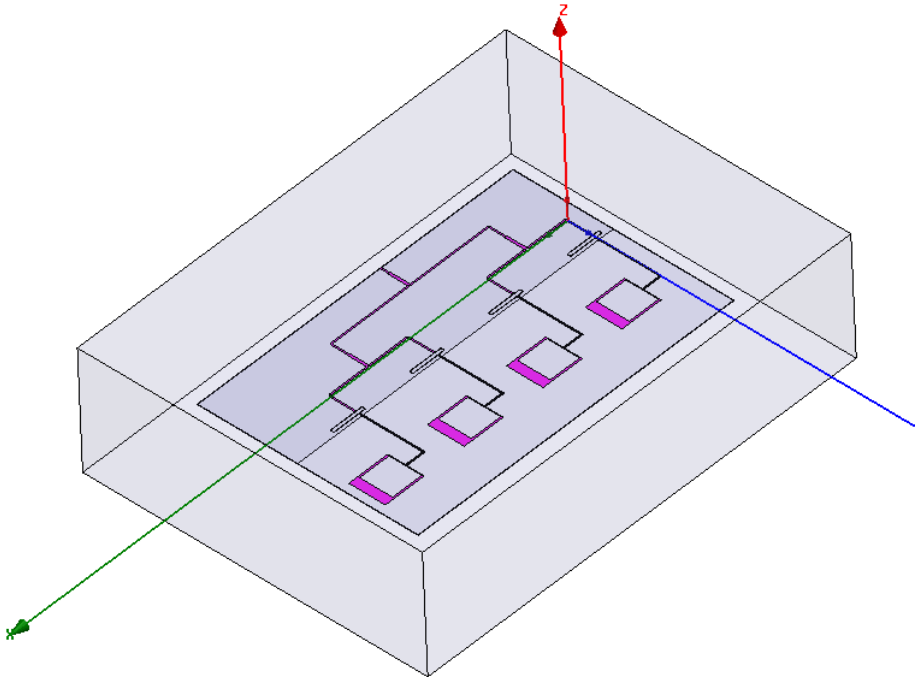

Figure 3- 64 Simulation model of the ACPS folded dipole array designed as configuration-II in Ansys HFSS®

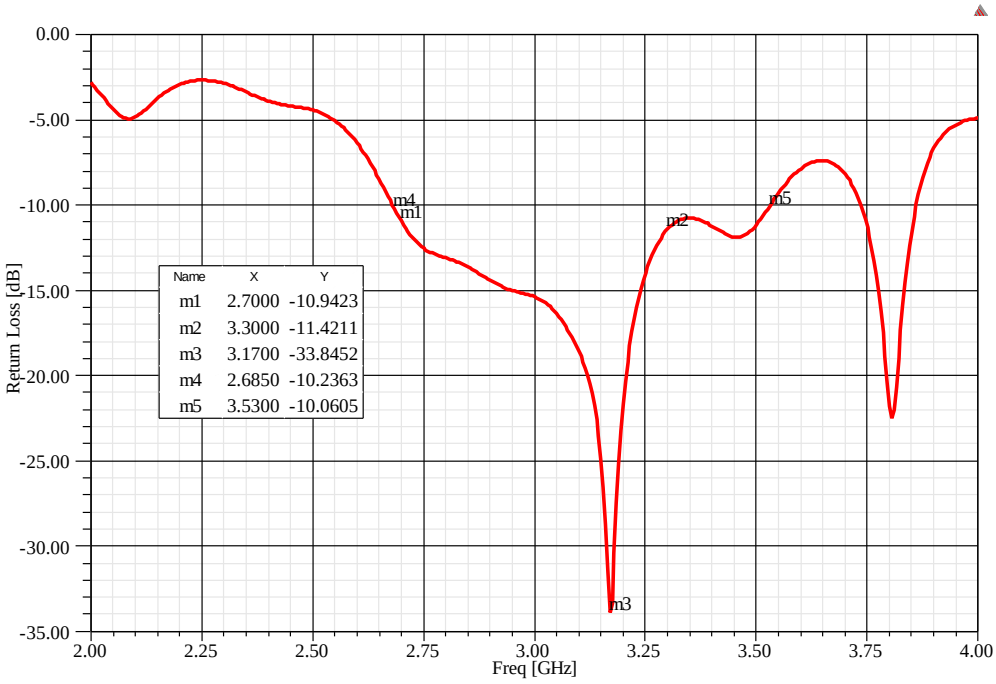

Figure 3- 65 Return loss of the ACPS folded dipole array designed as configuration-II

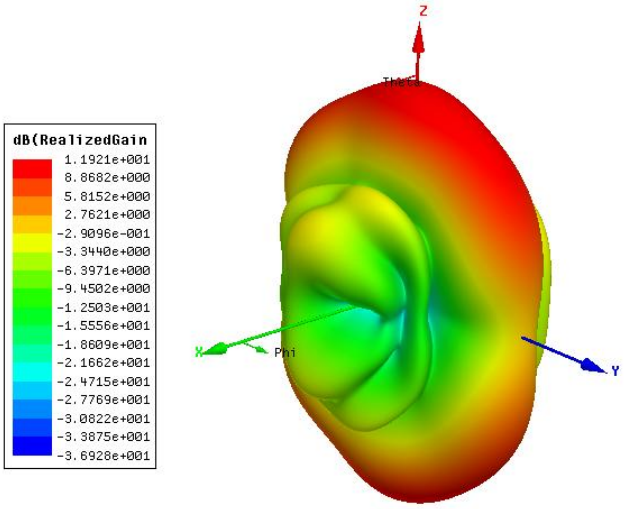

Figure 3- 66 3D radiation pattern of the ACPS folded dipole array designed as configuration-II at 3 GHz

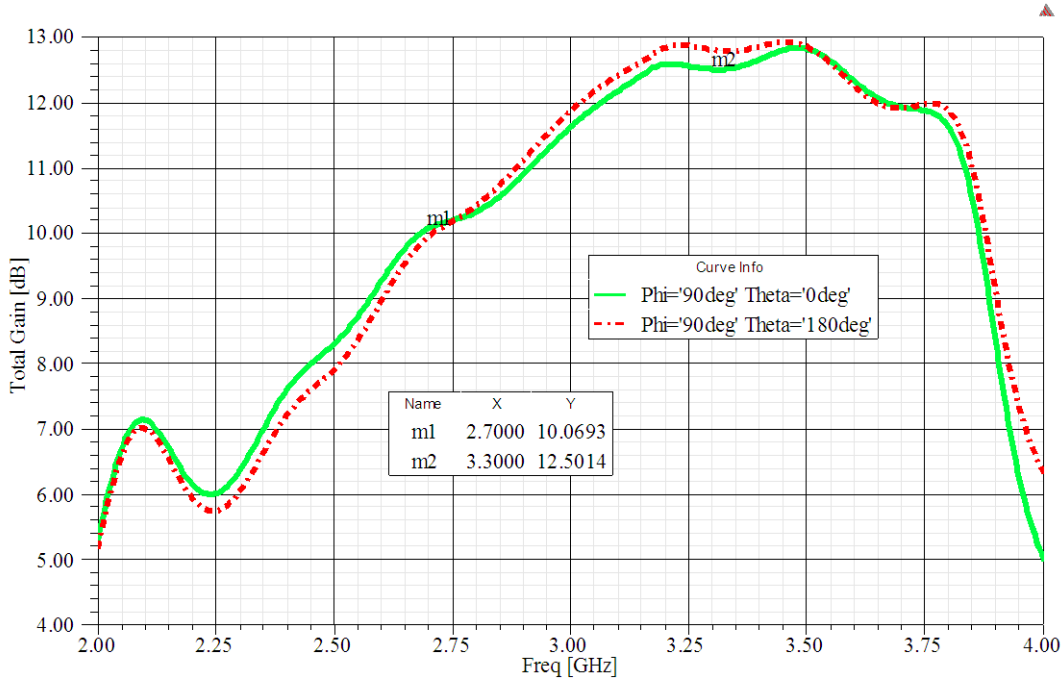

Figure 3- 67 Gains in bore-sight directions of the ACPS folded dipole array designed as configuration-II versus frequency

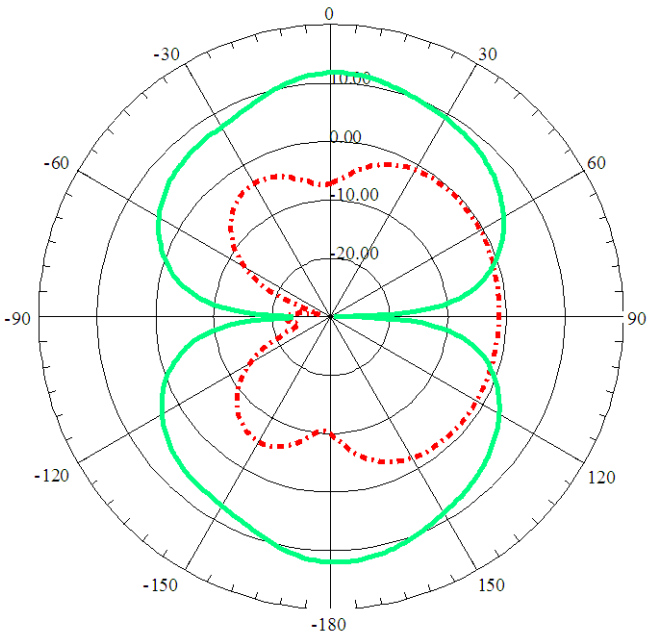

(a)

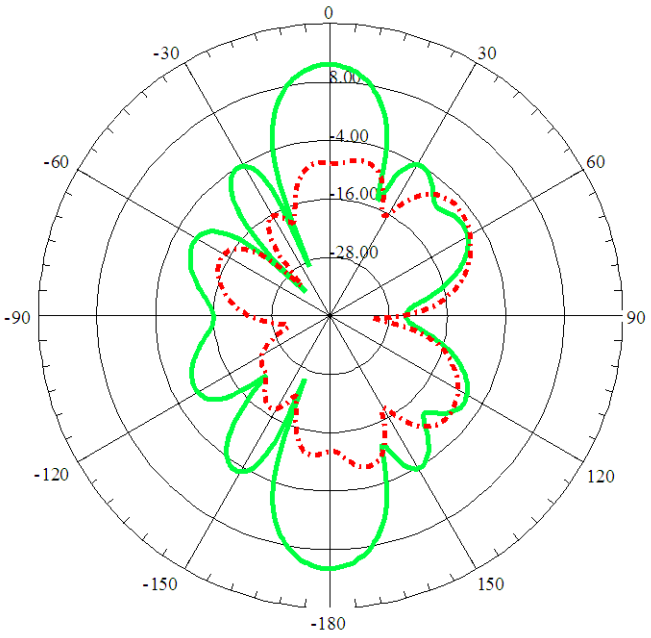

(b)

Figure 3- 68 Radiation patterns in terms of co and cross polarization of the ACPS folded dipole array designed as configuration-II at 3 GHz: (a) E-plane (b) H-plane

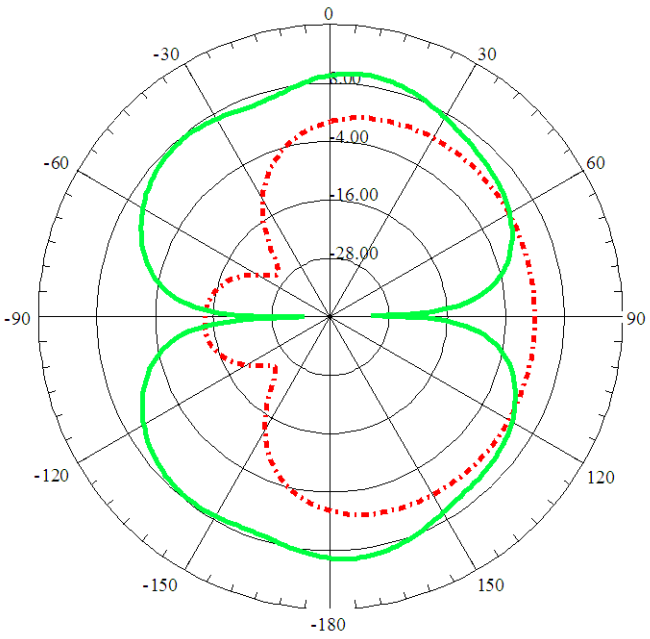

(a)

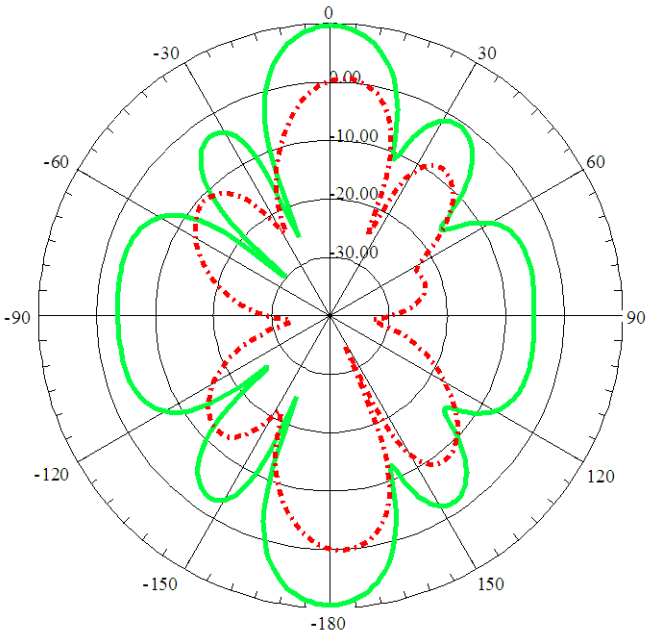

(b)

Figure 3- 69 Radiation patterns in terms of co and cross polarization of the ACPS folded dipole array designed as configuration-II at 2.7 GHz: (a) E-plane (b) H-plane

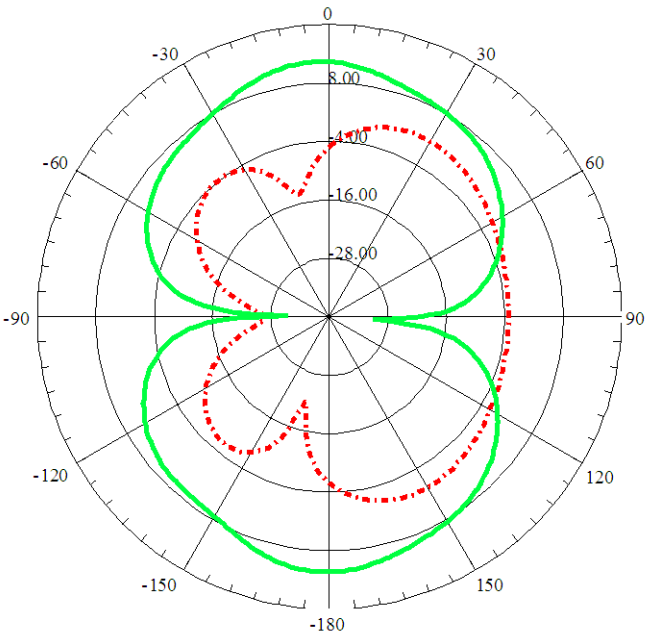

(a)

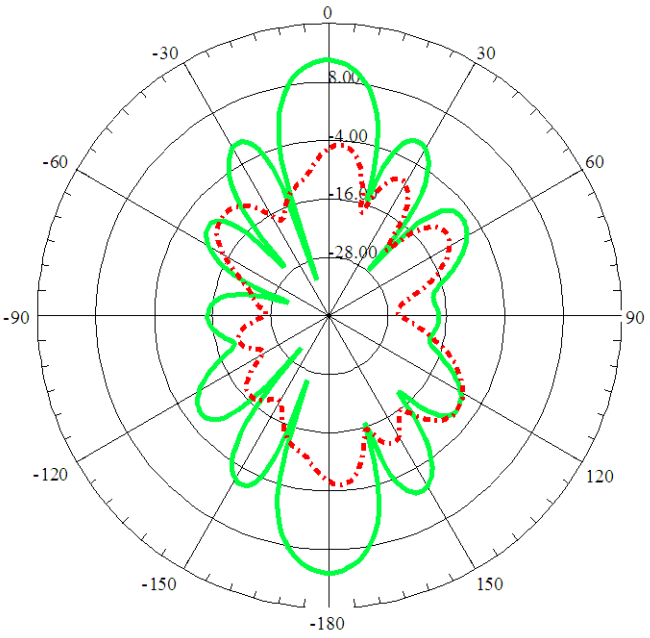

(b)

Figure 3- 70 Radiation patterns in terms of co and cross polarization of the ACPS folded dipole array designed as configuration-II at 3.3 GHz: (a) E-plane (b) H-plane

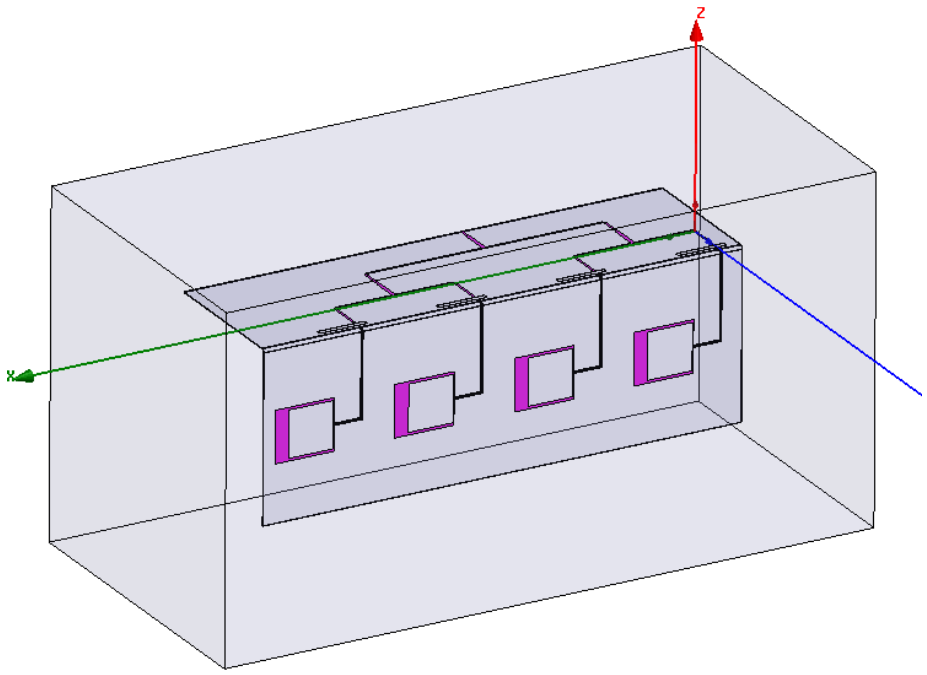

Figure 3- 71 Simulation model of the ACPS folded dipole array designed as configuration-III in Ansys HFSS®

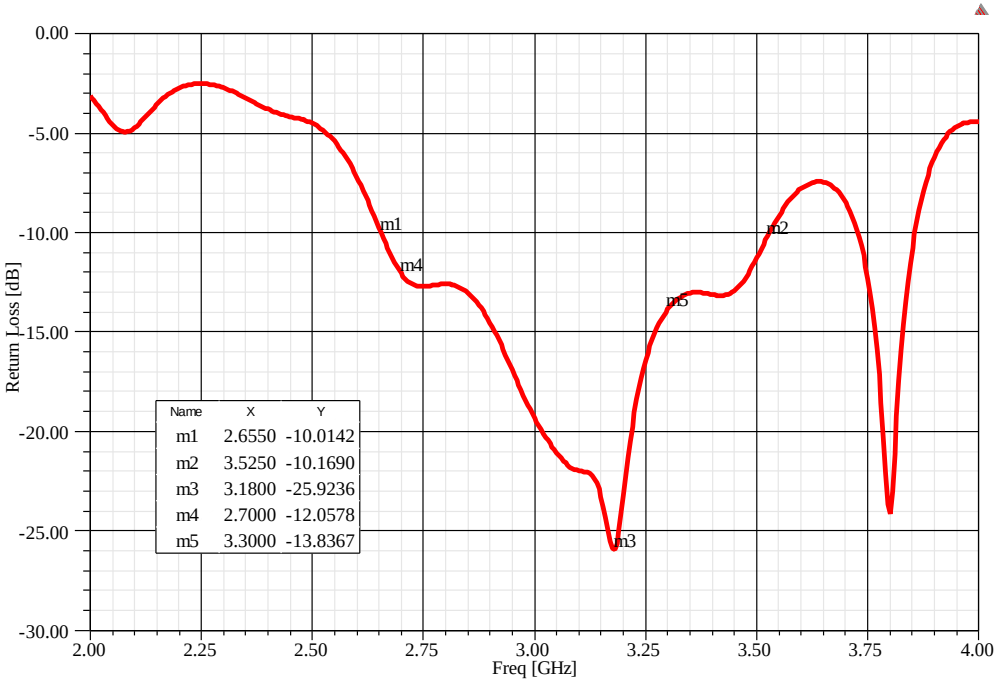

Figure 3- 72 Return loss of the ACPS folded dipole array designed as configuration-III

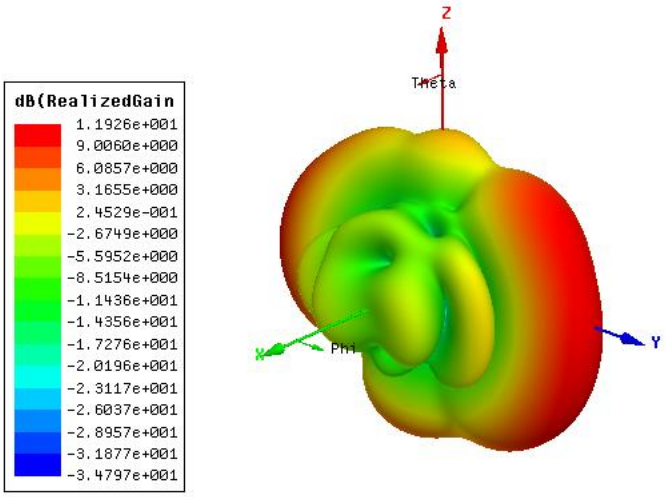

Figure 3- 73 3D radiation pattern of the ACPS folded dipole array designed as configuration-III at 3GHz

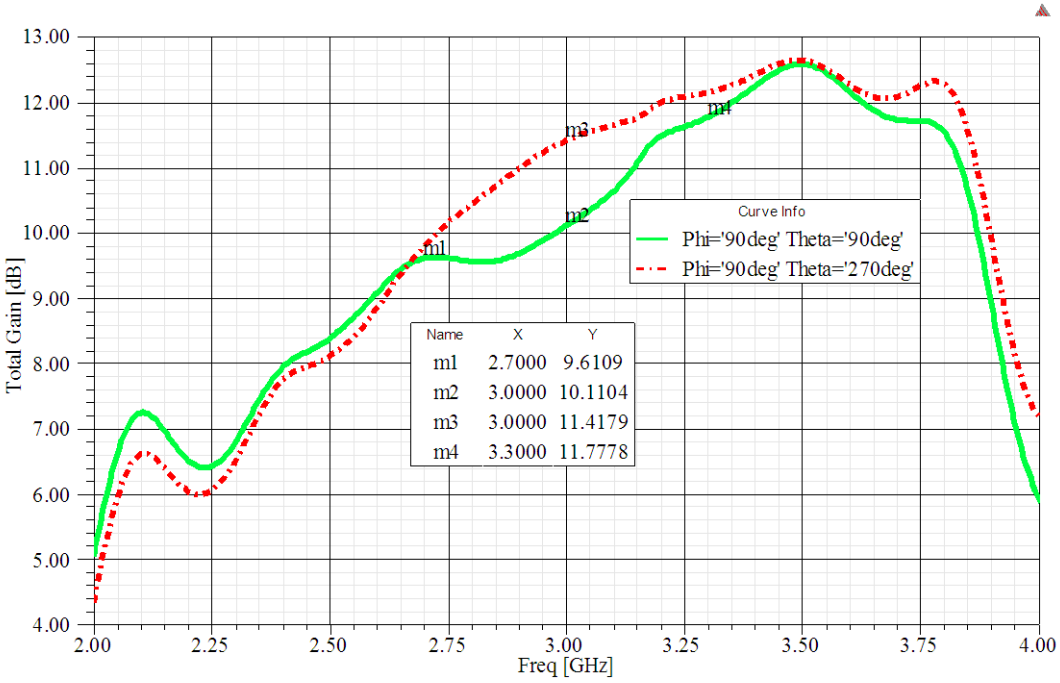

Figure 3- 74 Gains in bore-sight directions of the ACPS folded dipole array designed as configuration-III versus frequency

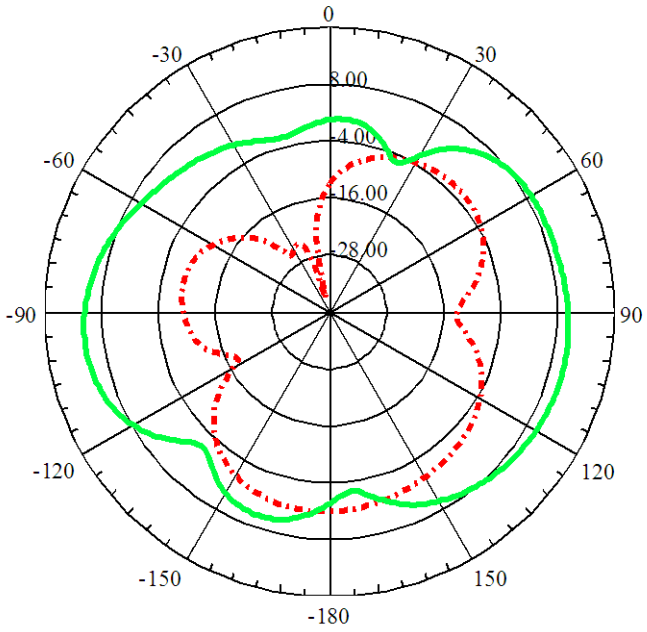

(a)

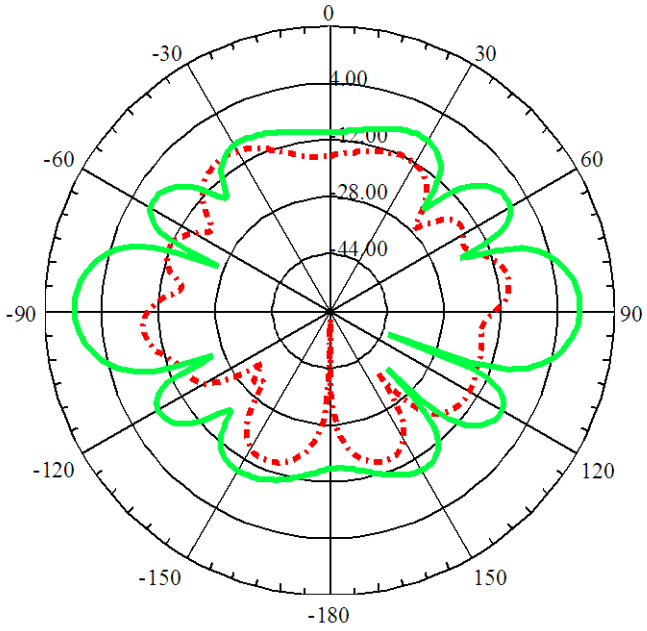

(b)

Figure 3- 75 Radiation patterns in terms of co and cross polarization of the ACPS folded dipole array designed as configuration-III at 3 GHz: (a) E-plane (b) H-plane

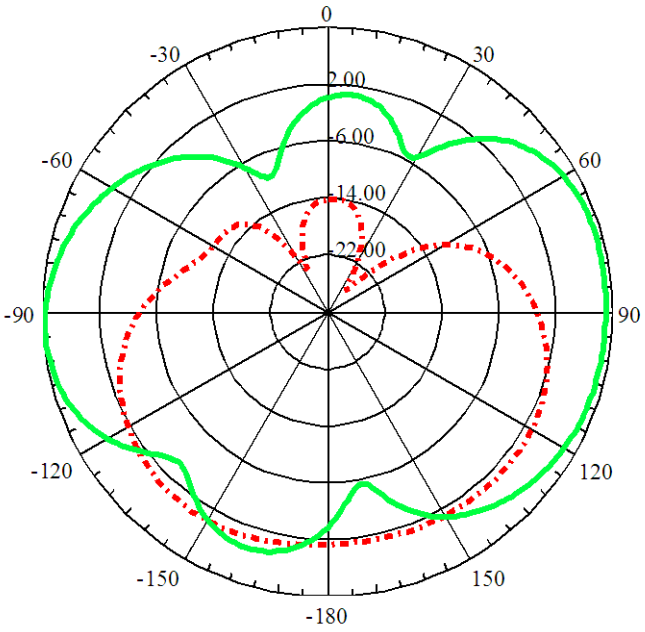

(a)

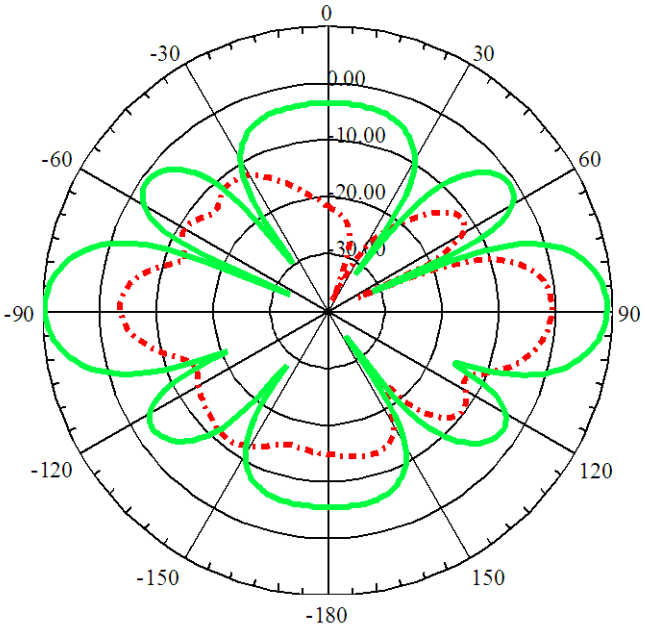

(b)

Figure 3- 76 Radiation patterns in terms of co and cross polarization of the ACPS folded dipole array designed as configuration-III at 2.7 GHz: (a) E-plane (b) H-plane

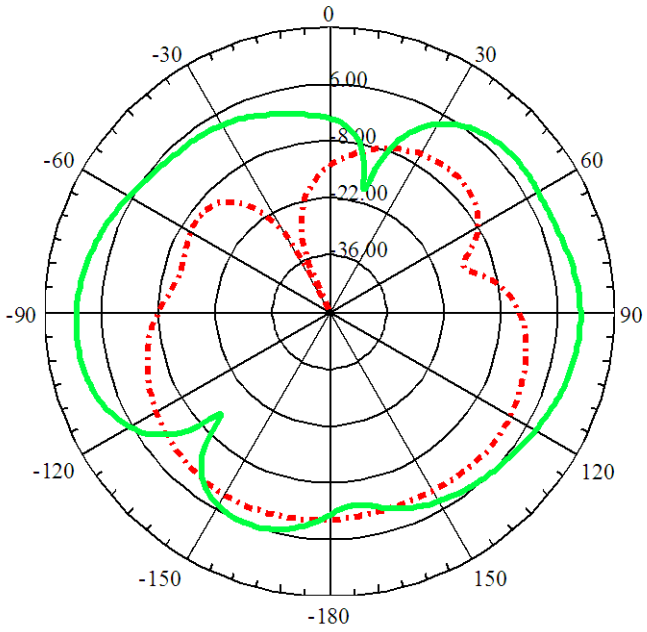

(a)

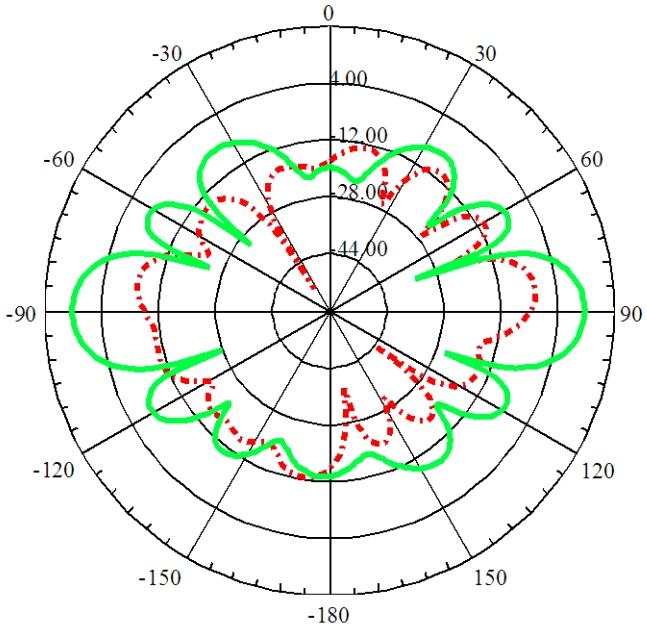

(b)

Figure 3- 77 Radiation patterns in terms of co and cross polarization of the ACPS folded dipole array designed as configuration-III at 3.3 GHz: (a) E-plane (b) H-plane

CHAPTER 4

FABRICATIONS AND MEASUREMENTS OF ACPS FOLDED DIPOLE ANTENNA AND ARRAY

4.1 Fabrications of Designed ACPS Folded Dipole Antenna and Array

To this point, the design methodology for the ACPS folded dipole antenna is detailed and the ACPS folded dipole antenna models are designed in different configurations. In order to prove the performance of the designed antennas, single element antenna and four-element linear array antenna prototypes are produced and measured. The antenna models designed as configuration-II in Chapter 3 are fabricated in the facilities of ASELSAN Inc. Laboratories. Laser PCB scraping equipment produced by LPKF Laser & Electronics Group is used for fabrication of both ACPS folded dipole antennas.

The material used as dielectric slab is RT/Duroid® 6002 High Frequency Laminate of Rogers Corporation [31]. For bending process of the fabricated as configuration-II both single element antenna and array, the base laminate material is required to be bendable on the curved surfaces. Thus, 6002 laminate is chosen due to its powerful elasticity features when compared to other PCBs as mentioned earlier. The antennas are designed for the 6002 laminate with copper metallization on both sides. The relative dielectric constant of this substrate is 2.94 where the substrate and metallization thickness are 0.508 mm and 0.018mm, respectively. The ACPS folded dipole, balun and microstrip feeding line are etched on the top layer of the dielectric substrate where the truncated ground plane is positioned on the bottom layer. The total area of the substrate for the single ACPS folded dipole antenna

element and array are chosen approximately 70 mm x 124.5 mm and 280mm x 181.5, respectively.

A 50 Ω SMA female connector of Huber & Suhner Corporation is used to feed the microstrip line. The center pin of the SMA connector is soldered to the microstrip feeding line, and the outer surface of the SMA connector is also soldered to the truncated ground plane in order to realize ground connection of the feeding. The fabricated single element ACPS folded dipole antenna and four element linear ACPS folded dipole array antenna are given in Figure 4- 1 and Figure 4- 2, respectively.

After the measurements of the single element antenna and array for configuration-II, bending process is implemented to this configuration of the antennas in order to form the configuration-III by using an adhesive substance and a foam backplane. Double sided tape of 3M™ is used as adhesive for bonding the antennas to the foam backplane along the truncated ground plane. The step by step bending processes for the single element ACPS folded dipole antenna and four element linear ACPS folded dipole antenna array are presented in Figure 4- 3 and Figure 4-4, respectively. Since these bending processes are done manually, the substrate and the strips cannot be curved with the radius $R_{subsbend}$ determined in Chapter 3 and cannot be curved at starting point of the rotation. The top side of the antennas is also pressed manually after bonding which may create some discrepancies on the performance of the antenna.

After the production of the antennas is completed, the characteristics of the antennas are measured.

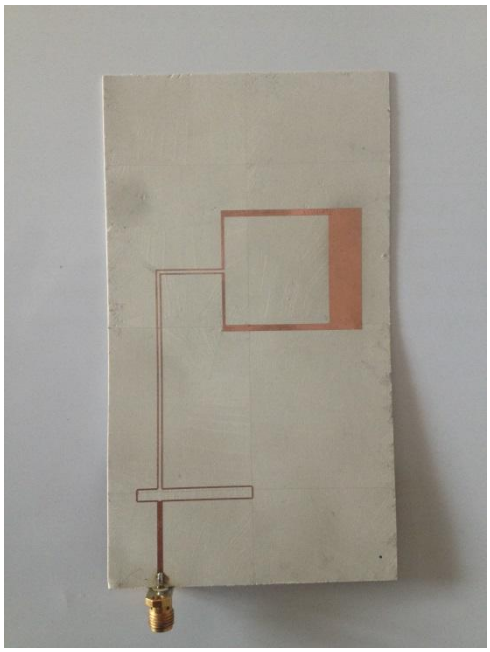

(a)

(b)

Figure 4- 1 Top and bottom side of the single element ACPS folded dipole antenna fabricated as configuration-II: (a) Top (b) Bottom

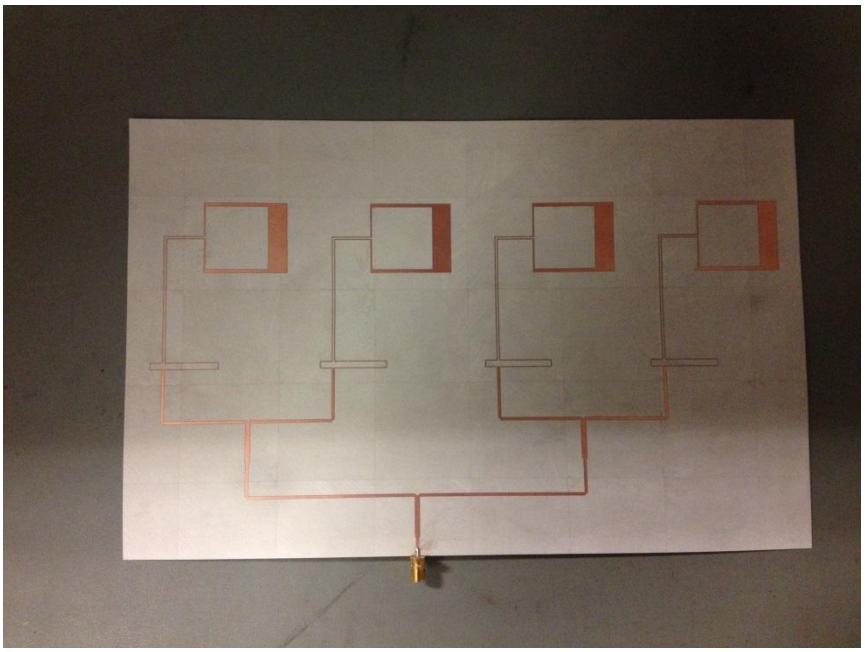

(a)

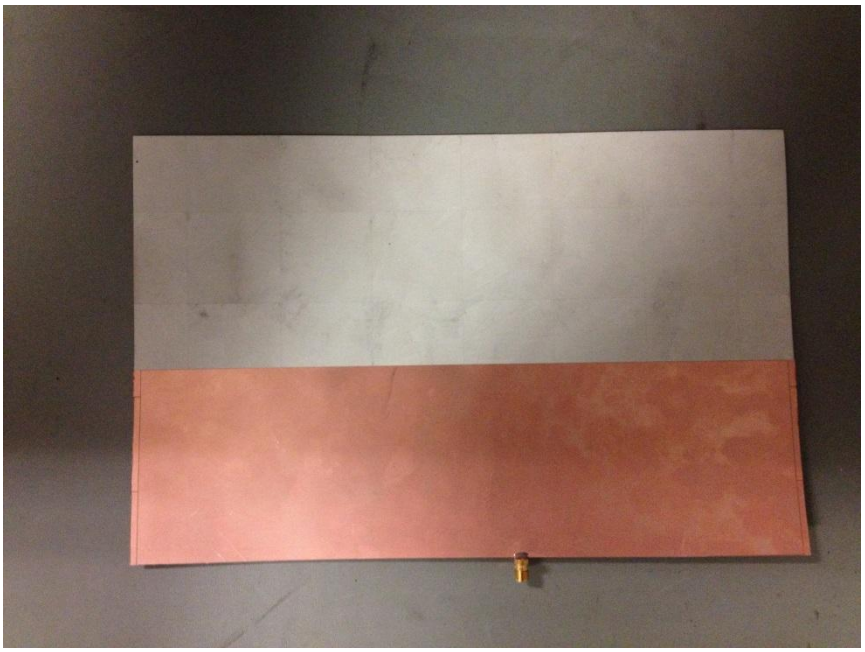

(b)

Figure 4- 2 Top and bottom side of the four element linear ACPS folded dipole array antenna fabricated as configuration-II: (a) Top (b) Bottom

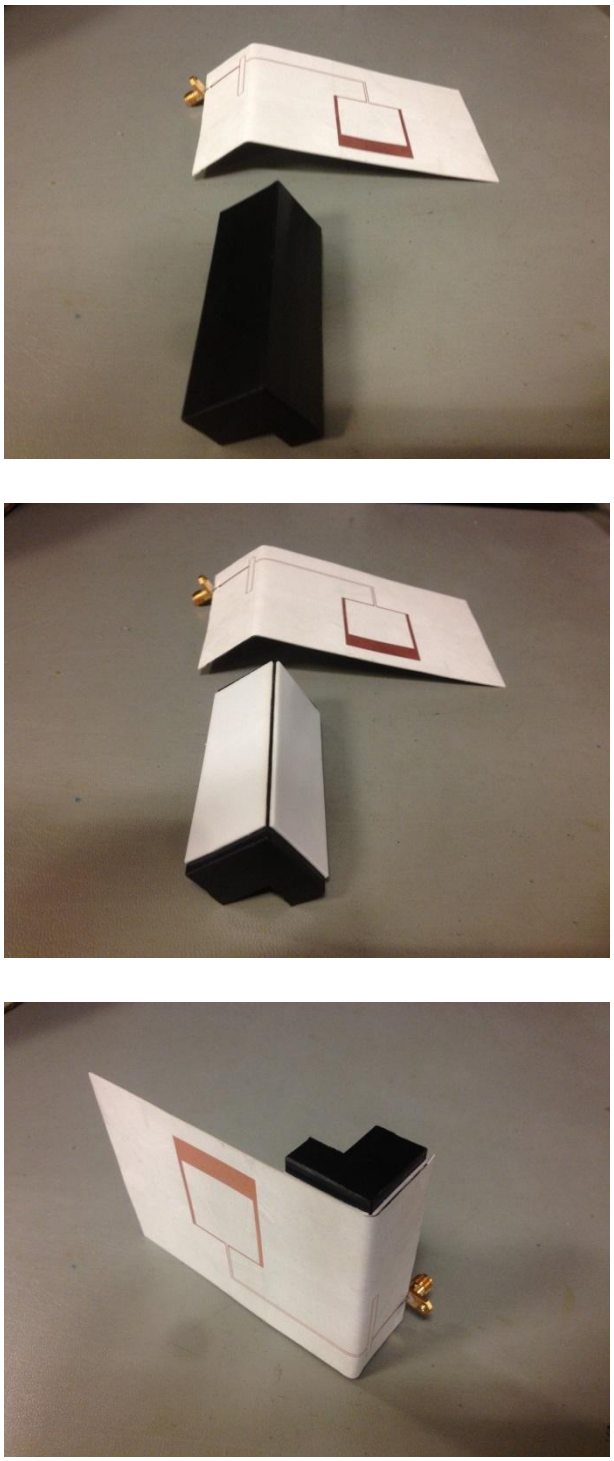

Figure 4- 3 Bending process of the single element ACPS folded dipole antenna fabricated as configuration-II in order to obtain the configuration-III

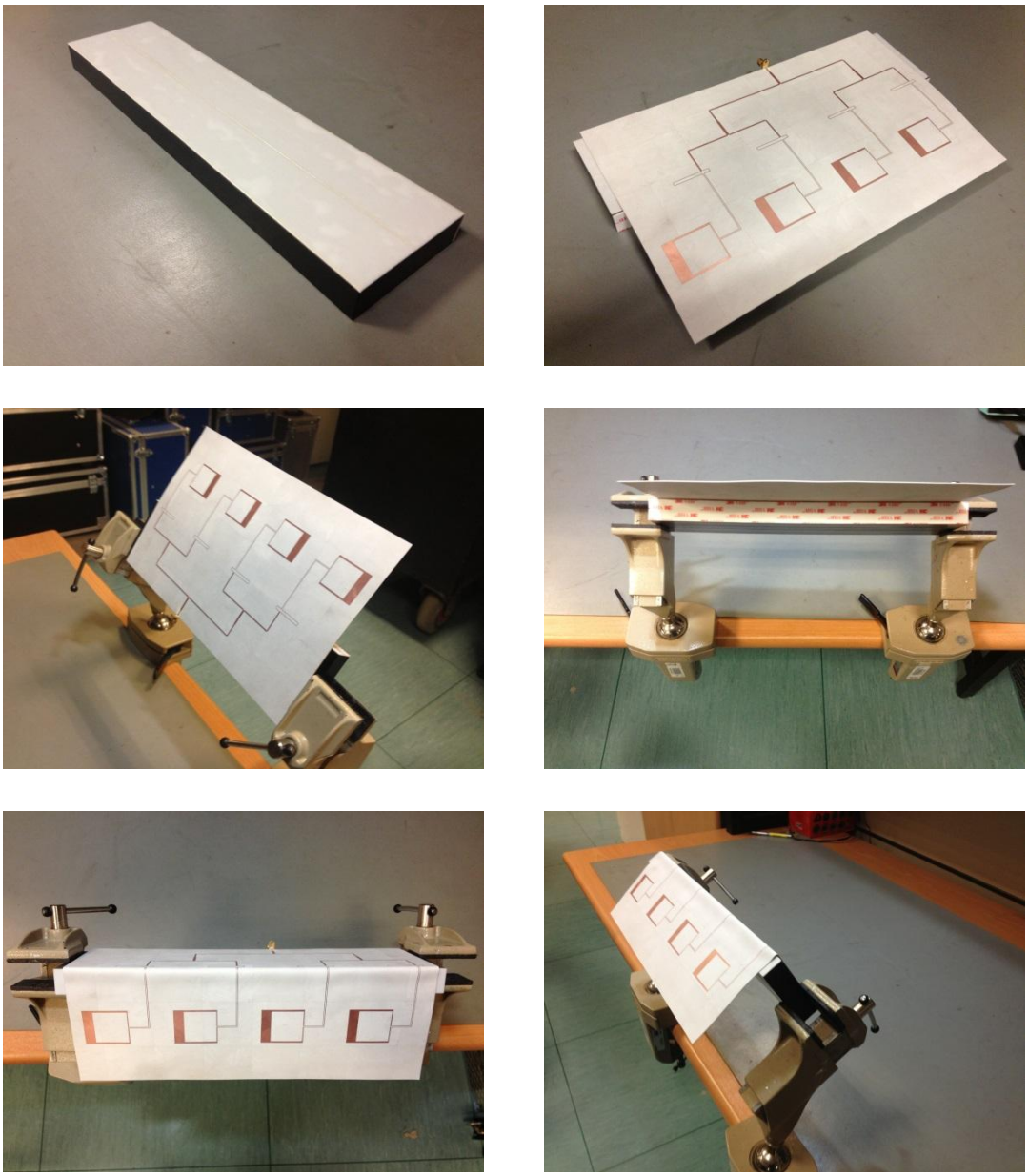

Figure 4- 4 Bending process of the four element linear ACPS folded dipole array antenna fabricated as configuration-II in order to obtain the configuration-III

4.2 Measurements of Fabricated ACPS Folded Dipole Antenna and Array

The return loss responses, radiation patterns and gains of the single element ACPS folded dipole antennas and the four-element ACPS folded dipole array antennas for two different configurations are measured and compared with simulation results in this section.

The return loss response is measured to see the matching between an antenna and its feeding structure. This measurement is done using the N5222A PNA network analyzer of Agilent Technologies. Before the measurement, the network analyzer is calibrated in the S-Band connecting open, short and load calibration standards to the Port-1 of the analyzer one by one. The single element antenna is connected to the same port next and return loss response of the antenna is obtained in dB through one port measurement with the calibrated network analyzer. The return loss response of the array is measured in the same way.

Return loss measurement are performed for the single ACPS folded dipole antennas and arrays which are fabricated as configuration-II and configuration-III. Return loss response measurement results compared to the simulation results for these antennas in S-band are displayed in Figure 4- 5, Figure 4- 6, Figure 4- 7 and Figure 4- 8, respectively.

Figure 4- 5 shows that the measurement result of the ACPS folded dipole antenna fabricated as configuration-II is in accordance with the simulation result.

In addition, as seen from Figure 4- 6, there exist differences in return loss characteristics between simulated and measured reflection coefficients of the ACPS folded dipole antenna fabricated as configuration-III. There is a shift in frequency of the order of 1.5%, estimated at 3.05 GHz.

Although small variations between the measured and simulated return loss response are seen from Figure 4- 7 and Figure 4- 8, the measured and simulated results of the four element ACPS folded dipole array antennas almost agree.

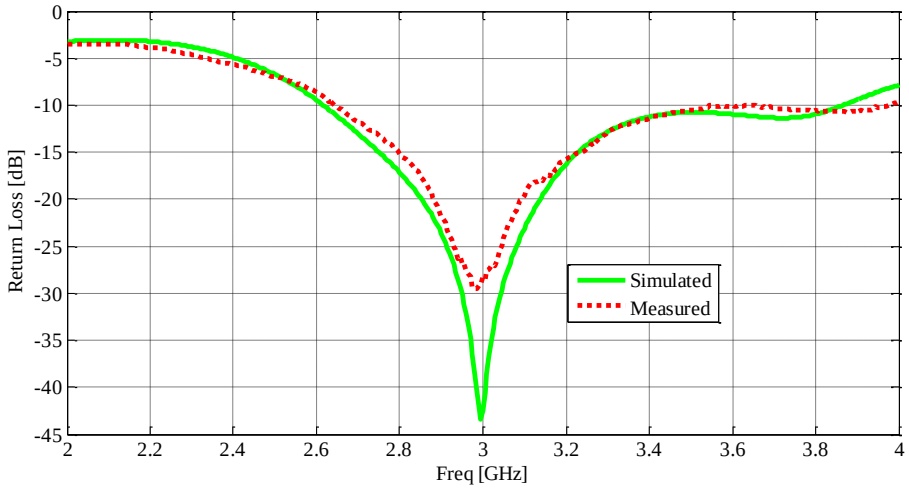

Figure 4- 5 Measured and simulated return loss of the ACPS folded dipole antenna element designed as configuration-II

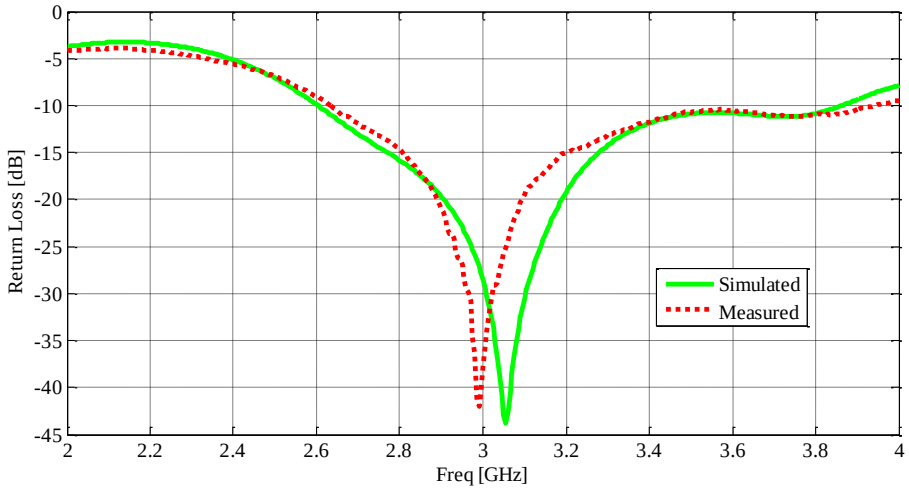

Figure 4- 6 Measured and simulated return loss of the ACPS folded dipole antenna element designed as configuration-III

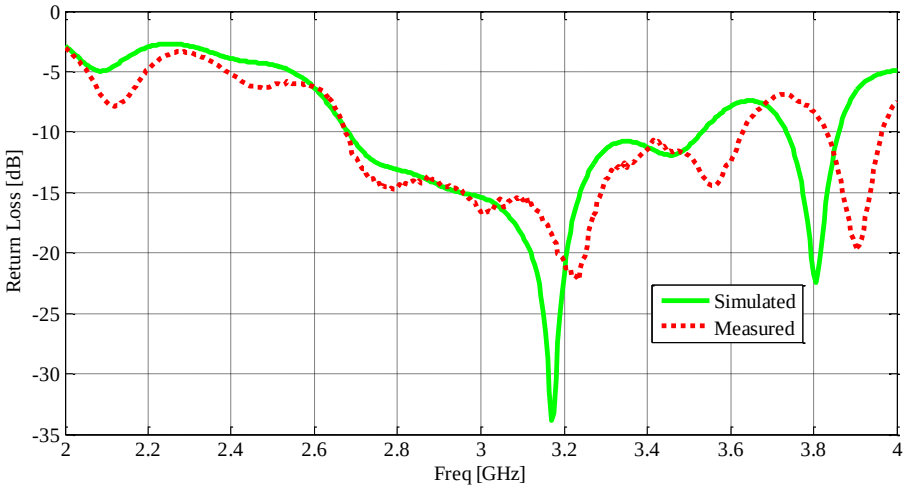

Figure 4- 7 Measured and simulated return loss of the ACPS folded dipole antenna array designed as configuration-II

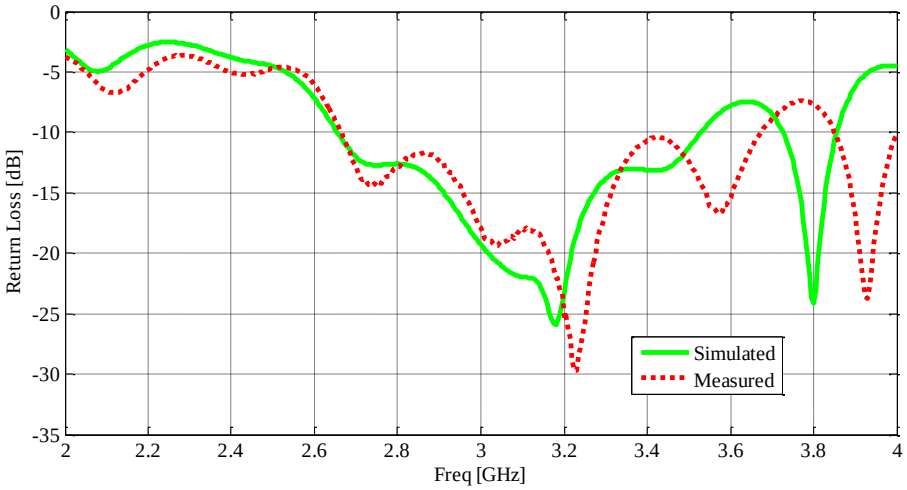

Figure 4- 8 Measured and simulated return loss of the ACPS folded dipole antenna array designed as configuration-III

After the bandwidth requirement of the antennas is fulfilled, radiation patterns of the antennas for both configurations are explored. StarLab Spherical Nearfield Measurement System of SATIMO is used for obtaining the far field patterns and far field measurement results are compared with simulation results in terms of gain and radiation patterns. The near field measurement setups are presented in Figure 4- 9, Figure 4- 10 and Figure 4- 11.

The simulated and measured gains versus frequency in the S-band for the single element ACPS folded dipole antennas and four-element linear array designed as configuration-III are presented in Figure 4- 12, Figure 4- 13 and Figure 4- 14, respectively. Variation between the measured and simulated gains of the single element ACPS folded dipole antennas, given in Figure 4- 12 and Figure 4- 13, is within 2.5 dB. This may result from the higher dielectric losses of the substrate or the measurement error in the anechoic near field measurement system.

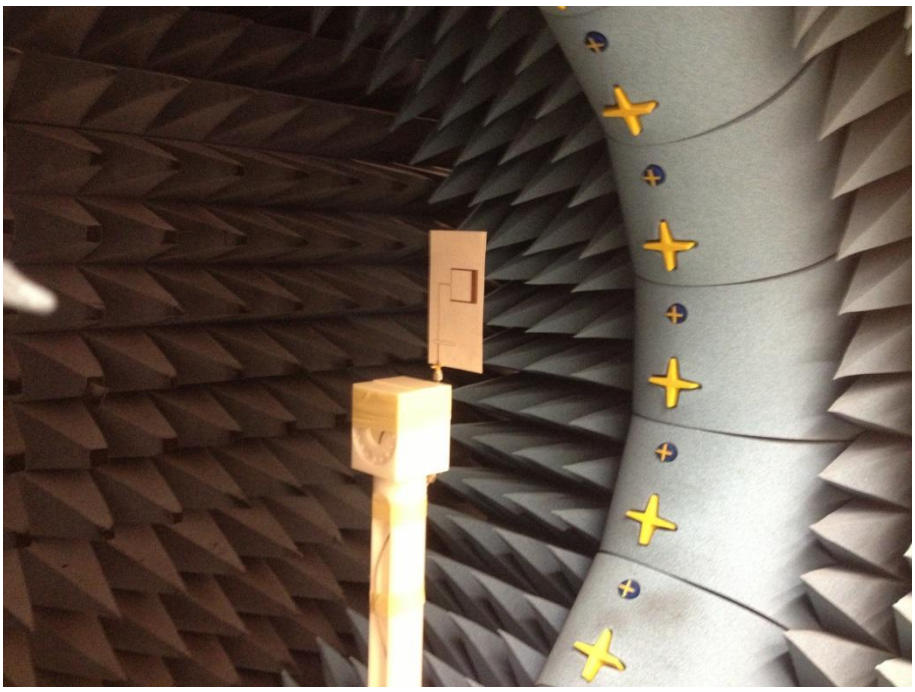

Figure 4- 9 Near field measurement set-up for the single element ACPS folded dipole antenna fabricated as configuration-II

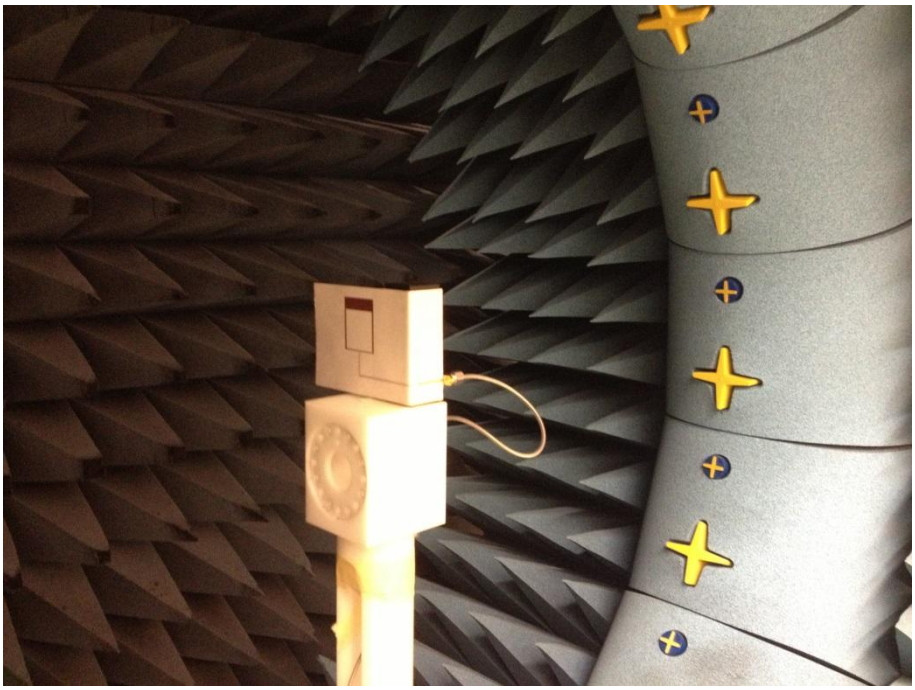

Figure 4- 10 Near field measurement set-up for the single element ACPS folded dipole antenna fabricated as configuration-III

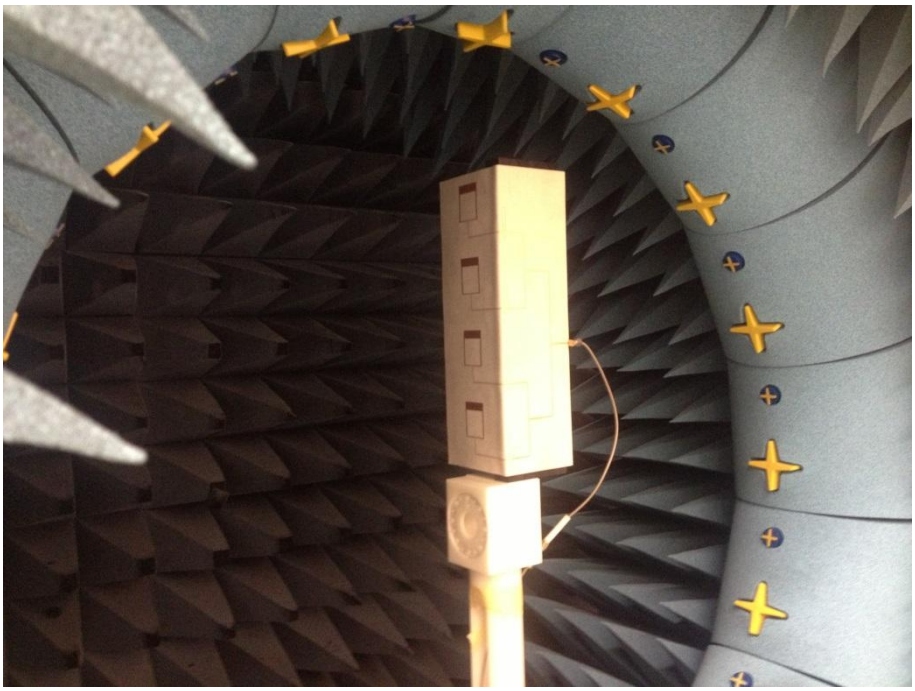

Figure 4- 11 Near field measurement set-up for the four element linear ACPS folded dipole array antenna fabricated as configuration-III

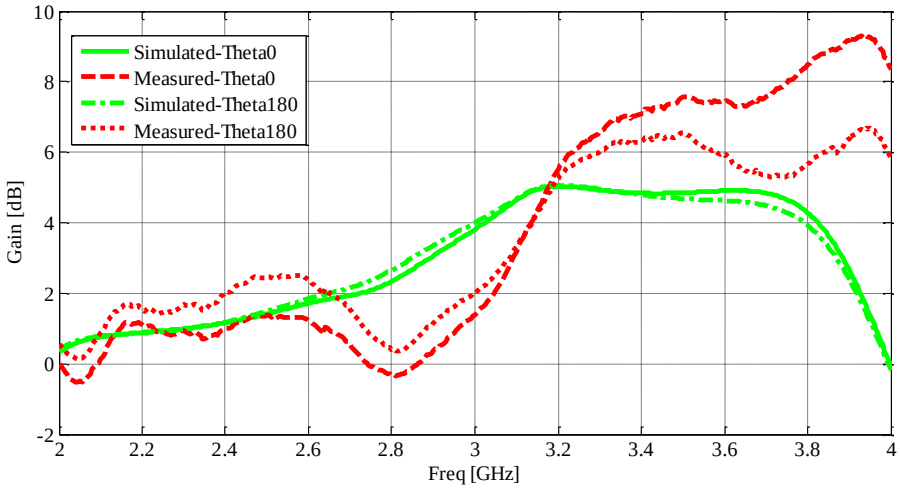

Figure 4- 12 Measured and simulated gains in bore-sight directions of the ACPS folded dipole antenna element designed as configuration-II

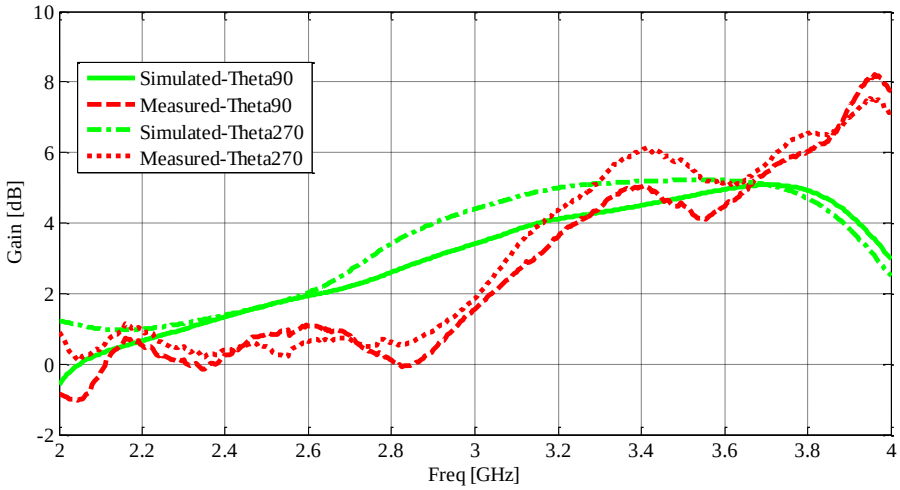

Figure 4- 13 Measured and simulated gains in bore-sight directions of the ACPS folded dipole antenna element designed as configuration-III

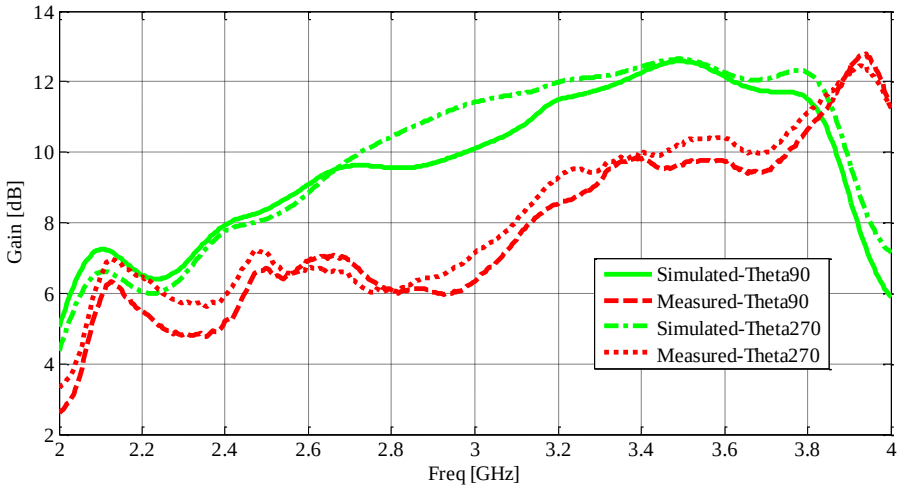

Figure 4- 14 Measured and simulated gains in bore-sight directions of the ACPS folded dipole antenna array designed as configuration-III

Radiation pattern measurements are done on the plane of polarization and the plane perpendicular to the polarization. The plane of polarization, also known as E-plane, is vertical in case of a vertically polarized ACPS folded dipole antenna configuration. H-plane is the plane perpendicular to the polarization and it is the horizontal plane in case of a vertically polarized ACPS folded dipole antenna configuration. In addition, the radiation patterns are measured at three different frequencies corresponding to the lowest, middle and highest frequencies of the operating band of the antennas in order to determine any frequency dependence of the patterns.

The comparison of measured and simulated results for the radiation patterns in terms of co and cross polarization in both E-plane and H-plane are illustrated in Figure 4- 15 through Figure 4- 32. It can be said that the measured and simulated patterns of the single element ACPS folded dipole antenna are fairly the same.

Radiation patterns in terms of co and cross polarization of the array for the E-plane and H-plane are exhibited in Figure 4- 33 through Figure 4- 41. The measured and simulated co and cross polar radiation patterns of the array with the main beams in the broadside directions are consistent in operating frequency band.

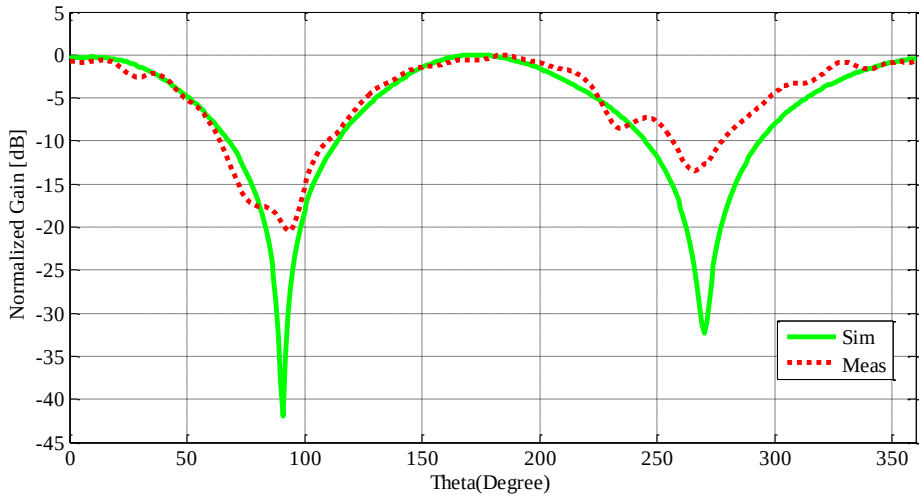

(a)

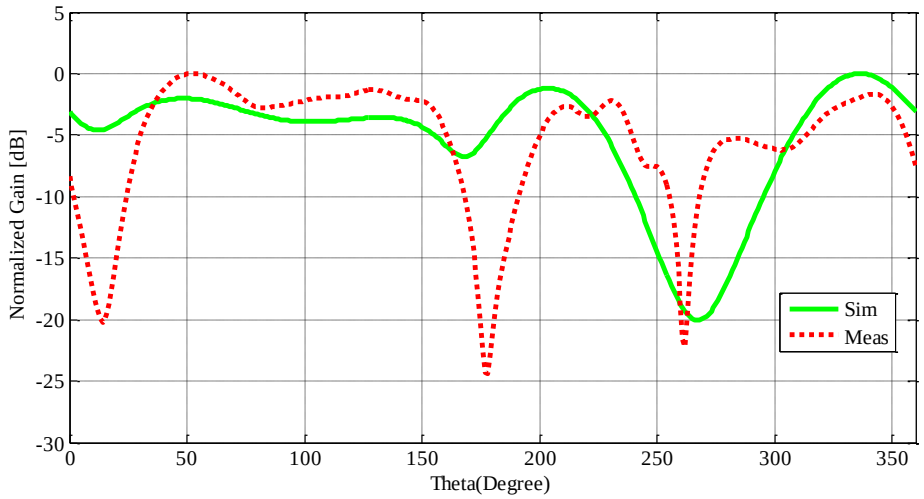

(b)

Figure 4- 15 Measured and simulated E-plane radiation patterns of the ACPS folded dipole antenna element designed as configuration-II at 3 GHz with the normalized gain: (a) Co-polar (b) Cross-polar

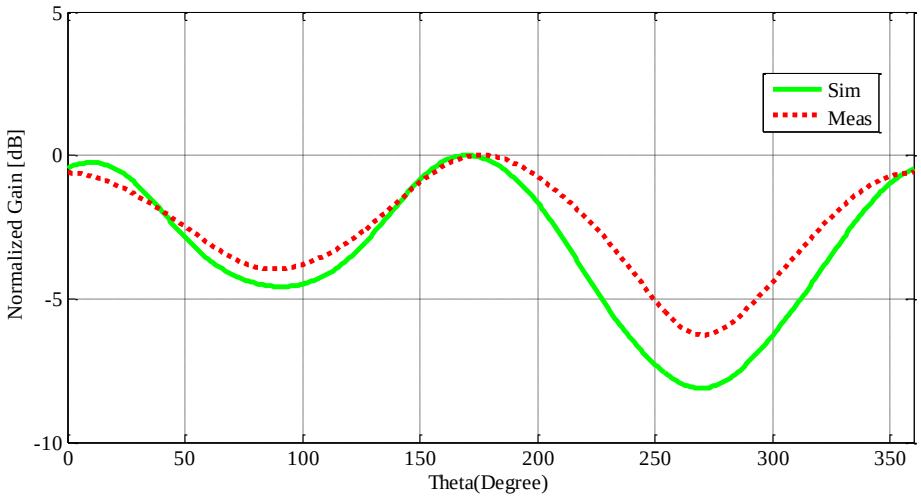

(a)

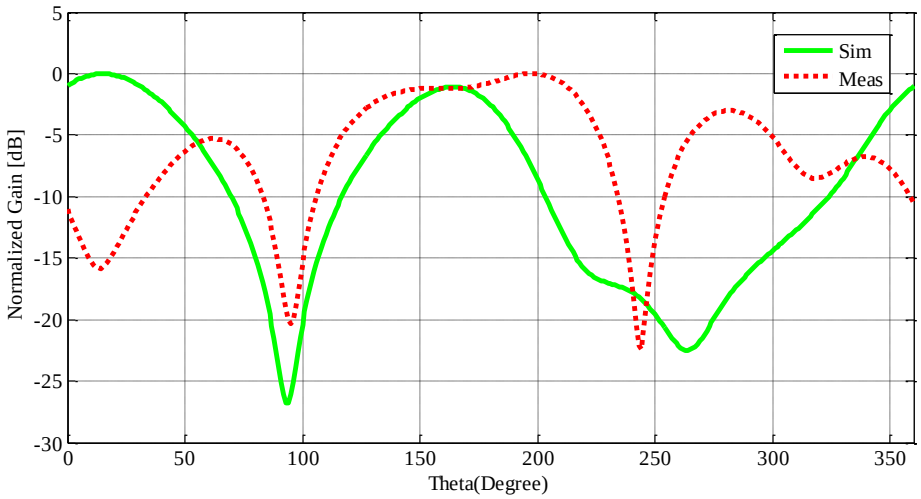

(b)

Figure 4- 16 Measured and simulated H-plane radiation patterns of the ACPS folded dipole antenna element designed as configuration-II at 3 GHz with the normalized gain: (a) Co-polar (b) Cross-polar

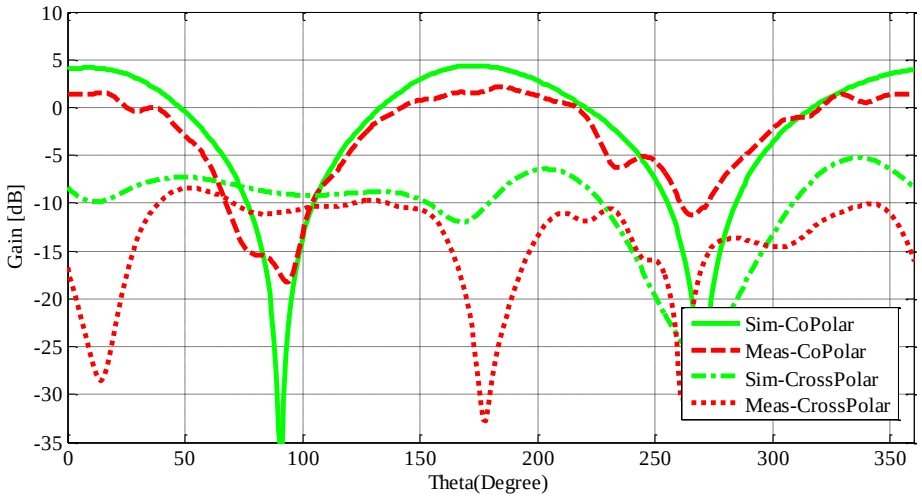

(a)

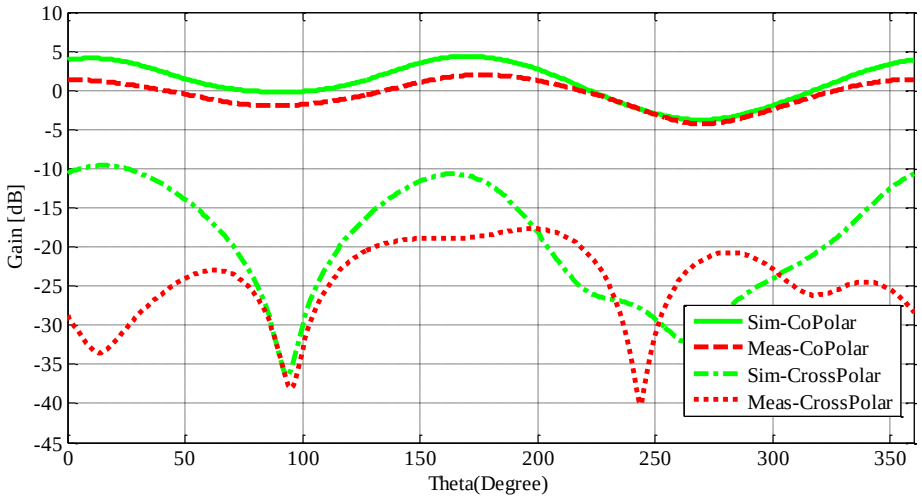

(b)

Figure 4- 17 Measured and simulated radiation patterns in terms of co and cross polarization of the ACPS folded dipole antenna element designed as configuration-II at 3 GHz: (a) E-plane (b) H-plane

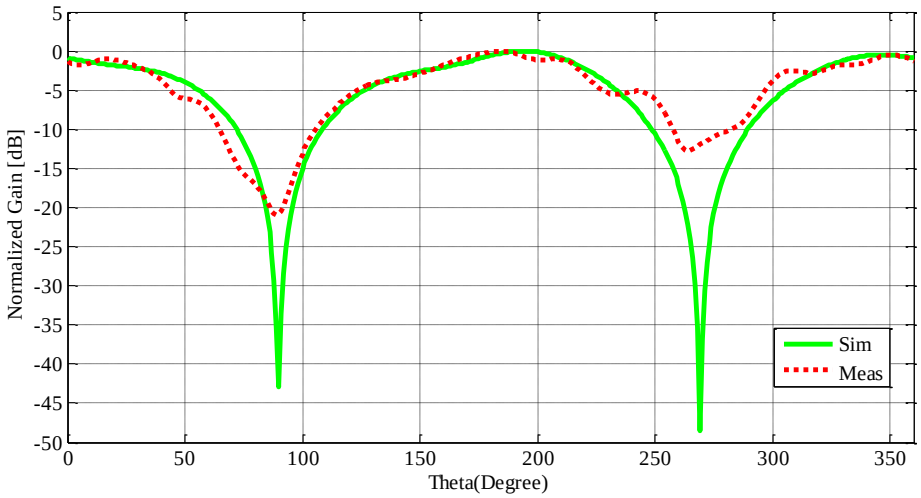

(a)

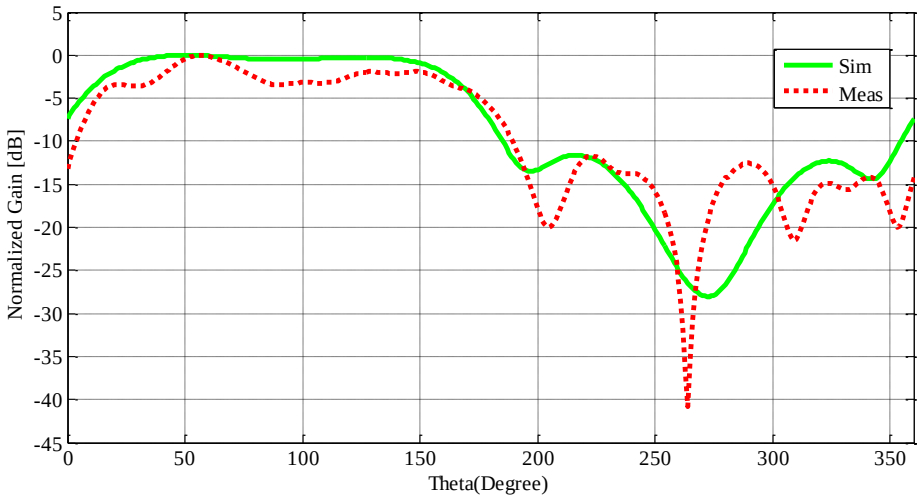

(b)

Figure 4- 18 Measured and simulated E-plane radiation patterns of the ACPS folded dipole antenna element designed as configuration-II at 2.7 GHz with the normalized gain: (a) Co-polar (b) Cross-polar

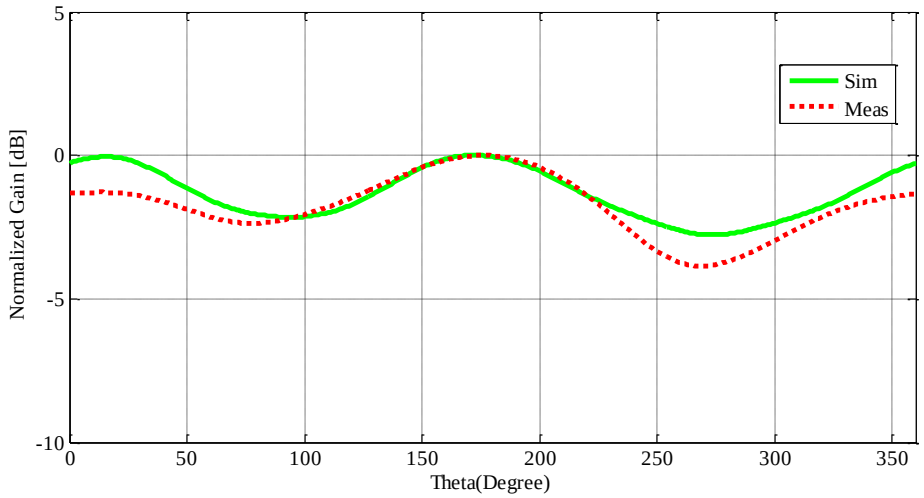

(a)

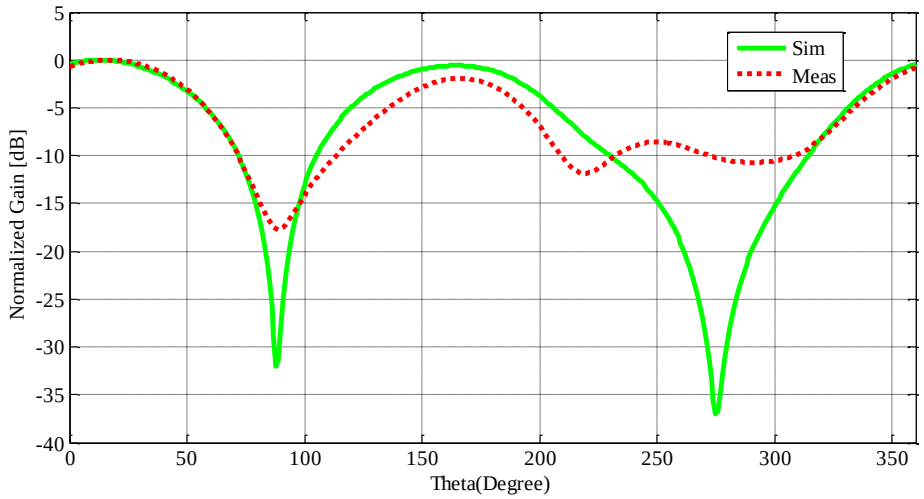

(b)

Figure 4- 19 Measured and simulated H-plane radiation patterns of the ACPS folded dipole antenna element designed as configuration-II at 2.7 GHz with the normalized gain: (a) Co-polar (b) Cross-polar

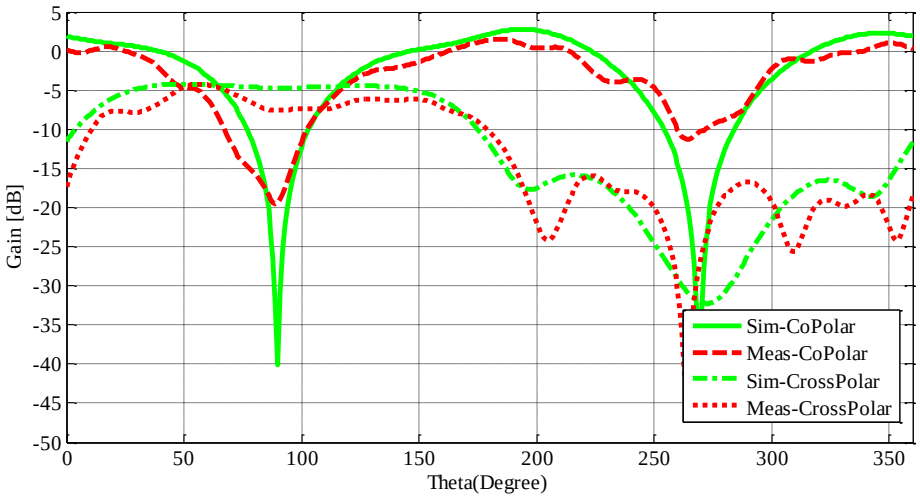

(a)

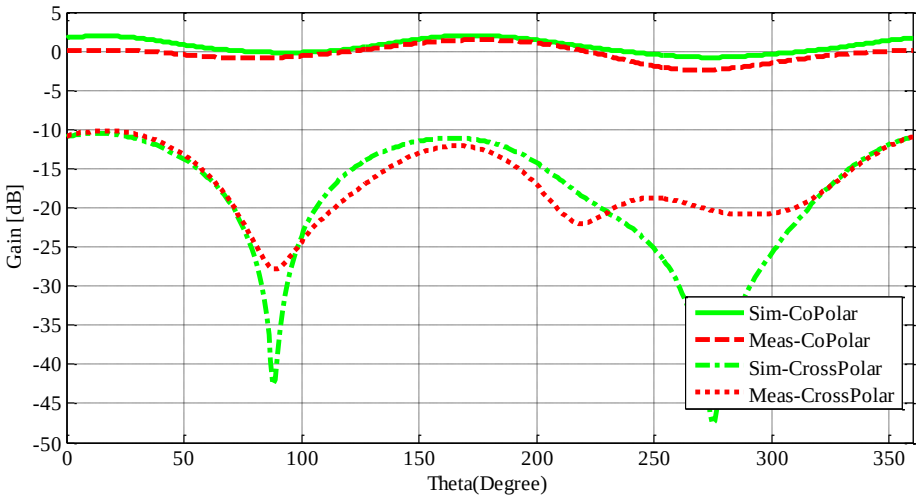

(b)

Figure 4- 20 Measured and simulated radiation patterns in terms of co and cross polarization of the ACPS folded dipole antenna element designed as configuration-II at 2.7 GHz: (a) E-plane (b) H-plane

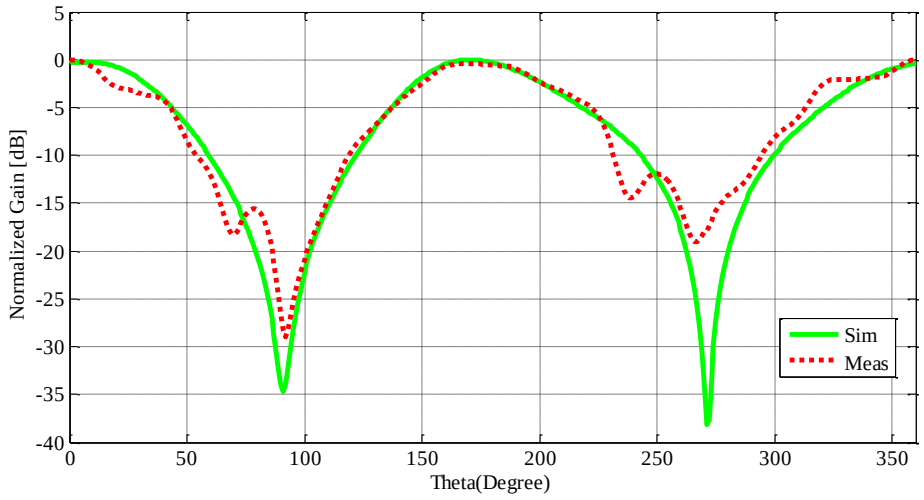

(a)

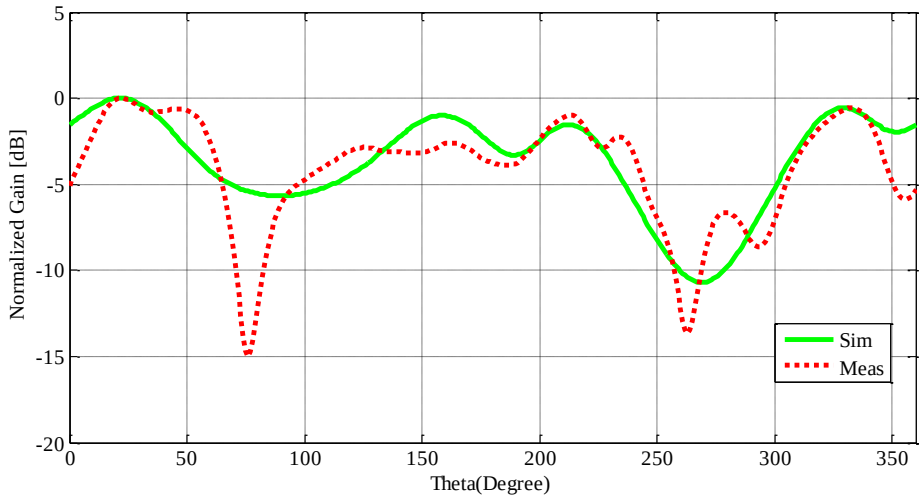

(b)

Figure 4- 21 Measured and simulated E-plane radiation patterns of the ACPS folded dipole antenna element designed as configuration-II at 3.3 GHz with the normalized gain: (a) Co-polar (b) Cross-polar

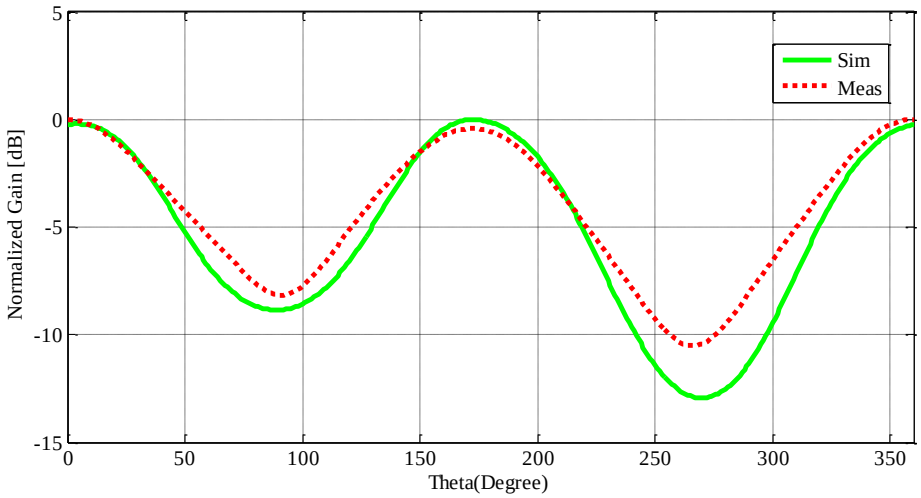

(a)

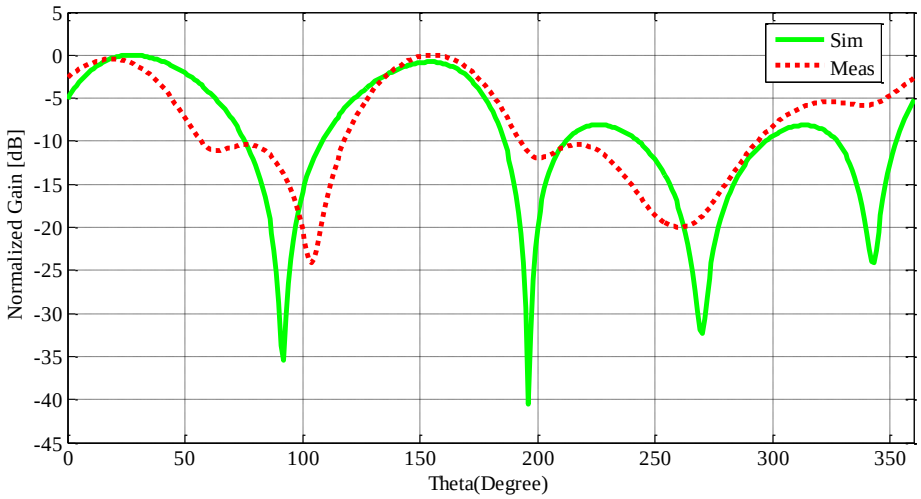

(b)

Figure 4- 22 Measured and simulated H-plane radiation patterns of the ACPS folded dipole antenna element designed as configuration-II at 3.3 GHz with the normalized gain: (a) Co-polar (b) Cross-polar

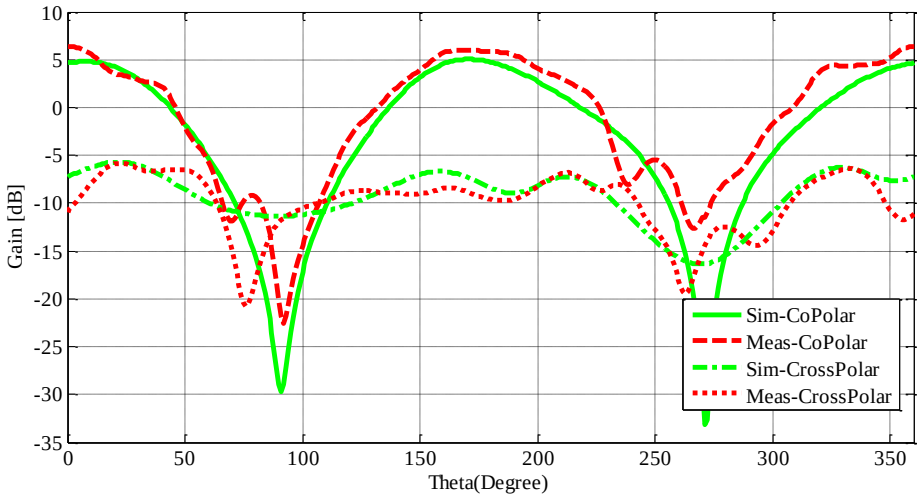

(a)

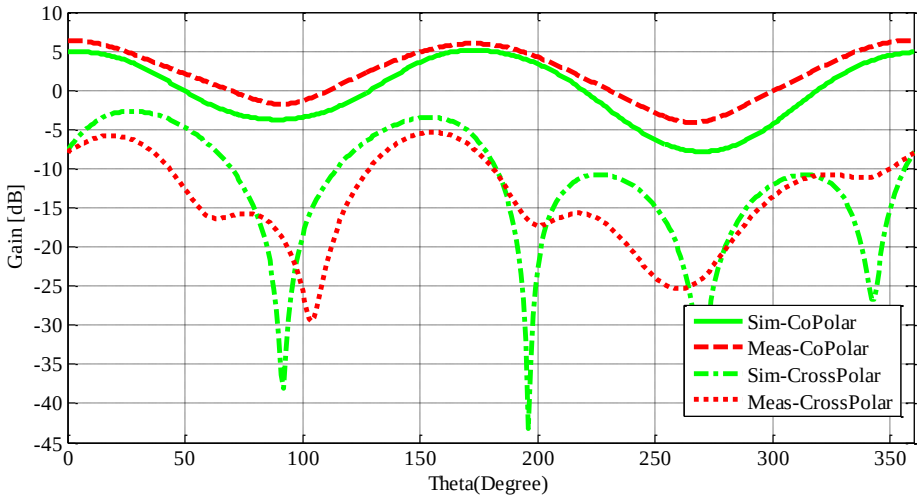

(b)

Figure 4- 23 Measured and simulated radiation patterns in terms of co and cross polarization of the ACPS folded dipole antenna element designed as configuration-II at 3.3 GHz: (a) E-plane (b) H-plane

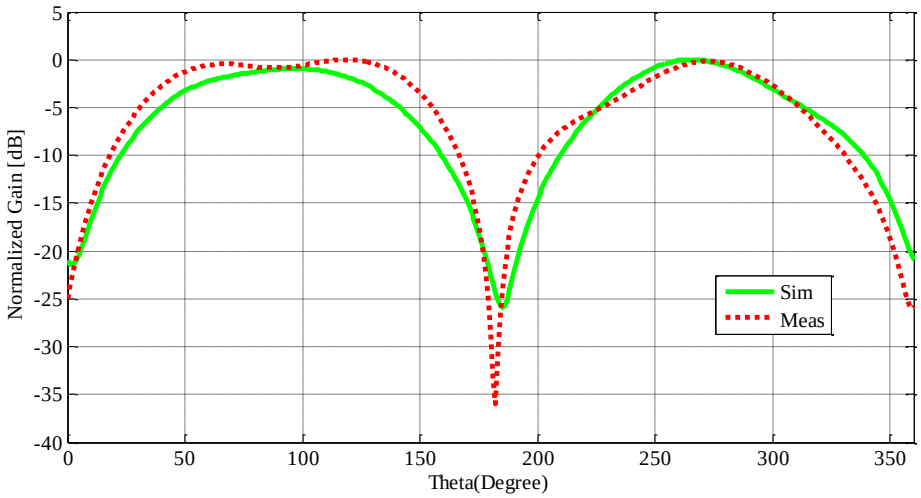

(a)

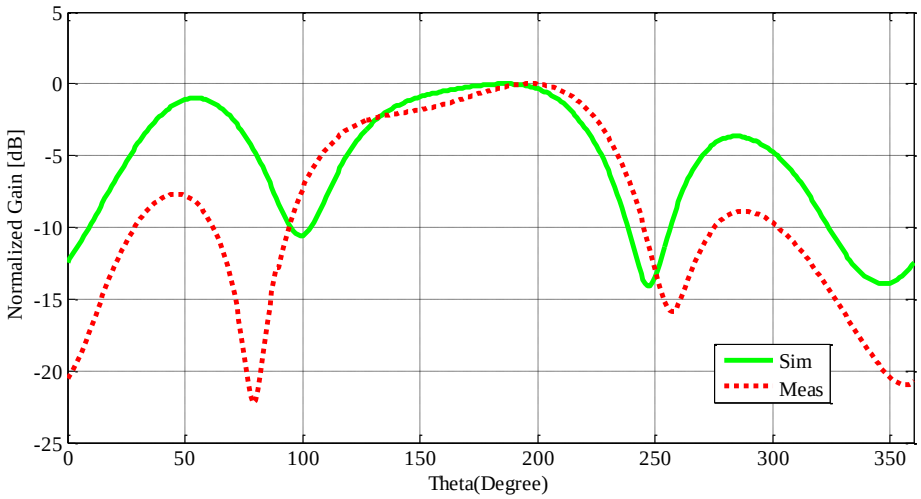

(b)

Figure 4- 24 Measured and simulated E-plane radiation patterns of the ACPS folded dipole antenna element designed as configuration-III at 3 GHz with the normalized gain: (a) Co-polar (b) Cross-polar

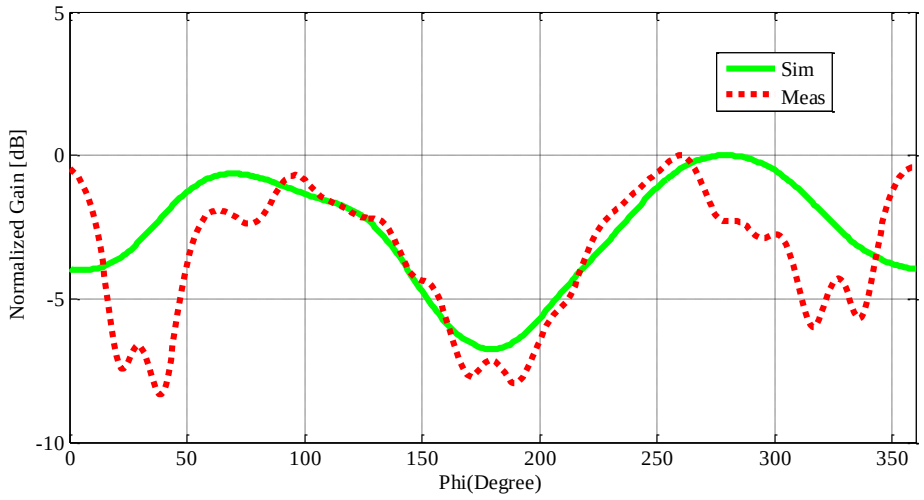

(a)

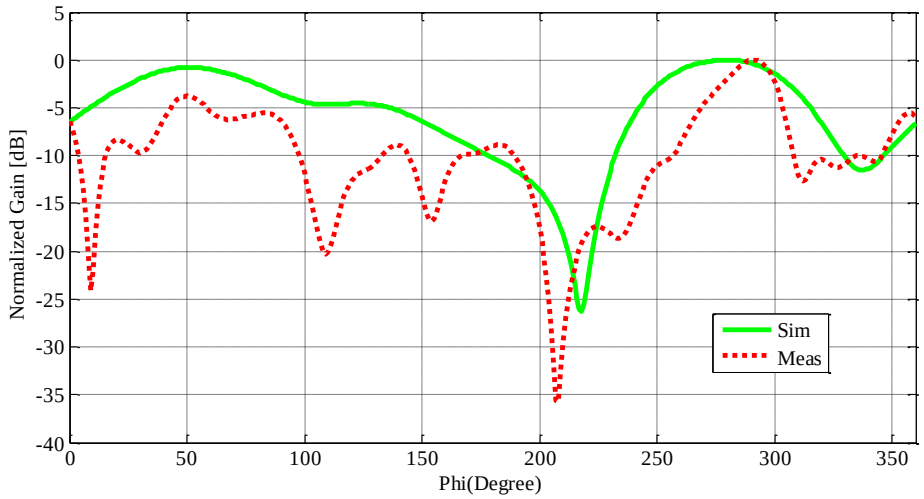

(b)

Figure 4- 25 Measured and simulated H-plane radiation patterns of the ACPS folded dipole antenna element designed as configuration-III at 3 GHz with the normalized gain: (a) Co-polar (b) Cross-polar

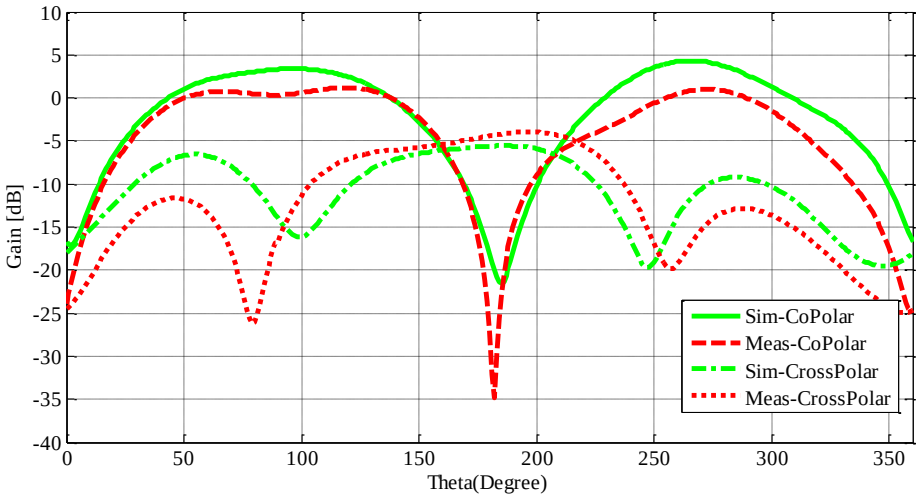

(a)

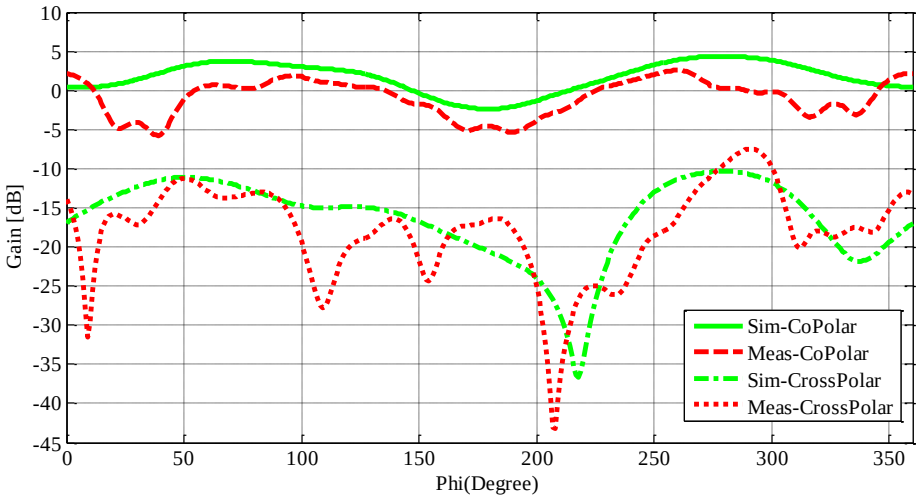

(b)

Figure 4- 26 Measured and simulated radiation patterns in terms of co and cross polarization of the ACPS folded dipole antenna element designed as configuration-III at 3 GHz: (a) E-plane (b) H-plane

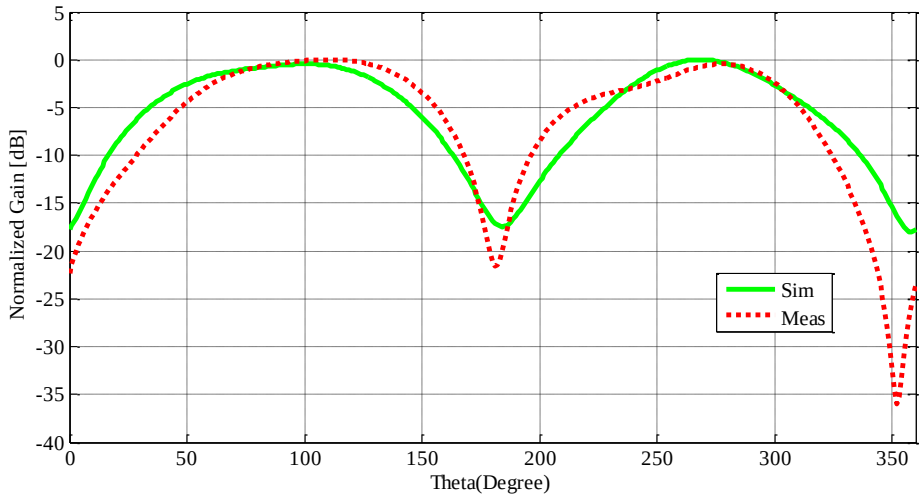

(a)

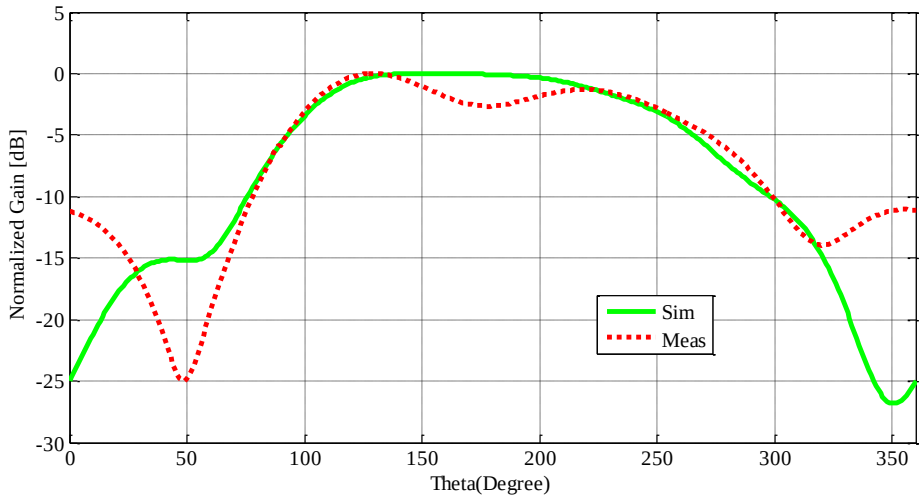

(b)

Figure 4- 27 Measured and simulated E-plane radiation patterns of the ACPS folded dipole antenna element designed as configuration-III at 2.7 GHz with the normalized gain: (a) Co-polar (b) Cross-polar

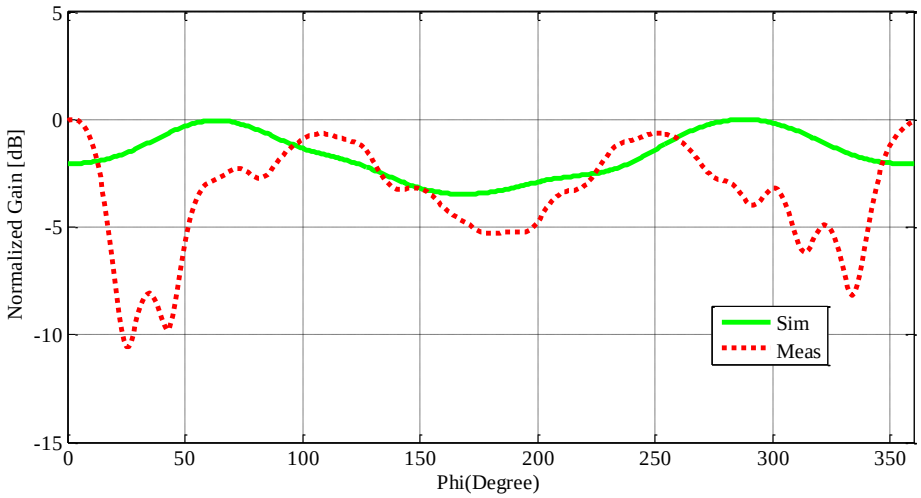

(a)

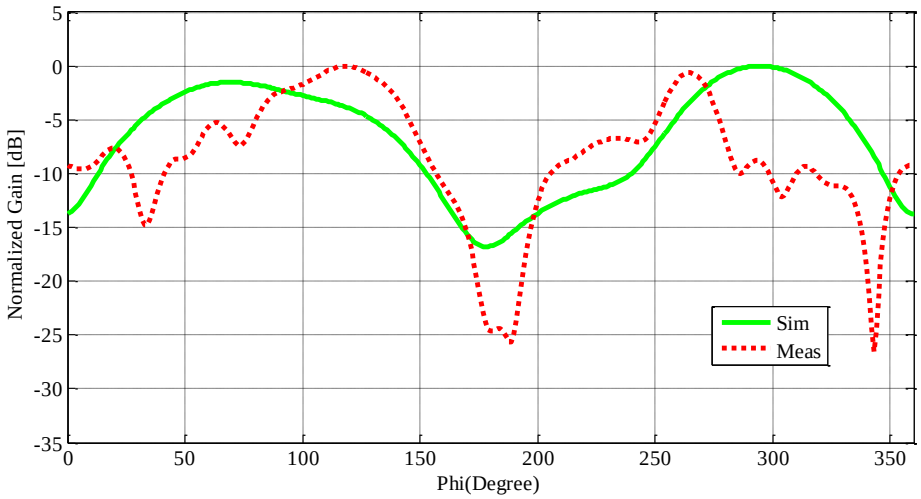

(b)

Figure 4- 28 Measured and simulated H-plane radiation patterns of the ACPS folded dipole antenna element designed as configuration-III at 2.7 GHz with the normalized gain: (a) Co-polar (b) Cross-polar

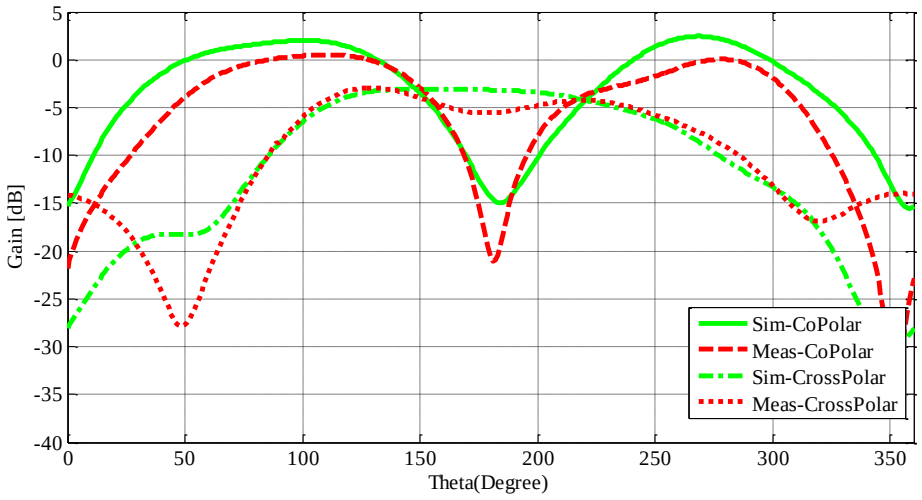

(a)

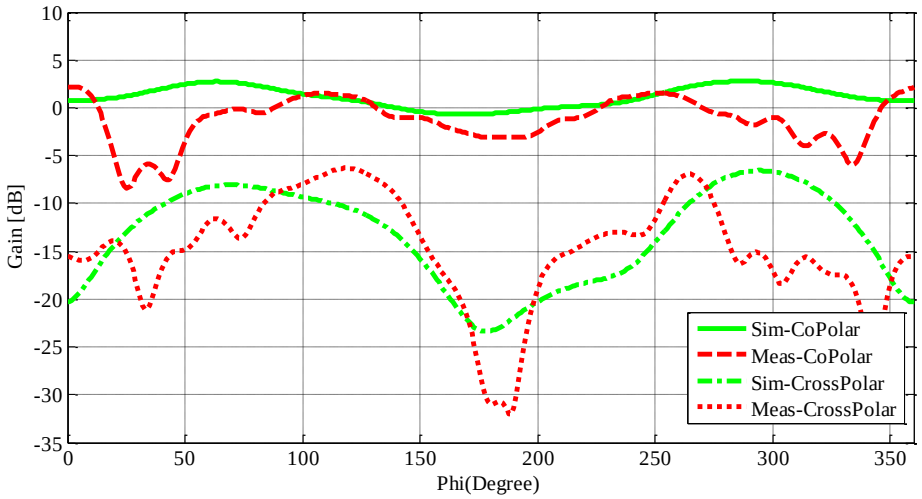

(b)

Figure 4- 29 Measured and simulated radiation patterns in terms of co and cross polarization of the ACPS folded dipole antenna element designed as configuration-III at 2.7 GHz: (a) E-plane (b) H-plane

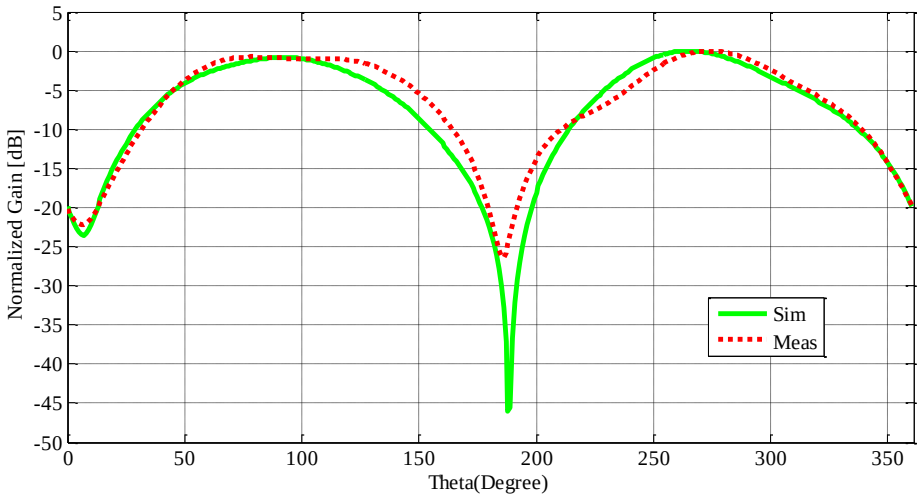

(a)

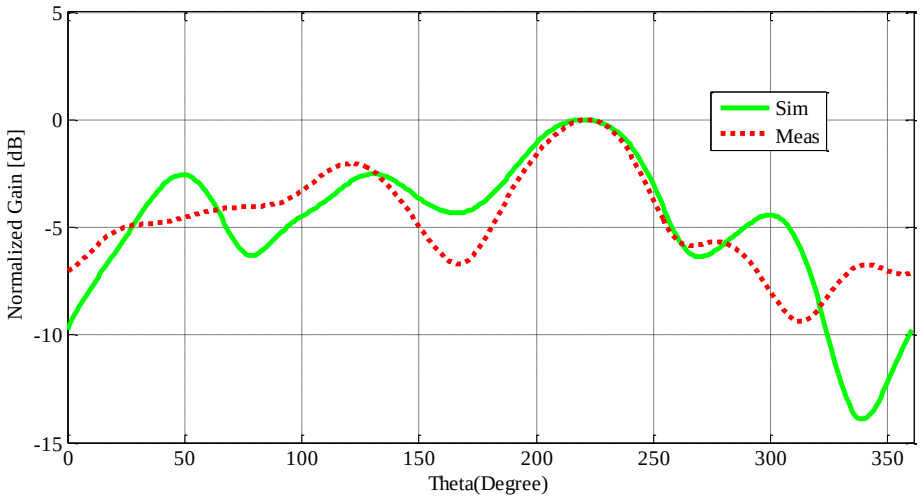

(b)

Figure 4- 30 Measured and simulated E-plane radiation patterns of the ACPS folded dipole antenna element designed as configuration-III at 3.3 GHz with the normalized gain: (a) Co-polar (b) Cross-polar

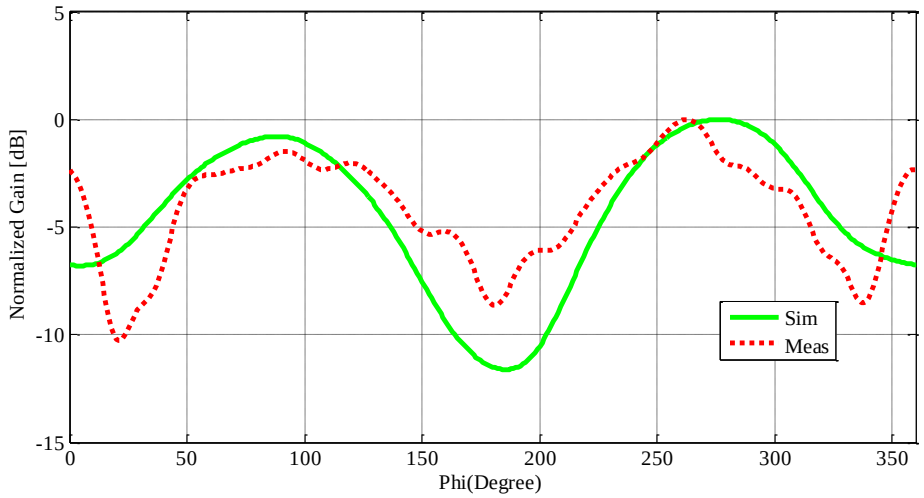

(a)

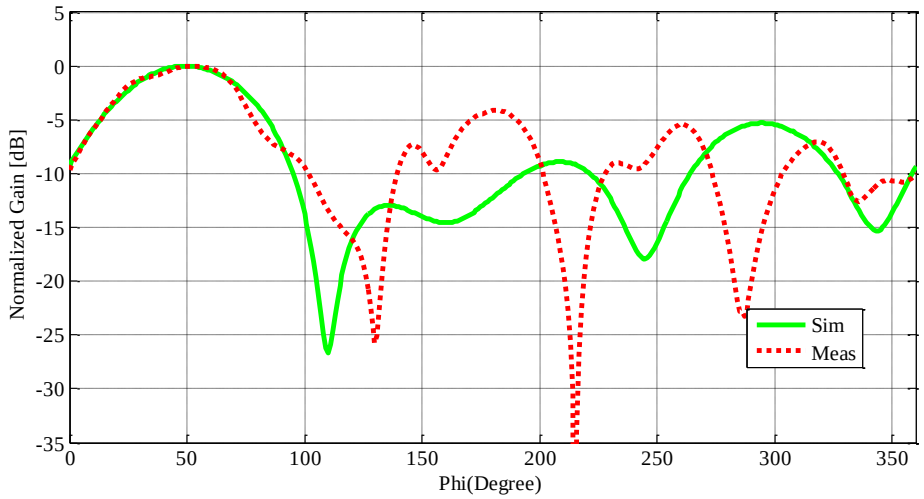

(b)

Figure 4- 31 Measured and simulated H-plane radiation patterns of the ACPS folded dipole antenna element designed as configuration-III at 3.3 GHz with the normalized gain: (a) Co-polar (b) Cross-polar

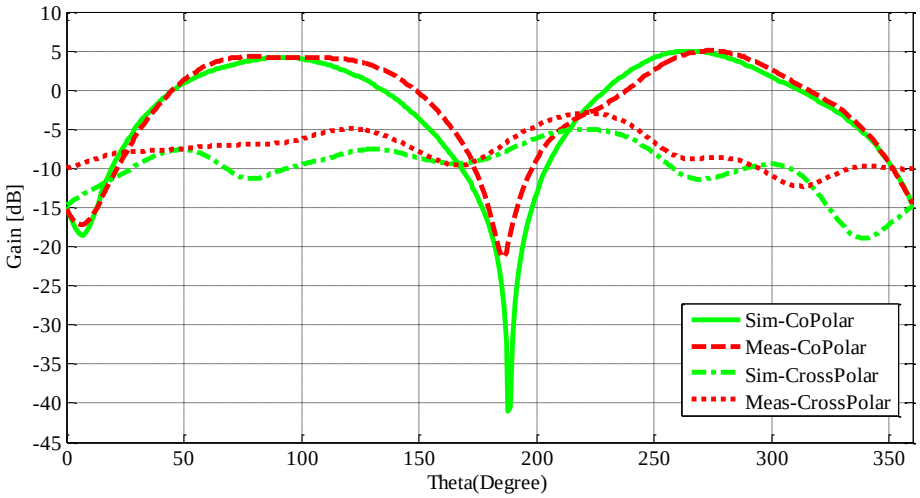

(a)

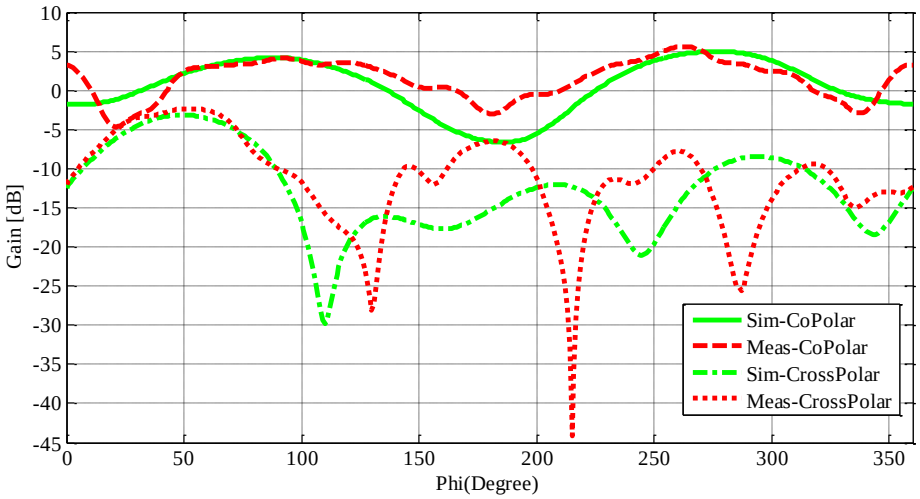

(b)

Figure 4- 32 Measured and simulated radiation patterns in terms of co and cross polarization of the ACPS folded dipole antenna element designed as configuration-III at 3.3 GHz: (a) E-plane (b) H-plane

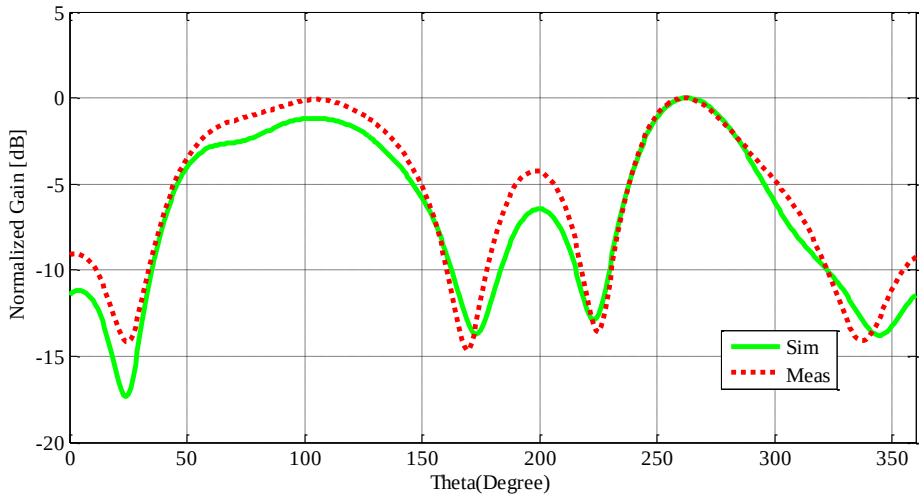

(a)

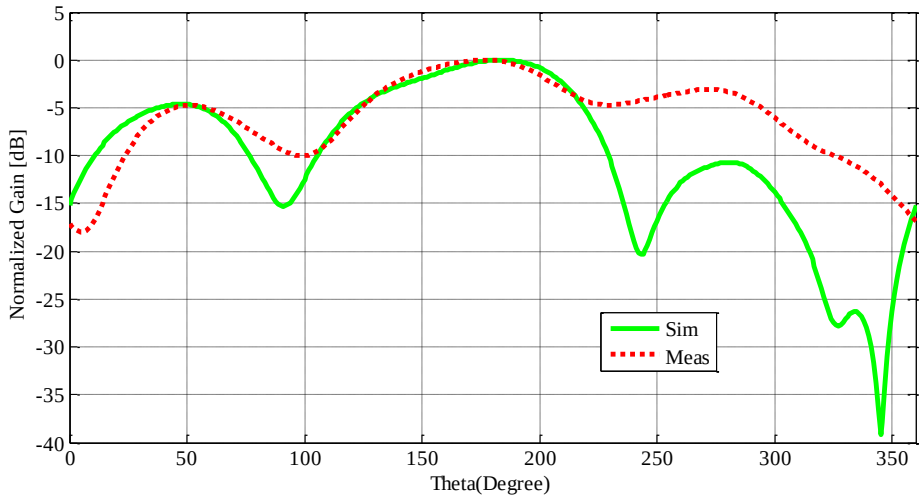

(b)

Figure 4- 33 Measured and simulated E-plane radiation patterns of the ACPS folded dipole antenna array designed as configuration-III at 3 GHz with the normalized gain: (a) Co-polar (b) Cross-polar

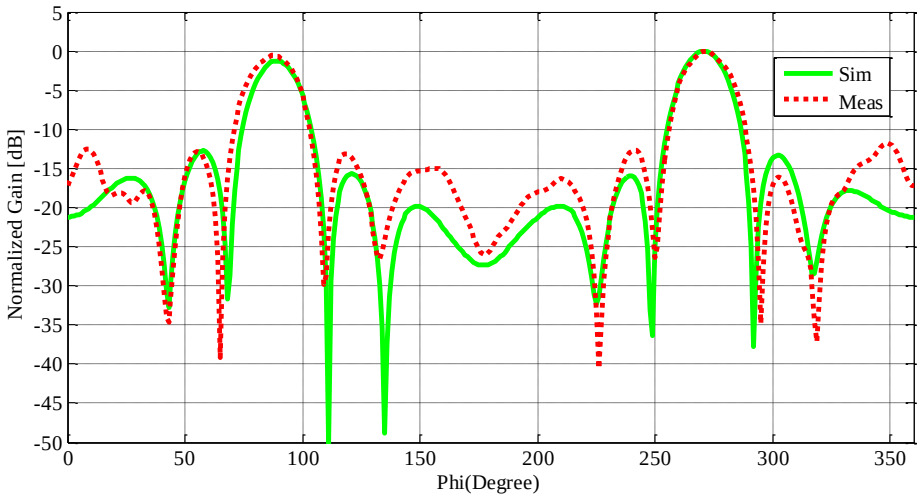

(a)

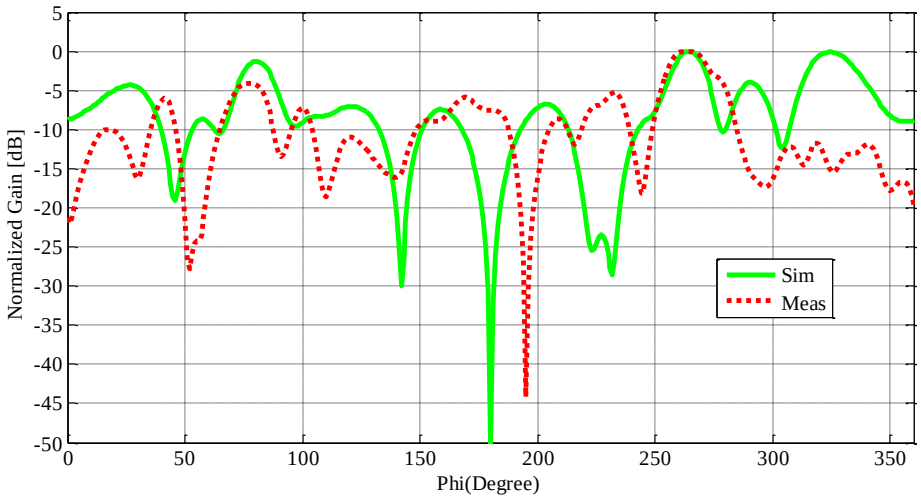

(b)

Figure 4- 34 Measured and simulated H-plane radiation patterns of the ACPS folded dipole antenna array designed as configuration-III at 3 GHz with the normalized gain: (a) Co-polar (b) Cross-polar

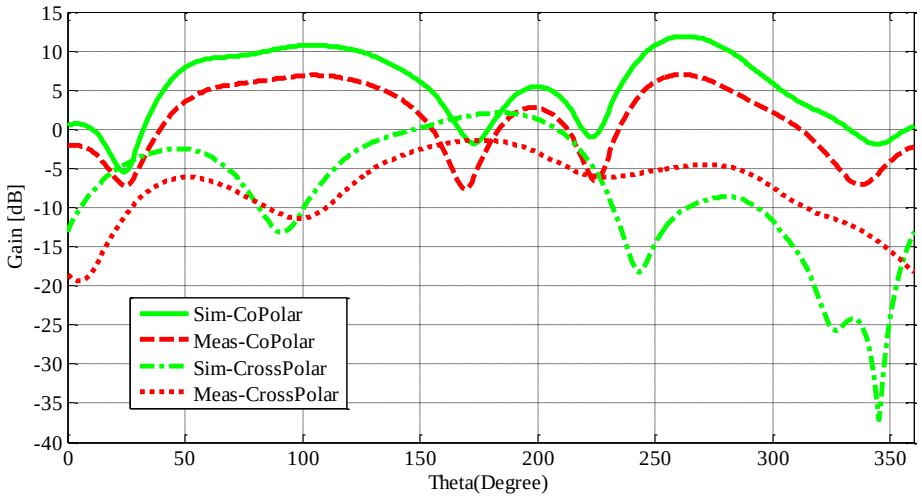

(a)

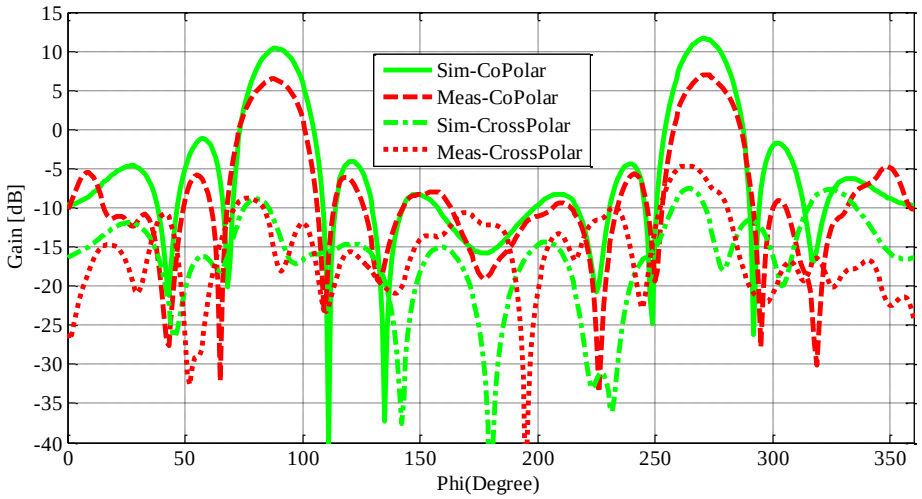

(b)

Figure 4- 35 Measured and simulated radiation patterns in terms of co and cross polarization of the ACPS folded dipole antenna array designed as configuration-III at 3 GHz: (a) E-plane (b) H-plane

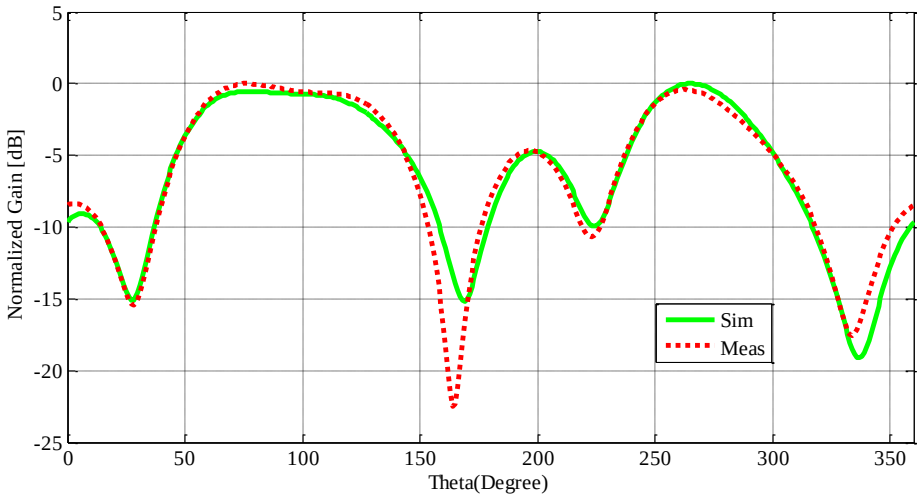

(a)

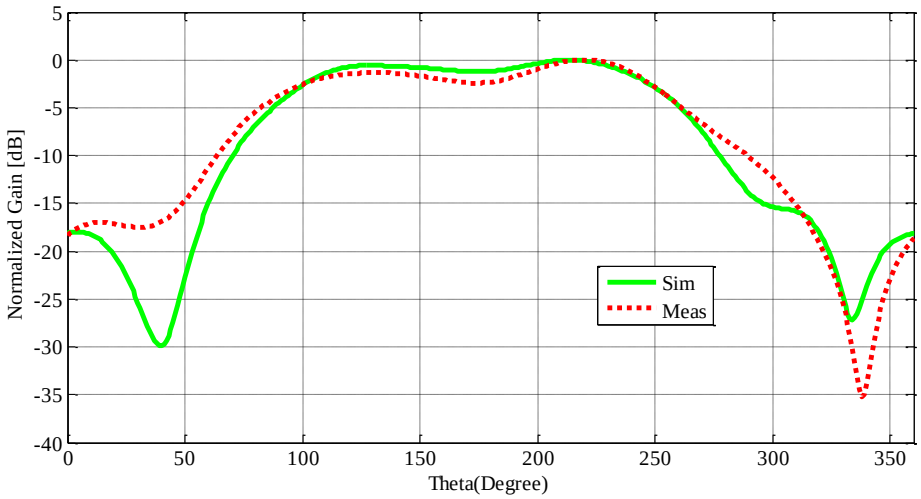

(b)

Figure 4- 36 Measured and simulated E-plane radiation patterns of the ACPS folded dipole antenna array designed as configuration-III at 2.7 GHz with the normalized gain: (a) Co-polar (b) Cross-polar

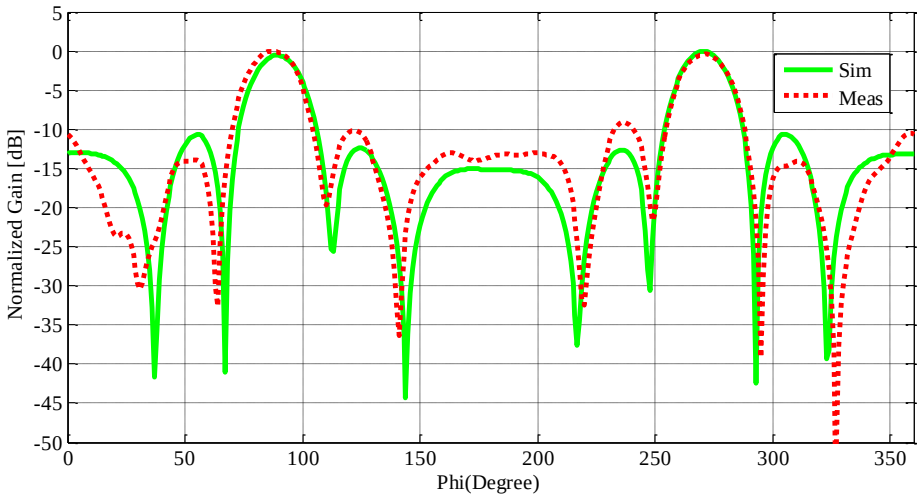

(a)

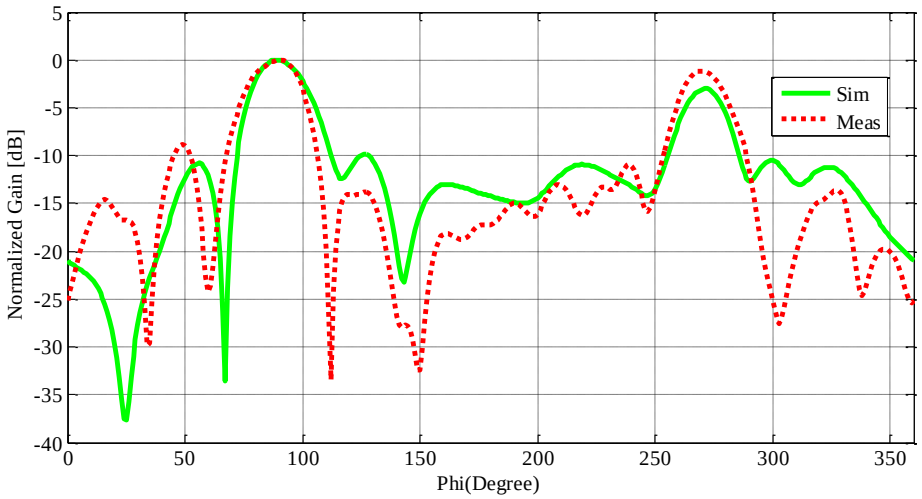

(b)

Figure 4- 37 Measured and simulated H-plane radiation patterns of the ACPS folded dipole antenna array designed as configuration-III at 2.7 GHz with the normalized gain: (a) Co-polar (b) Cross-polar

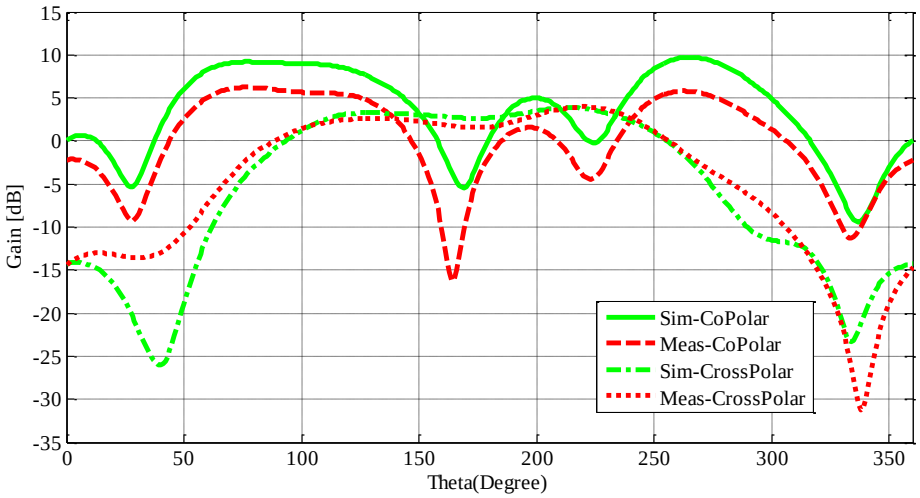

(a)

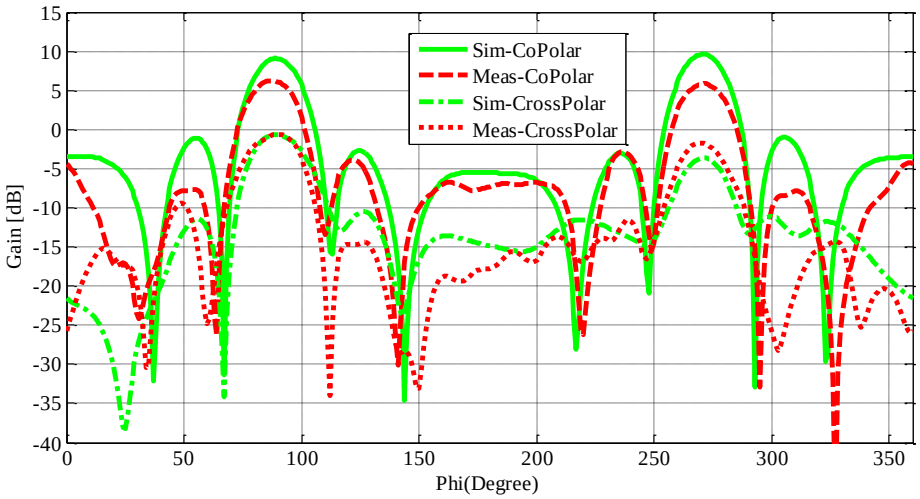

(b)

Figure 4- 38 Measured and simulated radiation patterns in terms of co and cross polarization of the ACPS folded dipole antenna array designed as configuration-III at 2.7 GHz: (a) E-plane (b) H-plane

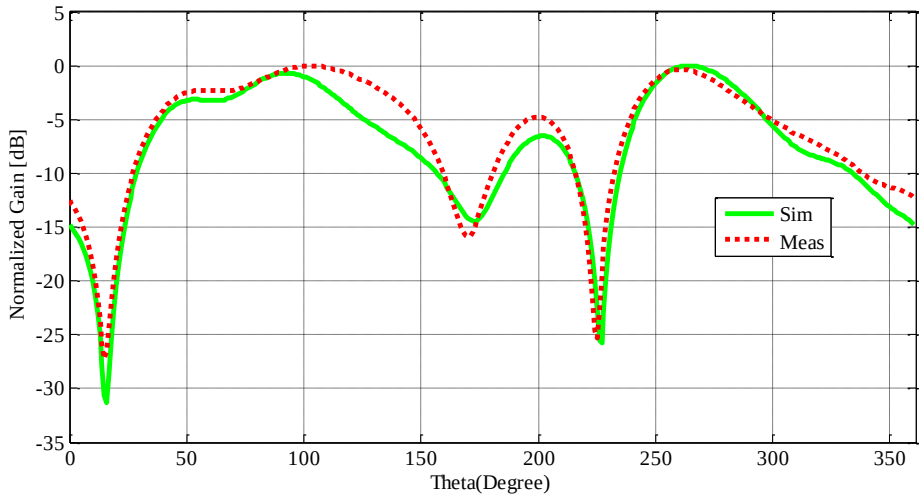

(a)

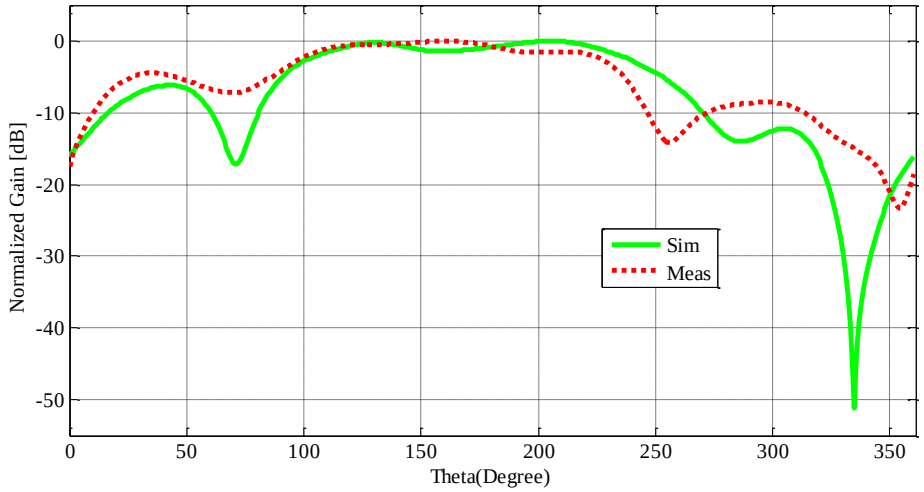

(b)

Figure 4- 39 Measured and simulated E-plane radiation patterns of the ACPS folded dipole antenna array designed as configuration-III at 3.3 GHz with the normalized gain: (a) Co-polar (b) Cross-polar

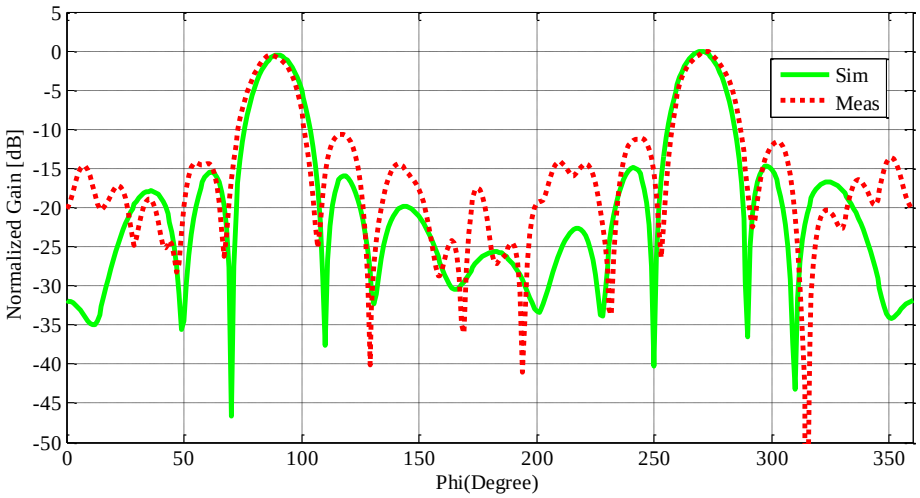

(a)

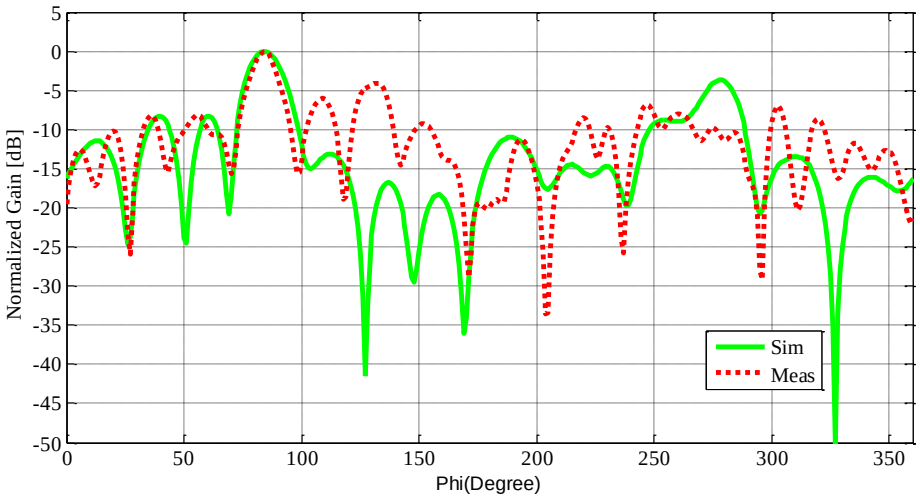

(b)

Figure 4- 40 Measured and simulated H-plane radiation patterns of the ACPS folded dipole antenna array designed as configuration-III at 3.3 GHz with the normalized gain: (a) Co-polar (b) Cross-polar

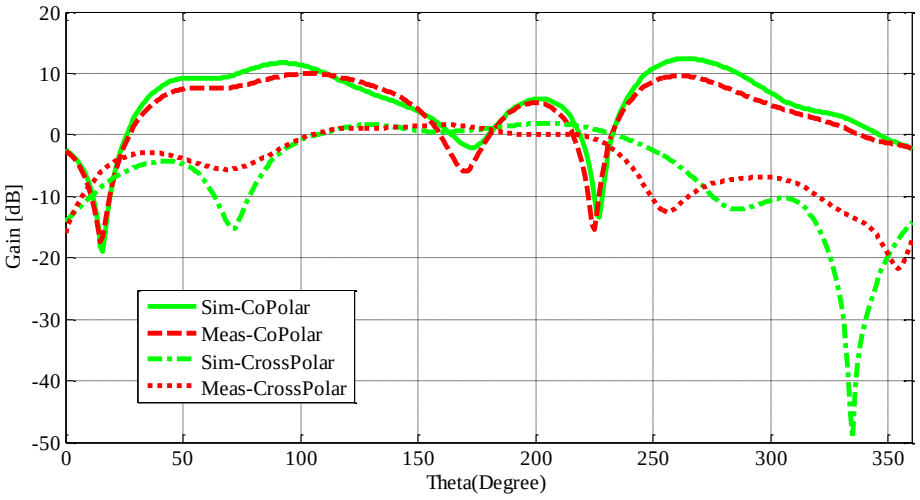

(a)

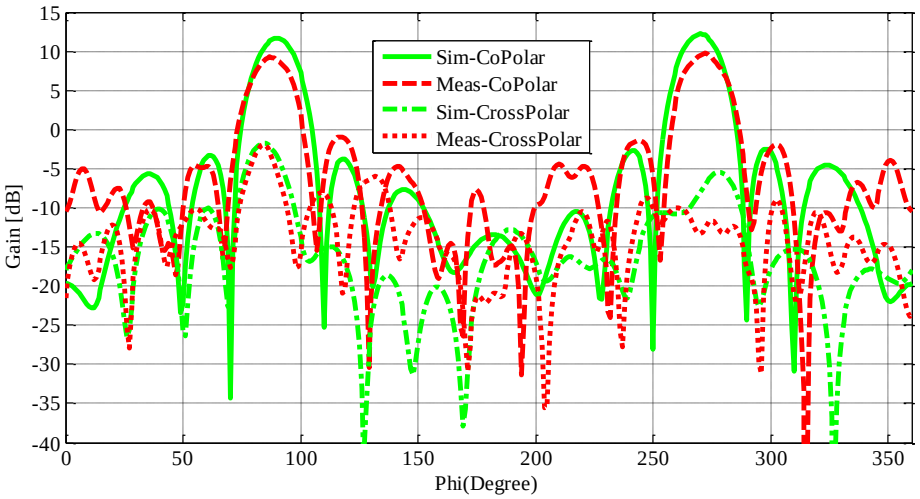

(b)

Figure 4- 41 Measured and simulated radiation patterns in terms of co and cross polarization of the ACPS folded dipole antenna array designed as configuration-III at 3.3 GHz: (a) E-plane (b) H-plane

CHAPTER 5

CONCLUSIONS

In this study a low profile printed ACPS folded dipole antenna with balun operating in S-band is presented, and its usefulness as a single element in array antenna is explored by constructing four-element linear array with corporate feed network. The appropriately arrangement of the physical parameters of the ACPS folded dipole enables us to tune the input impedance and resonance frequency of the ACPS folded dipole antenna and this property of the antenna gives an opportunity for optimization of a single element compared to the conventional dipole or folded dipole. The advantages of the designed antenna are that it has low cost, it is more compact and easy to fabricate due to printed circuit technology used for the construction of this antenna. Also, the beamwidth and radiation properties of this antenna make it attractive choice as either an array element or a standalone antenna with broad pattern.

ACPS folded dipole antenna design parameters are investigated in this work. The parametric analysis is done for each design parameters to explore the effect of these antenna parameters on input impedance, resonant frequencies and bandwidth characteristics of the antenna. Based on the results of this study, an ACPS folded dipole antenna with the requirements of 2.7 GHz – 3.3 GHz frequency bandwidth, return loss better than 10 dB and 200 Ω input impedance is designed. In order to feed the balanced ACPS folded dipole antenna, the balun consists of a microstrip to coplanar stripline transition is designed and the performance of this balun is investigated over the frequency range of the S-band by performing simulations in

detail. These simulation results show that the designed balun is suitable for integration with planar balanced antennas in a compact form and has any effects on the antenna performances.

After the design process of the ACPS folded dipole antenna and balun is completed, three different architectures which are the configuration-I, II and III for both the single element antenna and array are studied in this work in order to fulfill design requirements. At the beginning, the ACPS folded dipole antenna designed as configuration-I is simulated in terms of return loss response, gain and radiation patterns any optimization for the obtained design parameter values of the ACPS folded dipole and balun in previous section. According to the simulation results, design of a single element antenna with a 20% bandwidth is achieved. Step by step other configurations for the single element antenna and array are designed and simulated individually in the same aspects with configuration-I. The designed feed network for the four-element linear array divides power equally between the arms thereby supplying equal power, both in amplitude and phase. Simulation results of the single element and array designed as configuration-III demonstrates that the return loss response and radiation patterns of the antennas fulfill the requirements and expectations of the design.

Finally, the design and simulation process of the ACPS folded dipole antenna element and four-element linear array designed as configuration-II and III is completed, these antennas with determined parameters are fabricated and measured. Fabrication of these antennas is accomplished in the facilities of ASELSAN Inc. using printed circuit board technology. Bending process of the single element and four-element linear array antenna fabricated as configuration-II in order to obtain the configuration-III are done manually, therefore it is very crucial in order to achieve desired antenna performances. Return loss responses, gains and radiation patterns of the fabricated single element antennas and arrays are measured, and measurement results are compared with the simulation results in

order to reveal the crucial fabrication parameters resulting in deviation from the simulation.

Good agreement between the simulated and measured results of the single element ACPS folded dipole antenna fabricated as configuration-II and III are obtained in terms of the reflection coefficient, far field radiation patterns and gain. The measured bandwidth of the antenna for return loss responses better than 10 dB is over 20% for the center frequency of the design. Fluctuation between the simulated and measured total realized gain is within 2.5 dB across the bandwidth of 2.7 GHz – 3.3 GHz, and this may be due to some additional losses based on bending process, higher losses in the dielectric substrate or measurement errors result from the near field measurement system. The radiation patterns are measured for three different frequencies, and observed to be in accordance with the simulation results in the operating bandwidth.

The measured return loss responses of the four-element linear ACPS folded dipole array for both configuration-II and III are excellent agreement with the simulation results. It is observed to have return loss response, better than 10 dB across the bandwidth of 2.7 GHz – 3.3 GHz. The measured radiation pattern of the each arrays are fairly consistent with the simulated patterns in the operating bandwidth.

All these results prove that the ACPS folded dipole antenna radiates well and it is a good candidate for the next stage in order to form an array structure.

For the future work ACPS folded dipole antenna for different input impedance and resonant frequencies can be developed. Metallic backplane can be used to overcome the problem of bidirectional radiation, thus metallic backplane reflects radiations in the opposite direction and improve forward radiation of the array construction. The designed four-element linear ACPS folded dipole array can be extended to any number of elements for maximum directivity in broadside direction. The ACPS folded dipole array can be designed to obtain the scanning capabilities. Hence, microstrip delay lines can be employed to achieve the

appropriate phase difference between the elements and lengths of the each microstrip delay lines can be optimized at operating frequency. Lastly, the tapered excitation instead of the simple equal-amplitude excitation is used in order to obtain the desired sidelobe levels for the ACPS folded dipole array.

REFERENCES

[1] D.M. Pozar, *Microstrip Antennas*, Proc. IEEE, Vol. 80, No.1, pp.79-81, January 1992.

[2] R. Garg, P. Bhartia, I. Bahl and A. Ittipoon, *Microstrip Antenna Design Handbook*, Artech House, Boston, London, 2001.

[3] C. A. Balanis, *Antenna Theory - Analysis and Design*, John Wiley & Sons, Inc. Third Edition, New York, 2005.

[4] J. F. Zurcher and F. E. Gardiol, *Broadband Patch Antennas*, Artech House, United States of America, 1995.

[5] K. S. Yngvesson, T. L. Korzeniowski, Y. Kim, E. L. Kollbuerg and J. F. Johansson, *The Tapered Slot Antenna – A New Integrated Element For Millimeter-Wave Applications*, IEEE Transactions on Microwave Theory and Techniques, Vol. 37, pp. 365-374, February 1989.

[6] W. R. Deal, N. Kaneda, J. Sor, Y. Qian and T. Itoh, *A New Quasi-Yagi Antenna for Planar Active Antenna Arrays*, IEEE Transactions on Microwave Theory and Techniques, Vol. 48, No. 6, pp. 910-917, June 2000.

[7] C. W. Ling, C. Y. Lee, C. L. Tang and S. J. Chung, *Analysis and Application of an On-Package Planar Inverted-F Antenna*, IEEE Transactions on Antennas and Propagation, Vol. 55, No. 6, pp. 1774-1780, June 2007.

[8] Q. Xue, S. W. Liao and J. H. Xu, *A Differentially-Driven Dual-Polarized Magneto-Electric Dipole Antenna*, IEEE Transactions on Antennas and Propagation, Vol. 61, No. 1, pp. 425-430, January 2013.

[9] R. J. Mailloux, *Phased Array Antenna Handbook*, Artech House, Second Edition, Boston, London, 2005.

[10] H. J. Visser, *Approximate Antenna Analysis for CAD*, John Wiley & Sons, Inc., Chichester, UK, 2009.

[11] R. W. Lampe, *Design Formulas for an Asymmetric Coplanar Strip Folded Dipole*, IEEE Transactions on Antennas and Propagation, Vol. AP-33, No. 9, pp. 1028-1031, September 1985.

[12] R. W. Lampe, *Corrections to Design Formulas for an Asymmetric Coplanar Strip Folded Dipole*, IEEE Transactions on Antennas and Propagation, Vol. AP-34, No. 4, p. 611, April 1986.

[13] H. J. Visser, *Improved Design Equations for Asymmetric Coplanar Strip Folded Dipoles on a Dielectric Slab*, Proceedings of the Second European Conference on Antennas and Propagation EuCAP 2007, Edinburgh, UK, pp. 1-6, November 2007.

[14] J. P. German and F.E. Brooks, *The Effects of the Physical Parameters on the Bandwidth of a Folded Dipole*, IRE Transactions on Antennas and Propagation, pp. 186-190, April 1958.

[15] R. Guertler, *Impedance Transformation in Folded Dipoles*, Proceedings of the IRE, Vol. 38, pp. 1042-1047, September 1950.

[16] ANSYS HFSS®, <http://www.ansys.com/hfss>.

[17] J. A. Flint and J.C. Vardaxoglou, *Exploitation of Nonradiating Modes in Asymmetric Coplanar Strip Folded Dipoles*, IEE Proceedings of Microwave Theory and Antennas Propagation, Vol. 151, No. 4, pp. 307-310, August 2004.

[18] G. A. Thiele, E. P. Ekelman and L. W. Henderson, *On the Accuracy of the Transmission Line Model of the Folded Dipole*, IEEE Transactions on Antennas and Propagation, Vol. AP-28, No. 5, pp. 700-703, September 1980.

[19] V. F. Hanna and D. Thebault, *Analysis of Asymmetrical Coplanar Waveguides*, Int. J. Electron., Vol. 50, pp. 221-224, March 1981.

[20] V. F. Hanna and D. Thebault, *Theoretical and Experimental Investigation of Asymmetric Coplanar Waveguides*, IEEE Transactions on Microwave Theory and Techniques, Vol. MTT-32, No. 12, pp. 1649-1651, December 1984.

[21] W. Hilberg, *From Approximations to Exact Relations for Characteristic Impedances*, IEEE Transactions on Microwave Theory and Techniques, Vol. MTT-17, No. 5, pp. 259-265, May 1969.

[22] E. Hallen, *Theoretical Investigations into the Transmitting and Receiving Qualities of Antennae*, Nova Acta Regiae Soc. Sci. Upsaliensis, Ser. IV, Vol. 11, No. 4, pp. 3-44, 1938.

[23] S. Keyrouz, H. J. Visser and A. G. Tijhuis, *Novel Empirical Equations to Calculate the Impedance of a Strip Dipole Antenna*, Radio Engineering, Vol. 22, No. 4, pp. 1258-1261, December 2013.

[24] R. S. Elliot, *Antenna Theory and Design*, John Wiley & Sons, Inc., New Jersey, USA, 2003.

[25] S. Keyrouz, H. J. Visser and A. G. Tijhuis, *Novel Analytical Procedures for Folded Strip Dipole Antennas*, Sixth European Conference on Antennas and Propagation (EUCAP), pp. 2479-2482, 2012.

[26] Z. C. Zheng and G. Q. Luo, *Design of a Compact Wideband Balun between Microstrip and Coplanar Stripline*, Microwave Workshop Series on Millimeter Wave Wireless Technology and Applications (IMWS), 2012 IEEE MTT-S International, pp. 1-3, September 2012.

[27] J. B. Knorr and K. D. Kuchler, *Analysis of Coupled Slots and Coplanar Strips on Dielectric Substrate*, IEEE Transactions on Microwave Theory and Techniques, Vol. MTT-23, No. 7, pp. 541-548, July 1975.

[28] K. Goverdhanam, R. N. Simons and L. P. B. Katehi, *Coplanar Stripline Components for High-Frequency Applications*, IEEE Transactions on Microwave Theory and Techniques, Vol. 45, No. 10, pp. 1725-1729, October 1997.

[29] R. N. Simons, *Coplanar Waveguide Circuits, Components, and Systems*, John Wiley & Sons, Inc., New York, 2001.

[30] E. Chen and S. Y. Chou, *Characteristics of Coplanar Transmission Lines on Multilayer Substrates: Modelling and Experiments*, IEEE Transactions on Microwave Theory and Techniques, Vol. 45, No. 6, pp. 939-945, June 1997.

[31] Data Sheet, *RT/duroid® 6002 High Frequency Laminates*, ROGERS Corporation.

[32] K. H. Han, B. Lacroix, J. Papapolymerou and M. Swaminathan, *New Microstrip-to-CPS Transition for Millimeter-Wave Application*, Electronic Components and Technology Conference (ECTC), 2011 IEEE 61st, pp. 1052-1057, June 2011.

[33] T. Ma, C. Wang, R. Hua and J. Tsai, *A Modified Quasi-Yagi Antenna With a New Compact Microstrip to Coplanar Strip Transition using Artificial Transmission Lines*, IEEE Transactions on Antennas and Propagation, Vol. 57, No. 8, pp. 2469-2474, August 2009.

[34] Y. Suh and K. Chang, *A Wideband Coplanar Stripline to Microstrip Transition*, IEEE Microwave and Wireless Components Letters, Vol. 11, No. 1, pp. 28-29, January 2001.

[35] D. Woo, Y. Kim, K. Kim and Y. Cho, *A Simplified Design of Quasi-Yagi Antennas Using the New Microstrip-to-CPS Transitions*, Antennas and Propagation Society International Symposium, 2007 IEEE, pp. 781-784, June 2007.

[36] A. L. Amadjikpe, D. Choudhury, G. E. Ponchak and J. Papapolymerou, *High Gain Quasi-Yagi Planar Antenna Evaluation in Platform Material Environment for 60 GHz Wireless Application*, Microwave Symposium Digest, 2009. MTT '09. IEEE MTT-S International, pp. 385-388, June 2009.

[37] N. I. Dib, R. N. Simons and L. P. B. Katehi, *New Uniplanar Transitions for Circuit and Antenna Applications*, IEEE Transactions on Microwave Theory and Techniques, Vol. 43, No. 12, pp. 2868-2873, December 1995.

[38] Y. Qian and T. Itoh, *A Broadband Uniplanar Microstrip to CPS Transition*, Microwave Conference Proceedings, 1997. APMC '97, 1997 Asia-Pacific, pp.609-612, December 1997.

[39] D. M. Pozar, *Microwave Engineering*, John Wiley & Sons, Inc., Fourth Edition, New York, 2012.

[40] T. Maleszka, *Planar MS-CPS Bypass Balun for CPS-fed Textile Antennas*, Microwave Radar and Wireless Communications (MIKON), 2010 18th International Conference, pp. 1-4, June 2010.

[41] N. Nikolic and A.R. Weily, *Compact E-Band Planar Quasi-Yagi Antenna with Folded Dipole Driver*, IET Microwaves Antennas and Propagation, Vol.4, Iss. 11, pp. 1728-1734, 2010.

[42] C. J. Lee, K. M. K. H. Leong and T. Itoh, *A Broadband Microstrip to CPS Transition Using Composite Right/Left-Handed Transmission Lines with an Antenna Application*, Microwave Symposium Digest, 2005 IEEE MTT-S International, pp. 1949-1952, June 2005.

[43] R. J. P. Douville and D. S. James, *Experimental Study of Symmetric Microstrip Bends and Their Compensation*, IEEE Transactions on Microwave Theory and Techniques, Vol. MTT-26, No. 3, pp. 175-182, March 1978.

[44] R. Chadha and K. C. Gupta, *Compensation of Discontinuities in Planar Transmission Lines*, IEEE Transactions on Microwave Theory and Techniques, Vol. MTT-30, No. 12, pp. 2151-2156, December 1982.

[45] P. R. Grajek, B. Schoenlinner and G. M. Rebeiz, *A 24-GHz High-Gain Yagi-Uda Antenna Array*, IEEE Transactions on Antennas and Propagation, Vol. 52, No. 5, pp. 1257-1261, May 2004.